October 31, 1977

To the Graduate Council:

I am submitting herewith a thesis written by Chang-Pin D. Chou entitled "The Effect of Ferrite Level on the Corrosion Resistance of Austenitic Stainless Steel Weld Metal." I recommend that it be accepted in partial fulfillment of the requirements for the degree of Master of Science, with a major in Metallurgical Engineering.

J. E. Spruiell

Joe E. Spruiell, Major Professor

We have read this thesis
and recommend its acceptance:

E. E. Stansbury

Carl D. Lundin

Accepted for the Council:

L. Evans Cook

Vice Chancellor
Graduate Studies and Research

Thesis
77
C449
cop. 2

THE EFFECT OF FERRITE LEVEL ON THE CORROSION RESISTANCE OF AUSTENITIC STAINLESS STEEL WELD METAL

A Thesis

Presented for the

Master of Science

Degree

The University of Tennessee, Knoxville

Chang-Pin D. Chou

December 1977

1345660

ACKNOWLEDGEMENTS

The author wishes to express his sincere gratitude to his major professors, Dr. J. E. Spruiell and Dr. E. E. Stansbury, for their continued encouragement, advice, patience, and understanding during the course of this investigation.

Appreciation is expressed to Dr. C. D. Lundin for his kind guidence and help during this work.

The author wishes to thank Mr. H. B. Thompson and Mr. T. A. Long for their many contributions to the success of this work.

Thanks also to Mr. B. L. McGill for his assistance on the scanning electron microscopy work.

The author wishes to express his deepest appreciation and thanks to his wife, Pin-Ying, for her patience, understanding, and many hours of typing.

ABSTRACT

The purpose of this experimental study was to investigate the effect of initial ferrite content on the corrosion resistance of austenitic stainless steel weld metals after welding and aging at elevated temperatures. Various techniques such as optical metallography, X-ray diffraction of bulk extracted residues, and Magne Gage measurements of delta ferrite content were used to determine the precipitate identities, nucleation sites, morphology distribution, and kinetics of precipitation. Corrosion behavior was studied using anodic polarization curves. These were determined in a solution of 1N H_2SO_4 using a potentiostat. In order to selectively etch the specimen, a controlled potential etching test was run in a solution of 5% H_2SO_4 and 0.1 g/l NH_4SCN. The attacked surfaces of etched specimens were examined by optical microscopy and by scanning electron microscopy. Energy dispersive X-ray analysis was also applied to identify some of the etched particles.

It was found that the ferrite present in the as-deposited welds is replaced by the intermetallic sigma and chi phases during aging at elevated temperatures. Also the ferrite-austenite boundaries serve as easy nucleating sites for both carbides and the intermetallic phases, thus enhancing the rate of formation of such phases in welds containing ferrite as compared to materials of similar composition in which no ferrite exists.

Sensitization by carbide precipitation has a great effect on the anodic polarization curves for the high carbon grade welds. The passive current density increases at shorter aging times and then decreases after longer aging times. For the low carbon grade stainless steel welds the sensitization effect is not significant.

High ferrite content welds have both lower passive current densities and lower critical current densities than the low ferrite content welds have.

Chromium depletion in the grain boundaries itself is the cause of attack rather than the precipitates themselves. It is suggested that the distribution of chromium is a major cause of the intergranular corrosion in aged austenitic stainless steel weld metals.

From the etching test, it was found that a greater risk of intergranular attack occurred for the low ferrite content welds from the active region to the transpassive region. In high ferrite content welds the corrosive attack was uniformly distributed around the second phases, while in the low ferrite content welds attack was concentrated along the grain boundaries. It was also found that sigma phase can corrode rapidly beyond the transpassive region.

TABLE OF CONTENTS

CHAPTER		PAGE
I.	INTRODUCTION.	1
II.	LITERATURE REVIEW	4
	Ferrite in Austenitic Stainless Steel Weld Metal.	4
	Carbide Phases in Austenitic Stainless Steel Weld Metal.	8
	Sigma Phase in Austenitic Stainless Steel Weld Metal.	11
	Aging Characteristics of Austenitic Stainless Steel Weld Metal.	14
	Corrosion of Austenitic Stainless Steel Weld Metal.	17
	Electrochemical Behavior of Active-Passive Metals.	21
	Methods for Determining Current-Potential Polarization Curve.	26
	Alloy Evaluation by Using Potentiostatic Anodic Polarization Curve	30
III.	EXPERIMENTAL PROCEDURES	39
	Alloy Preparation	39
	Heat Treatment.	39
	Preparation of Specimens.	41

CHAPTER PAGE

Ferrite Determination 42

Optical Metallography 42

X-ray Diffraction 42

Potentiostatic Polarization Curve 43

Controlled Potential Corrosion Test 47

IV. RESULTS AND DISCUSSION. 49

Ferrite Contents and Microstructures of Aged Samples 49

Bulk Extraction and X-Ray Diffraction Studies of Precipitates 58

Anodic Polarization Curve Measurements. . . . 70

Controlled Potential Corrosion Test and Scanning Electron Microscope Studies. . . . 107

V. CONCLUSIONS 116

LIST OF REFERENCES. 118

VITA. 124

LIST OF TABLES

TABLE		PAGE
1.	Potentials for Selective Etching of Phases in 18-8 Stainless Steels	38
2.	Chemical Analyses and Ferrite Numbers of As-deposited Weld Pads	40
3.	Ferrite Number Readings Before and After Heat Treatments of Types 316L-D and 316-D Welds.	50
4.	Ferrite Number Readings Before and After Heat Treatments of Types 308L-D and 308-D Welds.	51
5.	The Equivalent Chromium Content of Austenitic Stainless Steel Weld Metals Used in this Investigation.	55
6.	Weight Percent of Extracted Precipitates from Aged Samples.	63
7.	Identified Phases and Fraction Content of Extracted Residue	64
8.	X-ray Diffraction Pattern Analysis of Weld Metal 308-D Aged 2000 Hours at 750°C	65
9.	Relative Contents of Extracted Residue from Type 308-D Weld Metal	66

TABLE PAGE

10. Electrochemical Parameters of Polarization Curves of Type 316-A Weld Metal. 86

11. Electrochemical Parameters of Polarization Curves of Type 316-D Weld Metal. 87

12. Electrochemical Parameters of Polarization Curves of Type 308-A Weld Metal. 88

13. Electrochemical Parameters of Polarization Curves of Type 308-D Weld Metal. 89

14. Electrochemical Parameters of Polarization Curves of Type 316L-A Weld Metal 90

15. Electrochemical Parameters of Polarization Curves of Type 316L-D Weld Metal 91

16. Electrochemical Parameters of Polarization Curves of Type 308L-A Weld Metal 92

17. Electrochemical Parameters of Polarization Curves of Type 308L-D Weld Metal 93

18. Average Values of Electrochemical Parameters for Each Type of Stainless Steel Weld Metal. 105

LIST OF FIGURES

FIGURE		PAGE
1.	Constitution Diagrams of (a) Fe-C, (b) Fe-Cr, and (c) 70% Fe-Ni-Cr	5
2.	Schematic Diagram of the Dissolution Behavior of an Active-Passive Metal	23
3.	Effect of Cathodic Exchange Current Density on the Stability of the Passive State.	25
4.	Comparison of Galvanostatic (Constant Current) and Potentiostatic (Constant Potential) Anodic Polarization Curves of Type 430 Stainless Steel in Normal Sulfuric Acid at 25°C.	27
5.	Experimental Arrangement for Potentiostatic Polarization Measurement	28
6.	Polarization Curves of Iron, Chromium, and Nickel in 1N H_2SO_4 at 25°C	31
7.	Effect of Alloy Chromium Content on Anodic Polarization in 2N H_2SO_4 at 90°C (Nickel Content in Range 8.32 to 9.85%, Balance Iron).	32
8.	Anodic Polarization Curves of an 18-9 Cr-Ni Stainless Steel after Sensitizing for the Indicated Time (Hours) at 650°C.	33

FIGURE PAGE

9. Anodic Polarization of Type 304 Stainless Steel in Deaerated H_2SO_4 (Schematic) (a) Solution Annealed, (b) Sensitized, and (c) Chromium Depleted Zone 35

10. Polarization Curves of Austenite, Delta Ferrite, and Sigma Phase with Potentials for Selective Etching. 37

11. Circuit Diagram of Electronic Potentiostat Used in this Investigation 44

12. Polarization Cell Used in this Investigation . . . 45

13. The Fraction of Ferrite Remaining as Function of Heat Treatment of Types 316 and 316L Weld. 52

14. The Fraction of Ferrite Remaining as Function of Heat Treatment of Types 308 and 308L Weld. 53

15. Effect of Aging Times on the Microstructures of 316-D Welds at 750°C (a) 0 Hours; (b) 2 Hours; (c) 20 Hours; (d) 200 Hours; (e) 2000 Hours; (f) 5000 Hours 56

16. Effect of Temperatures on the Microstructures of Types 308 Welds Aged for 2000 Hours. (a) 308-A, 550°C; (b) 308-D, 550°C (c) 308-A, 650°C; (d) 308-D, 650°C (e) 308-A, 750°C; (f) 308-D, 750°C 57

FIGURE PAGE

17. Effect of Solution Treatment on the Microstructures of Austenitic Stainless Steel Welds. (a) 308L-D, As-Welded; (b) 308L-D; Solution Treated; (c) 316L-D, As-Welded; (d) 316L-D, Solution Treated; (e) 308-A; As-Welded; (f) 308-A, Solution Treated 59

18. Effect of Ferrite Content on the Microstructures of Types 308 Welds Aged at 750°C. (a) 308-A, 0 Hours; (b) 308-D, 0 Hours; (c) 308-A, 200 Hours; (d) 308-D, 200 Hours (e) 308-A, 5000 Hours; (f) 308-D, 5000 Hours . 60

19. Microstructures of Aged Samples. (a) 308L-A and (b) 316L-A, Aged 2000 Hours at 750°C; (c) 308-D and (d) 316-D, Aged 2000 Hours at 750°C; (e) 308L-D and (f) 316L-D, Aged 5000 Hours at 750°C. 61

20. Weight Percent of Precipitates as Function of Heat Treatment for Types 316 and 316L Weld. 67

21. Weight Percent of Precipitates as Function of Heat Treatment for Types 308 and 308L Weld . . 68

22. Standard Band of the Polarization Curves of Stainless Steel 430 Under the Standard Procedures of ASTM G-1/XI. 71

23. Effect of the Scan Rate on the Polarization Curves 73

FIGURE PAGE

24. Effect of Surface Finish on the Polarization Curves 74
25. Effect of Immersion Time of Specimen on the Polarization Curves. 75
26. The Reproducibility of the Anodic Polarization Curves 76
27. Anodic Polarization Curves of Type 316-A Weld. . 78
28. Anodic Polarization Curves of Type 316-D Weld. . 79
29. Anodic Polarization Curves of Type 308-A Weld. . 80
30. Anodic Polarization Curves of Type 308-D Weld. . 81
31. Anodic Polarization Curves of Type 316L-A Weld . 82
32. Anodic Polarization Curves of Type 316L-D Weld . 83
33. Anodic Polarization Curves of Type 308L-A Weld . 84
34. Anodic Polarization Curves of Type 308L-D Weld . 85
35. Typical Anodic Polarization Curve Obtained in this Investigation 94
36. Passive Current Density as a Function of Heat Treatment for Type 316 Welds 96
37. Passive Current Density as a Function of Heat Treatment for Type 316L Welds. 97
38. Passive Current Density as a Function of Heat Treatment for Type 308 Welds 98
39. Passive Current Density as a Function of Heat Treatment for Type 308L Welds. 99

FIGURE PAGE

40. Critical Current Density as a Function of Heat Treatment for Type 316 Welds. 101

41. Critical Current Density as a Function of Heat Treatment for Type 316L Welds 102

42. Critical Current Density as a Function of Heat Treatment for Type 308 Welds. 103

43. Critical Current Density as a Function of Heat Treatment for Type 308L Welds 104

44. Microstructures of Type 308-A Weld Aged 20 Hours at 650°C. (a) Etched 2 Minutes at + 0.02 V. (SHE); (b) Etched 10 Minutes at + 0.10 V. (SHE); (c) Etched 1¼ Minutes at + 1.40 V. (SHE) 108

45. Microstructures of Type 308 Welds Aged Two Hours at 650°C. (a) 308L-A, 10 Minutes at + 0.10 V. (SHE); (b) 308L-A, 1½ Minutes at + 1.40 V. (SHE); (c) 308L-D, 10 Minutes at + 0.10 V. (SHE); (d) 308L-D, 1½ Minutes at + 1.40 V. (SHE). 109

46. Microstructures of Type 308L Welds Aged 2000 Hours at 750°C. (a) 308L-A, 8 Minutes at + 0.10 V. (SHE); (b) 308L-A, 2 Minutes at + 1.40 V. (SHE); (c) 308L-D, 8 Minutes at + 0.10 V. (SHE); (d) 308L-D, 2 Minutes at + 1.40 V. (SHE). 110

FIGURE PAGE

47. Microstructures of Type 308 Welds Aged 20 Hours at 650°C. (a) 308-A, 10 Minutes at + 0.10 V. (SHE); (b) 308-A, 1¼ Minutes at + 1.40 V. (SHE); (c) 308-D, 10 Minutes at + 0.10 V. (SHE); (d) 308-D, 1¼ Minutes at + 1.40 V. (SHE). 111

48. Effect of Etching Solution on the Microstructures of Austenitic Stainless Steel Weld Metal 113

49. Microstructures of Type 308 Welds Aged Two Hours at 750°C. (a) Low Ferrite Weld Etched Two Minutes at + 1.40 Volts (SHE); (b) High Ferrite Weld Etched Two Minutes at + 1.40 Volts (SHE). 114

50. Microstructures of Type 308L Welds Aged Two Hours at 750°C. (a) Low Ferrite Weld Etched Two Minutes at + 1.35 Volts (SHE); (b) High Ferrite Weld Etched Two Minutes at + 1.35 Volts (SHE) 115

CHAPTER I

INTRODUCTION

Recent interest in the high-temperature properties of austenitic stainless steel weld metals is in large measure due to the increased utilization of nuclear power.(1)[1] In such advanced applications the quality of the welds is of paramount importance. Fully austenitic weld metal often exhibits hot cracking and microfissuring, especially when applied under conditions of weld joint restraint.(2) In order to limit the extent of microfissuring in austenitic stainless steel weld metal, it has become common practice to control the chemical composition and welding process so as to provide a small quantity of ferrite phase in the as-deposited weld.(3) However, in the temperature range 500°-900°C, the chromium rich carbides and the intermetallic phases form at austenite grain boundaries and austenite/ferrite interfaces.(4) This causes a local reduction in the matrix chromium content with consequent loss of corrosion resistance and sensitization to intercrystalline attack in service.

---

[1]Superscript numbers in parentheses refer to those entries in the List of References.

The purpose of this research was to investigate the effect of ferrite level on the corrosion resistance of the austenitic stainless steel weld metal both after welding and after aging at elevated temperature, so that the corrosion behavior of real materials in service could be understood.

A potentiostat was employed in this investigation as it enables a variety of practical environmental conditions to be simulated in the laboratory,[5, 6] using only one solution. The sample was immersed in a suitable electrolyte and an external potential applied. The potentiostat maintains this potential constant with reference to a standard electrode and the resultant current flow may be related to the rate of electrochemical reactions on the sample at that potential.[5, 7] By altering the applied potentials, changes in oxidizing or reducing conditions can be experimentally produced. By plotting potential versus current, a "polarization curve" was obtained. Such a curve indicates how a material behaves when exposed to various environments, and in the basis of this, comparison could be made between materials for use in a particular type of environment, i.e., an estimate of the corrosion rate could be made.

The samples selected for this study were four types of austenitic stainless steel weld metal (308, 308L, 316, 316L) deposited by the shielded metal arc welding process.[2, 8] Each type was designed and fabricated to produce two different ferrite levels: 0-2 Ferrite Number (FN) and 6-8 FN. Aging times of up to 5000 hours at 650°C and 750°C were studied. For the metallographic examination standard light microscopy was employed to determine the nucleation sites, distribution, and morphology of the precipitates. X-ray diffraction patterns of the extracted precipitates provided identification of the phases obtained in the microstructure. Anodic polarization curves were obtained for as-welded samples, aged samples, and solution treated samples.

The corrosion potential and current density as function of composition, ferrite content, and heat treatments were then obtained. The correlation between microstructures and polarization curves of various specimens were examined by comparing micrographs and X-ray diffraction patterns of the precipitates. In addition, the controlled potential etching test was used to examine how the mode of attack varies with etching potential.[9-12]

CHAPTER II

LITERATURE REVIEW

In this chapter a brief summary of the significant results of published papers related to the problem to be studied in this research is given.

Ferrite in Austenitic Stainless Steel Weld Metal

Ferrite is the magnetic form of iron and has a body centered cubic space lattice with one atom per lattice site. In iron and in mild or low alloy steels it is both the high temperature form, which develops as the alloy freezes, and the room temperature form.[13] The iron-carbon equilibrium diagram is shown in Figure 1a.

The equilibrium diagram becomes more complex with the addition of alloy elements such as chromium. In Figure 1b it can be seen that chromium levels over about 13 weight percent can eliminate the austenite phase, which is the non-magnetic face centered cubic crystal form of iron. The elements which tend to make the alloy favor the ferrite phase are frequently referred to as "ferritizers" or "ferrite stabilizers."

Other alloying elements such as nickel and carbon tend to cause the alloy to favor the austenite phase and are thus often referred to as "austenitizers" or "austenite stabilizers."

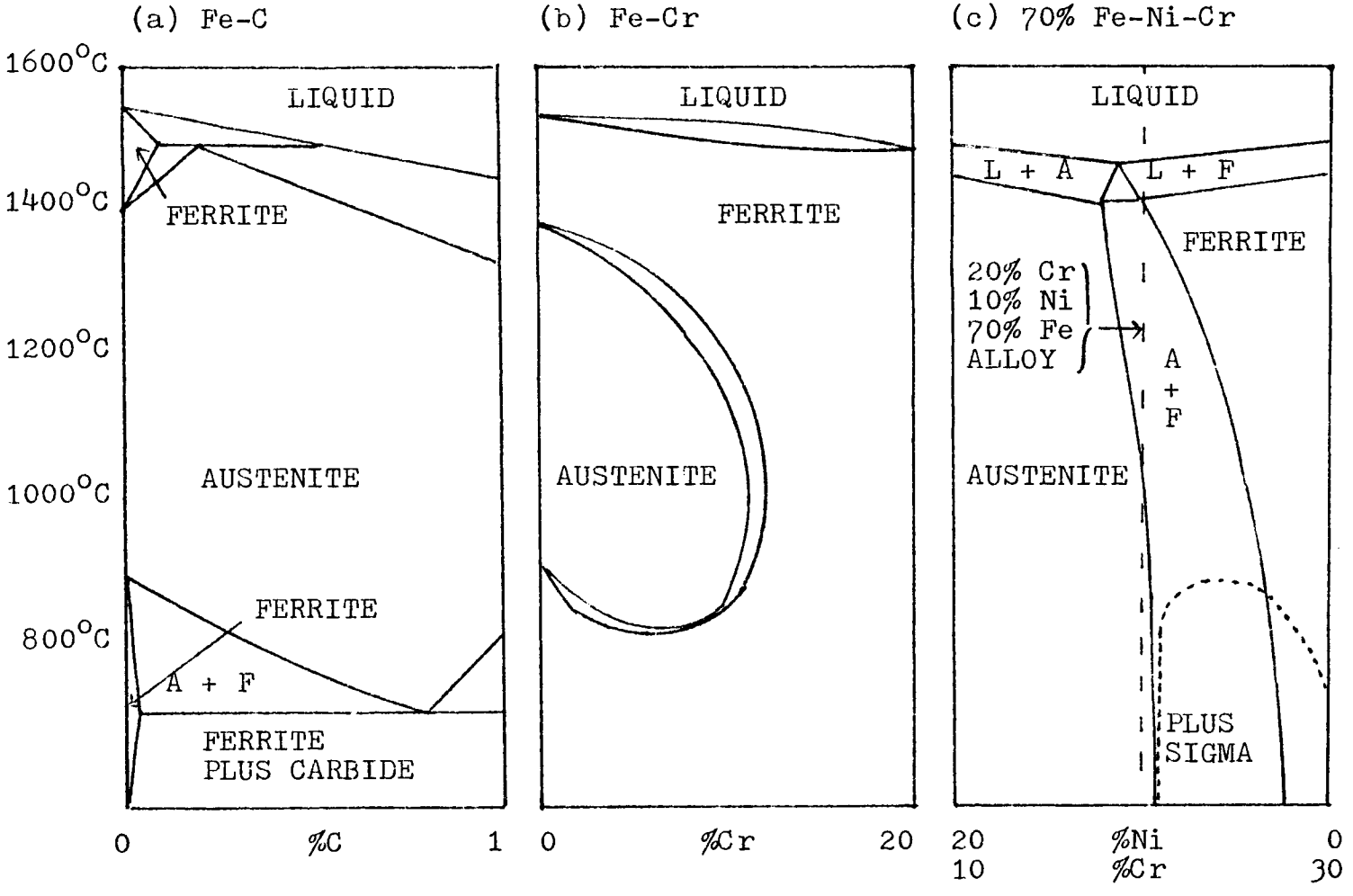


Figure 1. Constitution Diagrams of (a) Fe-C, (b) Fe-Cr, and (c) 70% Fe-Ni-Cr

With rather high levels of both chromium and nickel, for example in a type 308 weld metal typically containing 20% chromium and 10% nickel, a still more complex situation exists, as in the center of the 70% iron-nickel-chromium isopleth of Figure 1c.

The constitution diagrams shown in Figure 1 are useful in understanding the relationship between ferrite and austenite at various temperatures, but, aside from the usual questions of their accuracy, they only represent conditions at or close to equilibrium, i.e., with cooling rates slow enough to allow diffusion of the alloying elements so as to reach the stable condition for the alloy at each temperature. In contrast, cooling rates for welding processes are extremely rapid, and equilibrium is not attained.

Because of the fast freezing of weld metal, its ferrite-austenite structure tends to be very fine, with the ferrite generally occurring in a lacy, interlocked dendritic form. In the opinion of Delong,[13] who has studied ferrite in weld metal extensively, the ferrite distribution becomes continuous at levels beginning somewhere in the range of 4 to 7 volume percent. The dimensions and morphology of the austenite-ferrite substructure within the much larger crystals of weld metal vary depending on the welding process, bead size and shape, and cooling rate.

Thermal treatment at any temperature which allows some reasonable diffusion of the alloying elements can appreciably modify the size, shape, and the quantity of the ferrite.

For example, a conventional stainless steel solution annealing treatment at about 1038°C will often reduce the as-welded ferrite content by 5 volume percent or more.[13, 14] It also tends to spheroidize the remaining ferrite and make it noncontinuous, unless the ferrite level is quit high.

It was recongnized as early as 1938 that the presence of delta ferrite in the room temperature microstructure indicated a reduced fissuring tendency for austenitic stainless weld metals.[3] It was shown that weld metal containing 5 to 10% delta ferrite was more resistant to hot cracking than either fully austenitic or fully ferritic alloys. Recently, Spond[2] and Lundin, Delong and Spond[8] have quantitatively evaluated the ferrite requirements needed to eliminate fissuring in a variety of common austenitic stainless steel weld metals.

In 1967 Hull[3] summarized five theories that had been previously presented to explain the beneficial effect of ferrite in reducing fissuring tendency and then postulated his own theory. He postulated that the beneficial effect of ferrite results from the fact that the austenite:ferrite boundaries have a lower interfacial energy than the austenite:austenite boundaries. The austenite:austenite boundaries are wet by the last traces of liquid whereas the austenite:ferrite boundaries are not wet. Thus the austenite:ferrite boundaries can sustain the small but increasing stresses imposed by the contraction of the alloy as it freezes under restraint untill all the liquid has solidified

and the austenite:austenite boundaries can bear their share of the load.

The magnetic ferrite phase which is desirable in preventing microfissures can be converted to the brittle nonmagnetic sigma phase by aging treatments at temperatures in the range 650-900°C. The details of the ferrite decomposition will be described in a later section, but it is important to realize that the formation of sigma causes low temperature embrittlement of austenitic stainless steel weld metal and also appears to reduce creep rupture ductility.[15] A consideration which should not be overlooked is the fact that sigma has been found to form more rapidly from ferrite than from austenite, and since in many instances weld deposits joining the austenitic alloys consist of both ferrite and austenite, such deposits will sigmatize more rapidly than the base metal being welded. It appears, that electrodes should be so balanced as to contain the least ferrite consistent with the deposition of sound crack-free welds.[16]

Carbide Phases in Austenitic Stainless Steel Weld Metal

The chromium-nickel stainless steels which are primarily used for corrosion resistance generally contain less than 0.02% carbon. Since carbon exhibits a strong affinity for chromium, it tends to precipitate as a chromium bearing carbide at temperatures between 490°C and 870°C. The $M_{23}C_6$

carbide is commonly observed in heat treated stainless steels; it has a fcc crystal structure. In the solution treated and aged samples, $M_{23}C_6$ pricipitates successively on grain boundaries, incoherent twin boundaries, coherent twin boundaries, and finally intragranularly.[17] Non-metallic inclusions act also as nucleation sites with precipitation occurring approximately simultaneously with precipitation on incoherent twin boundaries.

The fact that precipitation occurs preferentially at the grain boundaries has far reaching consequences for these steels, In fact, in extreme cases when precipitation is considerable in alloys containing at least 0.15% carbon, a practically continuous network of carbides may surround each grain. Such a steel, lacking substantial cohesion between grains, is rather brittle.[18] Thus, intergranular precipitation has been believed to be responsible for reducing ductility and toughness in wrought grades, in castings, and in weld deposits. The carbide network also increases the susceptibility to stress-corrosion cracking of the intergranular type. This phenomenon has given a great deal of concern to the manufacturers of aircraft engine manifolds. Corrosion rates are also increased severely by the intergranular precipitation of carbides.[19]

Precipitation of carbides between 490 and 870°C is generally called sensitization. The temperature range in which this precipitation occurs is known as the sensitization range. The carbide network is most detrimental when

it is formed at the lower end of the sensitization range. Higher temperatures and longer holding periods cause agglomeration of the carbides which improves cohesion and resistance to intergranular corrosion. Nevertheless, short periods at the higher temperature may not be sufficient to allow agglomeration. Similar considerations hold true in weld deposits where a lower than normal ductility corresponds to a relatively continuous carbide network and higher ductility with agglomerated carbides in the dendritic structure.[18]

Carbides, in addition to their effects on intergranular corrosion, should also be recognized for their ability to increase tensile strength and reduce elongation. Thus, in severe cases of carbide embrittlement ductility may be lowered as severely as if sigma particles had been formed.

The cubic M_6C carbide was observed in type 316L stainless steel after aging for more than 1500 hours at 650°C.[17] The lattice parameter of this precipitate was determined as $a_o = 10.95 \pm 0.01$ A. The M_6C may be formed by a similar reaction sequence as suggested by Goldschmidt.[20]

$$M_{23}C_6 \xrightarrow[650^{\circ}C/1500\ hr.]{+\ Mo} (Fe,Cr)_{21}Mo_2C_6 \xrightarrow{+\ Mo} M_6C$$

The cubic MC carbide has been reported to be present as TiC in type 321 and titanium modified type 316 stainless steels.[28, 29] The early formation of TiC in those Ti bearing austenitic stainless steels may delay the precipitation of $M_{23}C_6$ and retard its growth.

Sigma Phase in Austenitic Stainless Steel Weld Metal

Sigma phase forms in the temperature range 650°-850°C for most austenitic stainless steels and results in considerable embrittlement at temperatures below 200°C. This phase exhibits a distorted complex tetragonal crystal structure which is highly brittle.

In alloys containing some ferrite dispersed in the austenite matrix, sigma seems to form preferentially from the ferrite. Four major factors are believed to be responsible for this.[18] They are: (1) the crystal structure of ferrite resembles that of sigma more closely than does the structure of austenite, (2) atomic mobility is greater in ferrite than in austenite, (3) the preferential precipitation of carbides in the ferrite sites concentrates the alloying elements locally or distorts the ferrite lattice and thereby facilitates the formation of sigma, and (4) the segregation of chromium in ferrite in preference to austenite tends to produce ferrite areas which are considerably higher in chromium than the average alloy composition would indicate. However, duplex compositions exposed for lengthy periods at precipitation temperatures may also show highly dispersed sigma particles in the austenite matrix.

In wrought annealed type 316 stainless steel the composition of the sigma phase was computed from the results of SEM-X-ray spectrometry. The following results of chemical

composition was obtained by Weiss and Stickler: Cr, 29%; Mo, 11%; Ni, 5%; Fe, 55%.

In type 316, the sigma phase appears sequentially beginning at triple points, then at grain boundaries, after longer times at higher temperatures also at incoherent twin boundaries, and finally intragranularly nucleating on oxide inclusions. The sigma phase dose not nucleate homogeneously in the austenitic matrix, but it always requires a high-energy interface for nucleation.(22,23)

The sigma phase in type 316 steel can form directly from austenite although some work has indicated that sigma tends to nucleate near previously formed carbides. In any event, it is a common observation that carbide precipitation precedes sigma phase formation. This is possibly a result of the highly mobile carbon atoms combining with chromium to form carbide. When the free carbon is exhausted, or nearly so, further diffusion of chromium in the unstable austenite will allow precipitation of the sigma phase. Weigand and Doruk proposed that carbon in solution prevents or retards the sigma formation because sigma cannot dissolve carbon. Another proposal is that the carbon will reduce the chromium level by forming carbide and thus reduces the driving force for sigma formation.(17) If the driving force is still sufficient, sigma will then form. Austenite which is rich in chromium will hold little carbon in solution and, therefore as the austenite becomes more depleted in chromium through sigma formation, the austenite can hold more carbon

in solution, hence the carbides may dissolve.

At temperatures above 400°C, sigma particles nucleate on triple points without any indications of the prior formation of $M_{23}C_6$ particles.[17] After long-time aging sigma phase is present in the form of massive grain boundary particles, or as bulky intragranular particles frequently exhibiting long needle-shaped tails.

The effect of alloying elements on the composition limits for formation of sigma phase in stainless steels are broadly summarized by stating that ferrite stabilizers (Cr, Si, Mo, Al, Ti, and Nb) promote sigma. The austenite stabilizers (C, N, Ni, and Mn) generally retard sigma formation.[17] Trace elements can be important, for example, intragranular nucleation of sigma phase occurred on oxide particles in type 316 stainless steel and trace quantities of boron retarded sigma formation.[25]

In order to provide a semi-quantitative relationship between embrittlement tendencies of weld metals and composition, the concept of "equivalent chromium" content of austenitic stainless steels was introduced by Hull.[26] The chromium equivalent of an element is defined as the % Cr that could be replaced in an alloy by 1% of the given element without altering the embrittling tendencies on aging. The "equivalent chromium" content of austenitic stainless steels with respect to embrittlement on aging at 816°C, is given by the equation:[26]

$$\text{"Equiv. Cr"} = \text{Cr} + 0.31\,\text{Mn} + 1.76\,\text{Mo} + 0.97\,\text{W} + 2.02\,\text{V} + 1.58\,\text{Si} + 2.44\,\text{Ti} + 1.70\,\text{Cb} + 1.22\,\text{Ta} - 0.226\,\text{Ni} - 0.177\,\text{Co}$$

Since this tendency toward embrittlement is associated mainly with the formation of intermetallic phases, the equivalent chromium content may also be used as an indicator of sigma forming tendencies.[26,29]

Little is known about the influence of sigma phase on the corrosion resistance of austenitic stainless steels other than in acid solutions. It has been established that the sigma phase can cause accelerated corrosion in boiling 65% nitric acid and in hot, concentrated (40 to 80%) sulphuric acid solutions.[27] There has been no evidence to indicate that sigma phase is necessarily deleterious to the corrosion resistance in other media. Moreover, there are no records of failures of austenitic steel structures that can be definitely attributed to the presence of sigma phase.[28]

Aging Characteristics of Austenitic Stainless Steel Weld Metal

The effect of microstructure on strength, ductility, impact resistance, and corrosion resistance of austenitic stainless steels has led to many reports relating the microstructural stability of these steels to aging treatments.[14-23, 29, 30] Time, temperature, and composition, as well as thermal and mechanical history, are factors that determine the formation and morphology of the secondary

phases that may occur in austenitic stainless steels.

Several investigations[14, 31-33] have been made on the effects of ferrite in the microstructure on the aging instabilities of various weld metal compositions. The brittle sigma phase formed rapidly from ferrite, and its morphology depended upon whether the welds had been solution annealed before aging. In addition, the formation of carbide networks differed with heat treatment, and the location of the carbides varied with the amount of ferrite. Within the welds, carbides preferred to precipitate within the ferrite at the ferrite-to-austenite boundary rather than at grain boundaries. When the amount of ferrite was small, carbides precipitated along grain boundaries as well as within the ferrite.[31]

The following results are from the investigation of type 316 and 16Cr-8Ni-2Mo filler metal welds by J. E. Scott,[14] who performed one of the most detailed investigations of weld metal microstructural instabilities to date:

(1) The ferrite content of welds which were not solution treated decreases during aging at both 650°C and 750°C; the rate of decrease was greater at 750°C; the ferrite content was reduced to a low level after 200 hours at 750°C and 2000 hours at 650°C.

(2) In as-welded samples $M_{23}C_6$ nucleates first at the ferrite-austenite interfaces and then also on the dislocation substructure. The σ or χ phases nucleate

primarily on the ferrite boundaries, and after long aging times the bulk of the ferrite appears to have transformed to one of these intermetallic phases. It is the replacement of the ferrite by $M_{23}C_6$, σ and/or χ that is primarily responsible for the reduction in ferrite number during aging at 650°C or 750°C.

(3) Cold work increased precipitation rates in the weld metal just as it does in wrought-annealed steels. However, easy nucleating sites at ferrite interfaces meant that σ and χ phases were readily formed in either as-welded or cold-worked samples.

(4) The decrease of ferrite content by solution treatment reduces the rate of nucleation of σ and χ at ferrite-austenite interfaces and, thus, greatly retards the rate of formation of these intermetallic phases.

(5) While solution treatment alone led to a reduction in the rate of precipitation as compared to as-welded material, cold-worked and solution treated material was observed to precipitate somewhat faster than the as-welded material. This increase in precipitation rate was attributed to the austenite grain refinement caused by this treatment and subsequent nucleation at the grain boundaries and triple grain junctions.

Corrosion of Austenitic Stainless Steel Weld Metal

The major use of the steels is in corrosive environments. The term "corrosive environment" can represent anything in which low alloy and carbon steels are expected to corrode or tarnish and thus covers conditions varying from the atmosphere to highly corrosive chemicals such as boiling nitric acid.[21] In steels containing 11% or more chromium, on exposure to an oxidizing atmosphere, an oxide of chromium forms on the surface.[34,35] This is extremely tenacious and the stainless characteristics of these steels depend on the formation and retention of this oxide film under the given environmental conditions.

General aqueous corrosion of stainless steel can occur where the environment is a reducing one or under severe oxidizing conditions.[35] The effect of a reducing environment is to break down the oxide film that already exists. In these circumstances the only practical solution is to use alloys containing elements such as nickel which do not rely on the formation of an oxide film for their corrosion protection. Most industrial corrosive applications are highly oxidizing, however, and if general corrosion of a particular stainless steel occurs under these conditions, then one with a higher chromium content is less likely to corrode; this is illustrated by the choice of steel for containing nitric acid. This is a highly oxidizing medium and therefore the 30% Cr steels are recommended in preference

to the more frequently used 18% Cr steels.

General corrosion can also be a problem where welding is involved. A weld metal of identical composition to a wrought material may show less corrosion resistance. This is probably a result of the heterogeneity of chemical composition associated with the solidification structure of the weld, but the exact cause is not known. However, if preferential corrosion of the weld metal should occur then a change to an "overmatching" weld metal composition, i.e., one containing a higher alloy content, particularly chromium, often reduces the corrosion problem. General corrosion of the stainless steels can therefore be controlled by choice of the right material composition and is not usually considered a serious problem. Most of the serious problems that arise in the corrosion application of stainless steels occur as a result of a local breakdown of corrosion resistance. Such a breakdown can occur under certain circumstances at the grain boundaries of the steel. This is termed intergranular corrosion[36-40] and is commonly encountered in welded austenitic stainless steel vessels in contact with corrosive media.

Stainless steels for corrosive environments are generally supplied in the fully annealed condition, i.e., carbides and other phases are absent from the microstructure having been taken into solution during the annealing treatment and retained in solution by rapid cooling. However,

if the material should subsequently be heated in the temperature range 550°C to 850°C and if a sufficient supersaturation of carbon exists then chromium carbide precipitates at the grain boundaries. This precipitation of a high Cr phase in a matrix of lower chromium content results in a region around the precipitate that is depleted in chromium.[19] It is this depleted region that is attacked by some corrosive media resulting in disintegration of the steel into individual grains. Such a phenomenon occurs near welds in stainless steels containing fairly high carbon contents; it is commonly referred to as "weld decay". A certain distance from the weld is a region which has been reheated to temperatures within the "sensitizing" range. In this region chromium carbide precipitates at grain boundaries resulting in a susceptibility to intercrystalline corrosion. Closer to the weld the temperature reached is sufficiently high to retain the carbon in solution and further away the temperature reached is too low to induce precipitation. Thus a narrow band of susceptible material is created on either side of the weld at a distance from it.[34]

There are a number of ways of ensuring that a stainless steel does not go into service in a condition liable to intergranular corrosion:[21, 34]

(1) The carbon content may be sufficiently low to be below the minimum necessary for precipitation to occur.

(2) The steel may be given a 1050°C anneal followed by rapid cooling.

(3) The steel may be heated in the sensitizing range for a sufficienly long time to allow the chromium depleted regions around the carbides to dissapear as result of the diffusion of chromium atoms from the matrix.

(4) The steel may contain either niobium or titanium. These are both strong carbide forming elements and form carbide in preference to chromium over the greater part of the chromium carbide precipitation range.

Of these four methods (1) and (4) are the most attractive in practical terms as heat treatment is not usually necessary after welding. On economic terms, the stabilized steels are more attractive than the extra low carbon variety, but in terms of the protection offered against the possibility of intergranular corrosion, the extra low carbon varieties have advantages. A stabilizing treatment prior to welding is inadequate, however, as the region adjacent to the weld has been heated to a high temperature taking the stabilizing carbides back into solution. Subsequent heat treatment in the appropriate temperature range can result in chromium carbide precipitation and a narrow region in the heat affected zone of the weld which is susceptible to intergranular corrosion. This can result in a phenomenon known as "knife-line" attack which differs from "weld decay".

The foregoing remarks all apply to wrought material particularly of the fully austenitic type. The same principles invoked apply to weld metal. Generally speaking therefore a stabilized or low carbon weld metal is advisable for most applications particularly where more than one pass of weld metal is involved.

In contrast to most wrought materials, weld metals are likely to contain significant amounts (5-15%) of ferrite. The presence of ferrite in austenitic steels reduces sensitivity to intergranular corrosion.[21, 40] If the material contains ferrite, carbide precipitation can occur along the austenite/ferrite interfaces as well as at austenite grain boundaries. As the number of precipitation sites is increased the density of carbide precipitation is reduced, and less severe chromium depletion occurs, Furthermore ferrite is a chromium-rich phase normally present as isolated islands. Thus, carbide precipitation may take place preferentially at ferrite/austenite interfaces over other sites in the material, but the consequent chromium depletion does not cause a continuous path through the material. For this reason the presence of ferrite in the steel does offer some resistance to intergranular corrosion.[21, 40]

Electrochemical Behavior of Active-Passive Metals

From an electrochemical viewpoint,[41-43] the phenomenon of passivity may be described by the schematic, anodic

polarization curve shown in Figure 2.[7] A logarithmic scale permits the presentation of a wide range of current densities. As the potential is made increasingly more noble, the dissolution rate of a typical active-passive metal passes through a maximum and then remains essentially independent of potential. At very noble potentials, dissolution rate again increases. As shown in Figure 2, the behavior of an active-passive metal can be divided into three different regions; active, passive, and transpassive. Almost all metals and alloys which demonstrate active-passive behavior can be characterized by a S-shaped curve such as Figure 2. The most important parameters describing the behavior of an active-passive metal are the potential and current corresponding to the current maximum. Here, these are termed the primary passive potential, E_{pp}, and critical anodic current density, I_{crit}.[5]

A polarization curve such as Figure 2 provides a unique means for describing and predicting the dissolution or corrosion behavior of a metal which demonstrates an active-passive transition. For example, it is possible to determine: (1) The passive potential region; (2) The passive corrosion rates; (3) The relative stability of the passive state; and (4) The conditions necessary for achieving passivity. Furthermore, it is possible to compare the behavior of two different alloys on the basis of these properties.

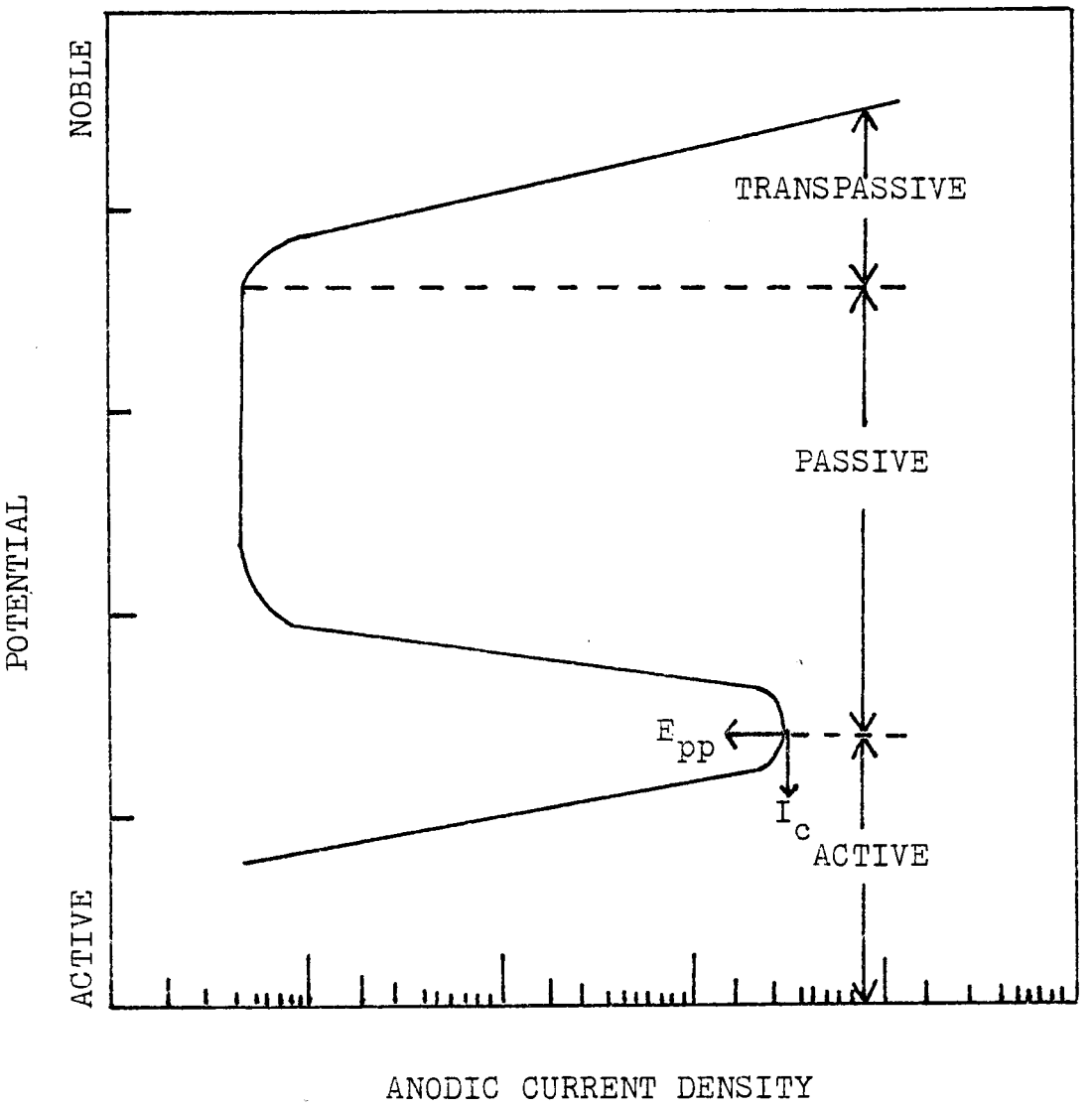


Figure 2. Schematic Diagram of the Dissolution Behavior of an Active-Passive Metal

When a metal is exposed to a corrosive media, two processes occur on its surface: oxidation and reduction. For a metal which demonstrates an active-passive transition, this can be illustrated by superimposing a cathodic reduction polarization curve. Figure 3 illustrates three different conditions which can arise when a cathodic process is superimposed. The three curves represent different activation control reduction processes with different exchange current densities. For case 1 there is only one stable corrosion potential and current at A. That is, at point A, the condition that the total rate of oxidation equals the total rate of reduction is fullfied. In case 2, there are three points (B, C, and D) where the rate equality criteria is fullfilled. However point C does not represent a stable state. Hence, only points B and D are stable. There is only one stable point, E, for case 3.

The above examples indicate there are three distinct possibilities: (1) The metal is stable only in the active state, (2) The metal is stable in either the active or passive states, or (3) Only the passive state is stable. From the standpoint of practical corrosion resistance, case 3 is desirable, since a metal-corrosive system illustrating these characteristics will spontaneously passivate.

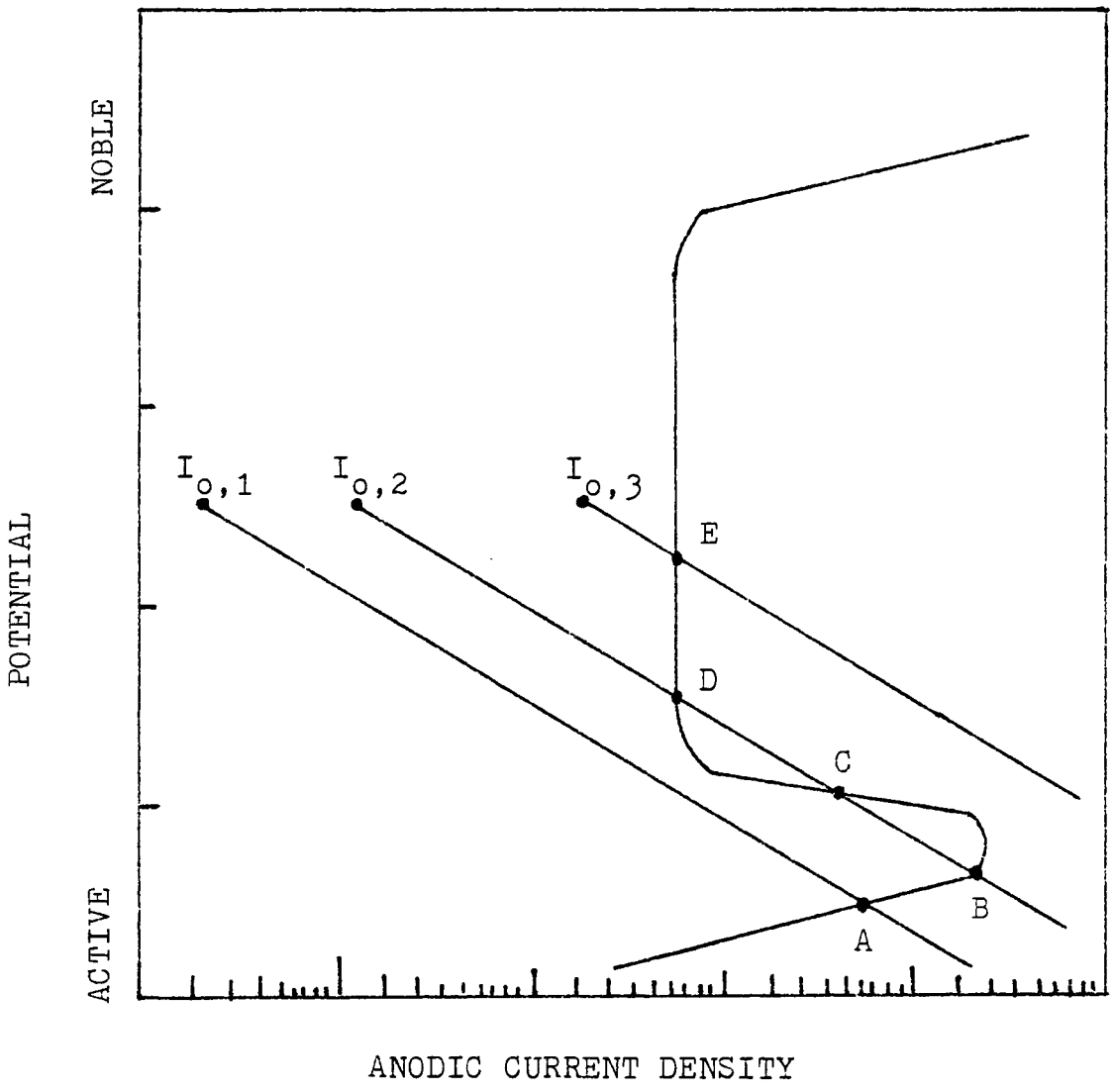


Figure 3. Effect of Cahtodic Exchange Current Density on The Stability of The Passive State

Method for Determining Applied Current-Potential Curves

There are two methods commonly used for determining applied current-potential curve.[5] In the first method, called the galvanostatic method, the applied current is held constant and the value of the electrode potential is measured relative to some standard potentials. The disadvantage in using the galvanostatic technique is that the active-passive transition in metals cannot be examined in detail. When the critical anodic current density is reached, the potential changes spontaneously to the transpassive region, since this is the next stable potential.[5] This is shown in Figure 4.

In the second method called the potentiostatic method, the potential of the electrode is held constant and the value of the resulting current is measured. A potentiostat functions by monitoring the potential between the working electrode and auxiliary electrode to maintain this potential constant. Thus, a potentiostat is a three-terminal device; there are terminals for the working, auxiliary, and reference electrodes. Figure 5 shows the experimental arrangement for potentiostatic polarization measurement. In this diagram, [44] a potentiostat with an external power supply is connected to the appropriate electrodes. An ammeter is placed in the lead to the auxiliary electrode and a short, low resistance lead is used to connect the test specimen to the potentiostat. The potential of the

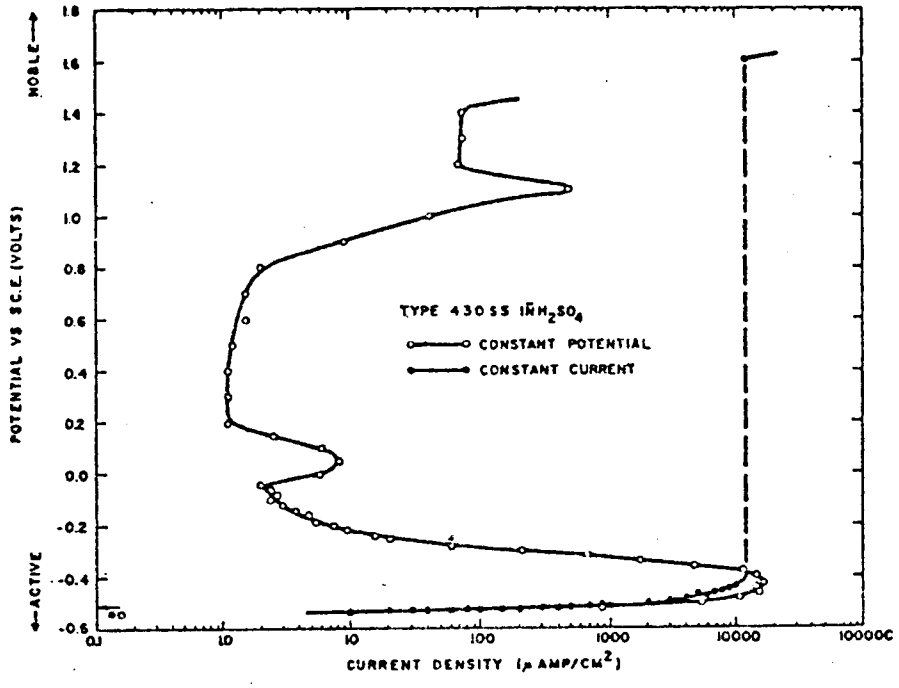


Figure 4. Comparison of Galvanostatic (Constant Current) and Potentiostatic (Constant Potential) Anodic Polarization Curves of Type 430 Stainless Steel in Normal Sulfuric Acid at 25°C

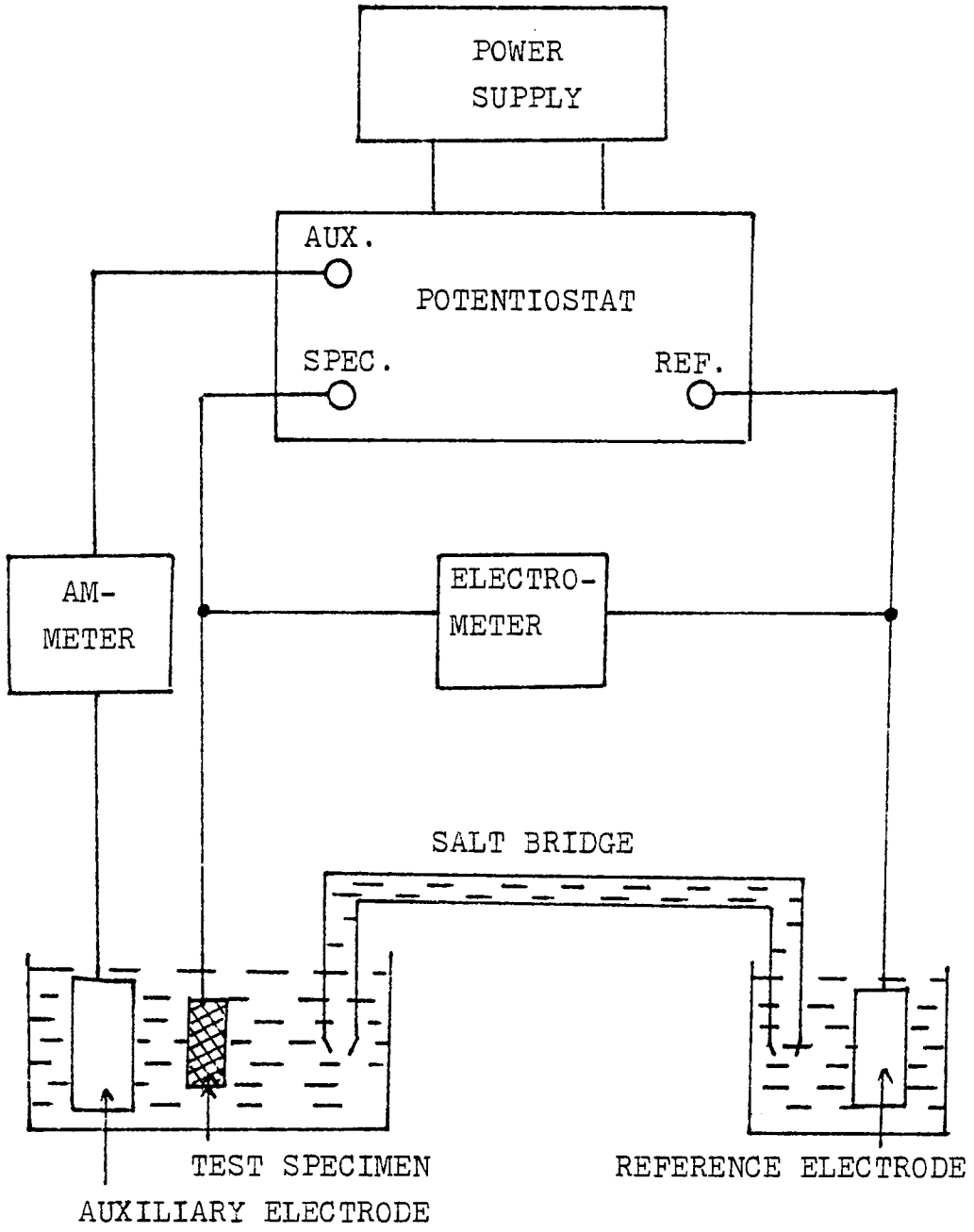


Figure 5. Experimental Arrangement for Potentiostatic Polarization Measurement

test specimen is measured by an electometer.

There are two general ways of conducting potentiostatic polarization measurements; manually and automatically. In the manual method, potential is increased in a stepwise fashion and current is measured after a predetermined time at each potential setting. Automatic potentiostatic polarization is accomplished by continuously varying the potential while simultaneously recording current.

Potentiostatic anodic polarization measurements of metals and alloys possessing active-passive transitions require several special precautions. Most active-passive metals demonstrate strongly time-dependent polarization behavior and therefore, it is necessary to control time parameters for maximum accuracy and reproducibility.[5,45,46] Electrodes should be pre-exposed to the electrolyte solution for constant time periods and potential step size, traverse rate and time at each potential setting must be carefully and reproducibly controlled. It is recommended that polarization be conducted in the anodic or positive direction starting at the mixed or corrosion potential. Cathodic pretreatment of the electrode is not recommended as it tends to distort the polarization curve shape.[47,48] Oxygen and other oxidizers should be excluded from the electrolyte as their presence complicates the analysis of the resulting polarization curves.[5]

Alloy Evaluation by Using Potentiostatic Anodic Polarization Curve

Many commercial metals and alloys depend on the achievement of passivity for their corrosion resistance, and there are two general ways for achieving passivity.[34] First, the environment may be made sufficiently oxidizing to cause spontaneous passivation, or in special instances, galvanic coupling can be used to achieve passivity as in the case of titanium. Both methods depend on establishing potentials in the passive range. One of the most common oxidizers encountered in practice is dissolved oxygen. Oxygen is very slightly soluble in water and aqueous solutions, and, as result, its reduction is usually under diffusion control. In air-saturated non-agitated solution, the limiting diffusion current for oxygen reduction is approximately 100 $\mu a/cm^2$. If an active-passive metal is exposed to an aerated corrosive medium, it spontaneously passivates if its critical anodic current density is equal to or less than approximately 100 $\mu a/cm^2$. Thus, if the anodic dissolution behavior of a metal or alloy is known, it is possible to predict whether or not it will passivate in an aerated solution.

To illustrate some of these concepts,[34] consider the anodic polarization behavior of several commercial alloys shown in Figures 6 to 8.[49-51] These figures represent experimental data determined in dilute sulfuric acid. The

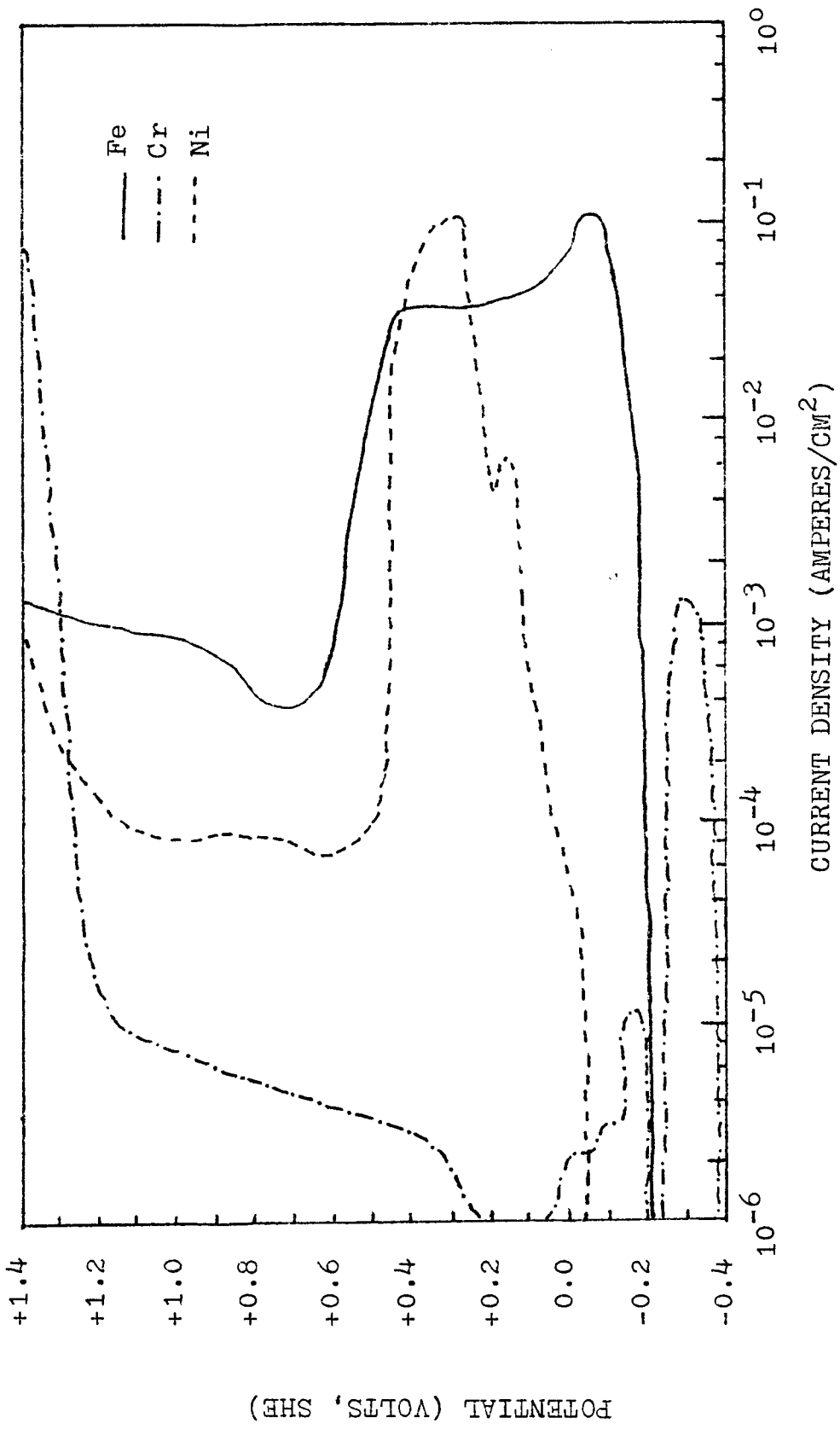


Figure 6. Polarization Curves of Iron, Chromium, and Nickel in 1N H_2SO_4 at 25°C

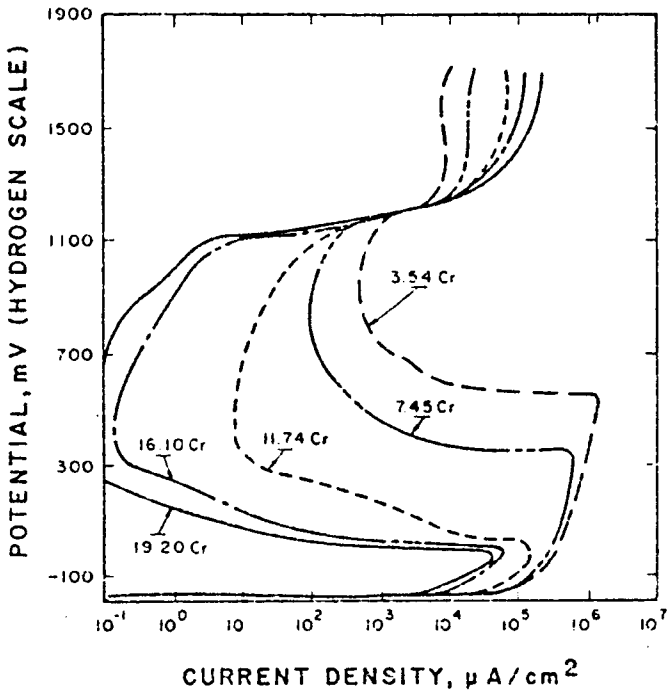


FIgure 7. Effect of Alloy Chromium Content on Anodic Polarization in 2N H_2SO_4 at 90°C (Nickel Content in Range 8.32 to 9.85%, Balance Iron)

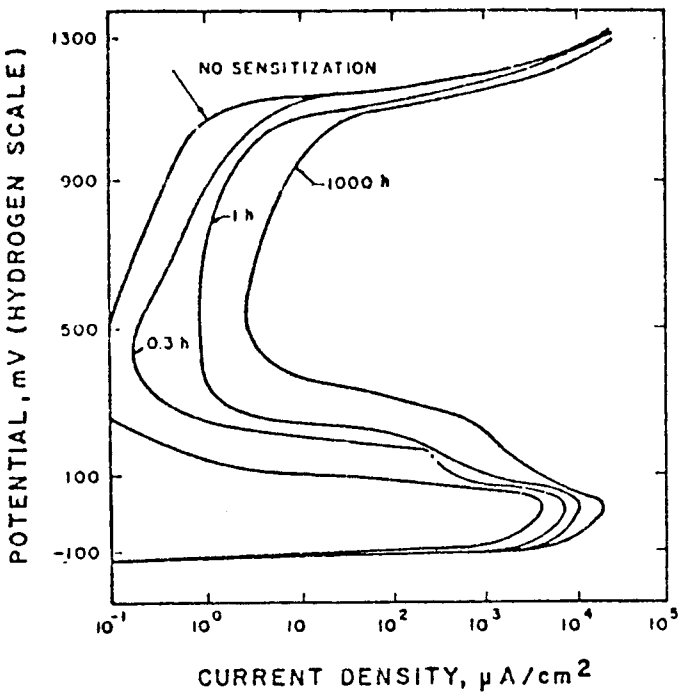


Figure 8. Anodic Polarization Curves of an 18-9 Cr-Ni Stainless Steel After Sensitizing for the Indicated Time (Hours) at 650°C

anodic polarization curves of iron, chromium, and nickel are shown in Figure 6. Because the iron has a very large critical anodic current density and relatively noble primary passive potential, it is difficult to passivate in acid solution. It is obvious that a limiting oxygen diffusion current of 100μa/cm^2 is insufficient to cause its passivation. The addition of chromium and nickel to iron markedly increases the ease of passivation, as is indicated in Figure 7.

Stainless steels which are susceptible to intergranular attack show anodic polarization behavior different to that of resistant material. Several examples of this have been reported, and typical behavior for austenitic stainless steels is shown in Figure 8. The polarization curve of the specimens sensitive to intergranular corrosion is considered to be the sum of the curve of the intergranular zone and that of the grain with current contributions weighted proportional to the respective exposed areas. This is shown in Figure 9. If the anodic polarization curve of the grain is assumed to be the same as that of the solution treated steel (curve a) and the polarization curve of the grain boundary (low chromium) is represented by curve c, then the polarization curve of a sensitized specimen should be curve b. This is consistent with the anodic polarization curves in Figure 7.

Anodic polarization curves can be useful in indicating which potential regions are most likely to cause attack.

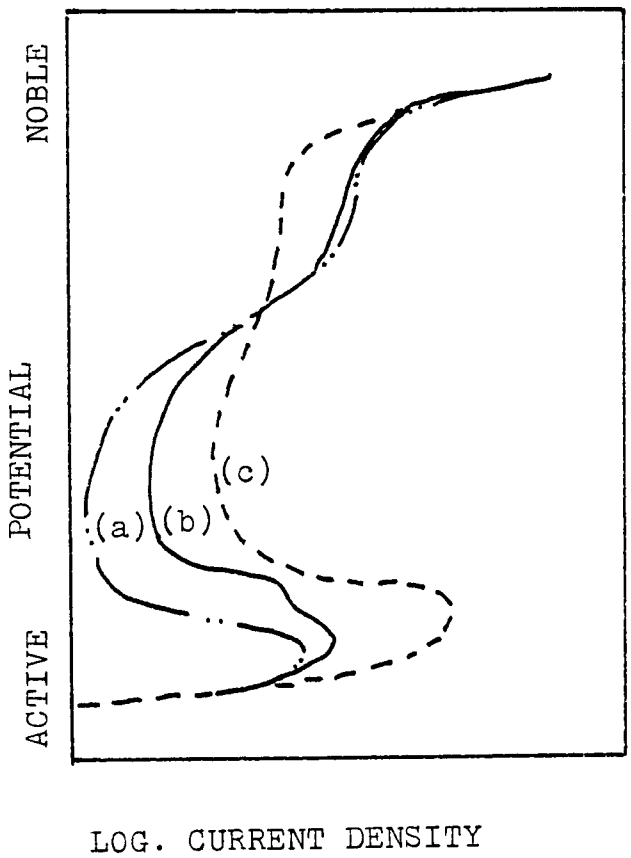


Figure 9. Anodic Polarization of Type 304 Stainless Steel in Deaerated H_2SO_4 (Schematic) (a) Solution Annealed, (b) Sensitized, and (c) Chromium Depleted Zone

In an alloy containing two or more phases, each phase has a certain characteristic polarization curve and by comparing these, it is possible to choose a potential at which one particular phase is preferentially attacked. This is the basic idea for the controlled potential etching test.[9,10,12]

There are several significant advantages in the controlled potential technique compared with conventional chemical corrosion tests;[9] these include the precise preselection of reproducible, stable potentials that are uninfluenced by environmental changes, and the instantaneous, accurate measurement of corrosion rates.

Controlled potential etching experiments on 18-8 stainless steels were carried out in a 5% sulphuric acid solution containing 0.1 g/l ammonium thiocyannate by Cihal and Prazak.[10] Figure 10 shows the polarization curves of austenite, delta ferrite, and sigma phase of 18-8 stainless steels. As the chromium content is raised, the active region and the primary passive potential becomes more negative. Thus by comparing the polarization curves for austenite, delta ferrite, and sigma, we can choose an etching potential so high that virtually only one phase is selectively attacked.

Edeleanu [12] distinguished delta ferrite and sigma phase from austenite by etching in 20% H_2SO_4 using the potentiostat, and the potentials he used are compared with of Cihal and Prazak in Table 1.

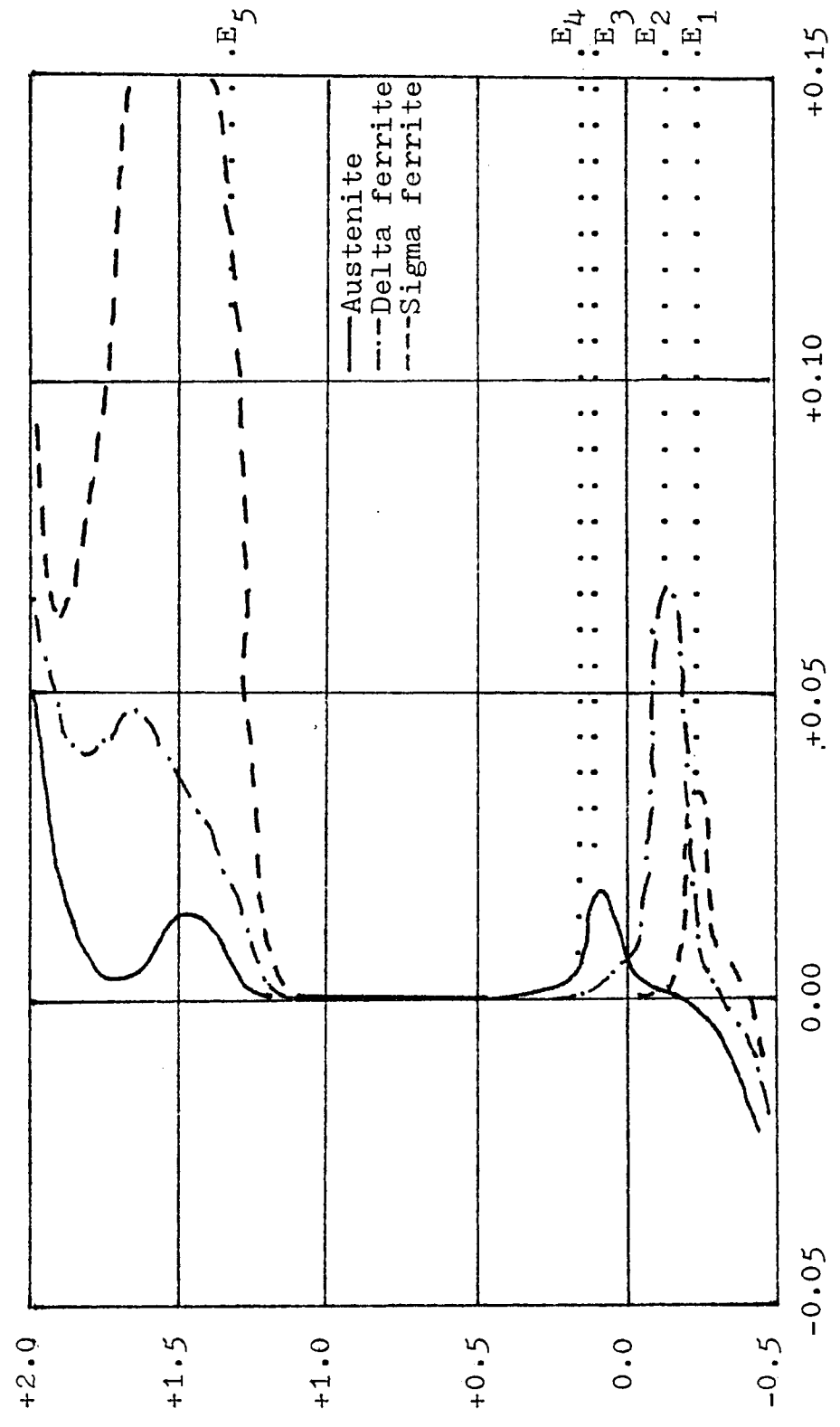


Figure 10. Polarization Curves of Austenite, Delta Ferrite, and Sigma Phase with Potentials for Selective Etching

Table 1. Potentials for Selective Etching of Phases in 18-8 Stainless Steels

Solution	20% H_2SO_4*		5% H_2SO_4 + 0.1 g/l NH_4SCN**		Potential from Figure 9
	Etching Potential (SHE)	Etching Time	Etching Potential (SHE)	Etching Time	
Delta ferrite	-0.20 V.	1 hr.	-0.10 V. -0.15 V.	60-250 sec.	E_1
Sigma phase	-----	-----	-0.15 V. -0.20 V.	60-150 sec.	E_2
Austenite	+0.10 V.	1 hr.	+0.10 V. +0.05 V.	20-120 sec.	E_3
Austenite Grain Boundaries	-----	-----	+0.15 V.	1-3 min.	E_4
Delat ferrite	+1.30 V.	3-5 min.	-----	-----	E_5

* Etching solution used by Edeleanu.
** Etching solution used by Cihal and Prazak.

CHAPTER III

EXPERIMENTAL PROCEDURES

In this chapter a discussion of the experimental procedures used in the course of this investigation is presented.

Alloy Preparation

The alloys selected for study were four types of austenitic stainless steel weld metals (308, 308L, 316, 316L) which had been used to investigate the ferrite-fissuring relationship by Dr. C. D. Lundin and D. F. Spond at The University of Tennessee.[2,6] The weld metals were deposited by the shielded metal arc welding process with 1/8" diameter AC-DC electrodes. The samples were produced as weld metal pads (1/4 inch thick) deposited on 1/2 inch thick 304 or 304L base plates. These weld metals were designed and fabricated to produce two different ferrite levels: 0-2 FN and 6-8 FN.

The chemical analyses and measured Ferrite Numbers of the as-deposited weld metal are presented in Table 2.[2] Ferrite numbers were obtained from the weld pad surfaces by Magne Gage.

Heat Treatment

The unbent portions of the samples previously used were sectioned into 3/8" x 3/8" x 3/4" chunks and then heat treated as follows:

Table 2. Chemical Analyses and Ferrite Numbers of As-deposited Weld Pads[2]

Weld Metal	Elements									Ferrite Number
	C	Mn	Si	P	S	Cr	Ni	Mo	N	
308-A	0.052	1.64	0.35	---	---	18.18	10.95	---	---	0.2
308-D	0.060	1.65	0.37	---	---	19.30	9.89	---	---	6.8
308L-A	0.020	1.62	0.38	---	---	18.40	10.80	---	---	0.5
308L-D	0.022	1.66	0.41	---	---	19.09	10.32	---	---	6.0
316-A	0.065	1.92	0.46	0.016	0.008	17.79	12.30	2.22	0.047	0.3
316-D	0.069	1.96	0.52	0.014	0.010	19.38	11.78	2.12	0.047	5.8
316L-A	0.035	1.85	0.40	0.008	0.015	17.88	13.07	2.15	0.047	0.2
316L-D	0.037	1.87	0.46	0.015	0.010	18.60	11.64	2.12	0.047	5.7

(1) As-welded.

(2) As-welded, then aged at 650°C for 2 hours, 20 hours, 200 hours, 2000 hours, and 5000 hours.

(3) As-welded, then aged at 750°C for 2 hours, 20 hours, 200 hours, 2000 hours, and 5000 hours.

(4) As-welded, then homogenized at 1100°C for one hour.

Short-time heat treatments were carried out in an argon purged furnace. For long-time heat treatments, the specimens were sealed in evacuated Inconel tubes. Furnace controllers utilized platinum-platinum 13% rhodium thermocouples to maintain set temperatures to within 1% of the operating temperature. After each heat treatment, the specimens were water quenched.

Preparation of Specimens

The corners of the specimens were rounded off and then the specimens were ground on metallographic papers to a 3/0 finish, degreased in hot benzene, and then mounted in bakelite. The absence of crevices between the specimen and the bakelite was carefully controlled when the metal surface was microscopically observed before the last grinding. The specimens were threaded from the back side with a 3/8" hole to provide electrical contact. The mounted samples were then re-ground to a 3/0 finish and polished to a metallographic finish using 1.0 and 0.06 micron Al_2O_3 abrasives and a high-grade microcloth.

Ferrite Determination

Ferrite Number (FN) readings were made on all metallographic specimens using the Aminco-Brenner Magne Gage. The instrument was calibrated by Calibration Procedure D with magnet 3.[55] In order to minimize the error due to weldment inhomogeniety, the average value of three determinations taken from different locations along the surface of the weld metal was recorded.

Optical Metallography

The specimens were re-ground and re-polished after taking FN readings. The specimens were then electrically etched with a stainless steel cathode at 9 volts for approximately 30 to 60 seconds. The etching solution consists of 25 grams CrO_3, 133 ml glacial acetic acid, and 7 ml distilled water. Then, a selected area was photographed at 200 X magnification using type 55 Polaroid film.

After all photomicrographs were taken, the specimens were carefully ground and polished to a 600 grit finish, washed in soap and water, and dried in methanol.

X-Ray Diffraction

Bulk extraction of the precipitates for X-ray diffraction analysis was carried out electrolytically in a 10% HCl in methanol electroyte with a current density of 200-300 mA/cm^2. The weight fraction of precipitate was determined by weighing the bulk sample before and after partial

dissolution and also weighing the extracted and dried residues. X-ray patterns of the extracted powder were made using a Debye-Scherrer camera. The X-ray source was Cu $K\alpha$ radiation with a nickel filter. Qualitative phase identification was carried out by comparison of the diffraction pattern of the residue with standard patterns from the phases expected to occur in austenitic stainless steels.

Potentiostatic Polarization Curve

The potentiostat used in this investigation was characterized by an input impedence of 100 megaohms, a maximum output current of $\pm$100,000 microamperes and an output voltage of $\pm$2.0 volts. In addition the instrument was equipped with a differential amplifier and logarithmic converter which permitted continuous plotting of polarization curves through five decades of log current. Figure 11 shows a circuit diagram of the potentiostat as used in this investigation. The potential sweep rate was set at 2.5 volts/hr. to establish quasi-steady-state conditions.

In order to use the metallographic samples as the test specimens, a conventional polarization cell was modified as shown in Figure 12. A transparent, thin walled hollow cylindrical PVC T-joint with three PVC caps was used as the polarization cell. The dimensions of this cell are also shown in Figure 12.

The desired gas is admitted continucusly through the gas inlet tube and dispersed throughout the solution by

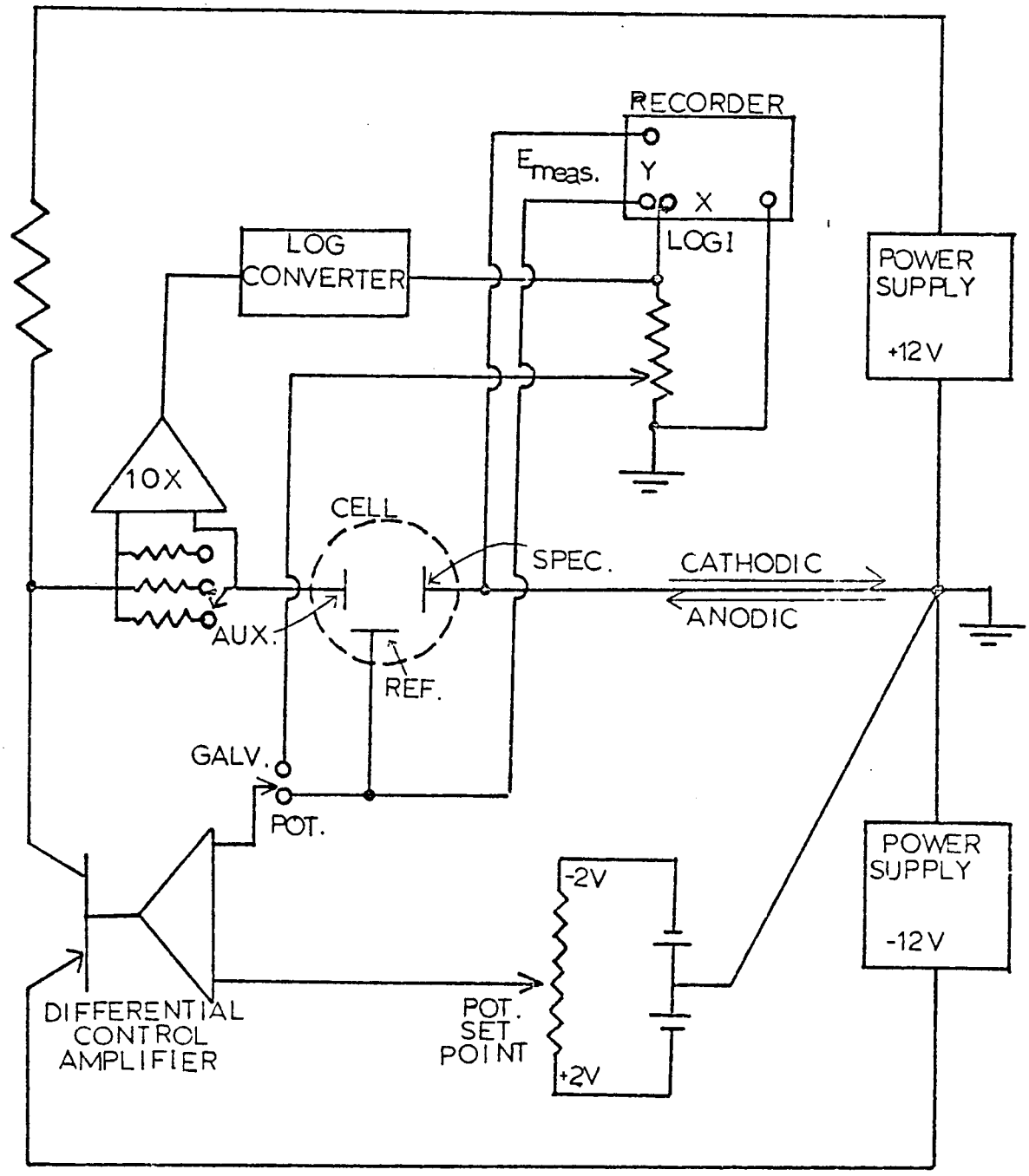


Figure 11. Circuit Diagram of Electronic Potentiostat Used in this Investigation

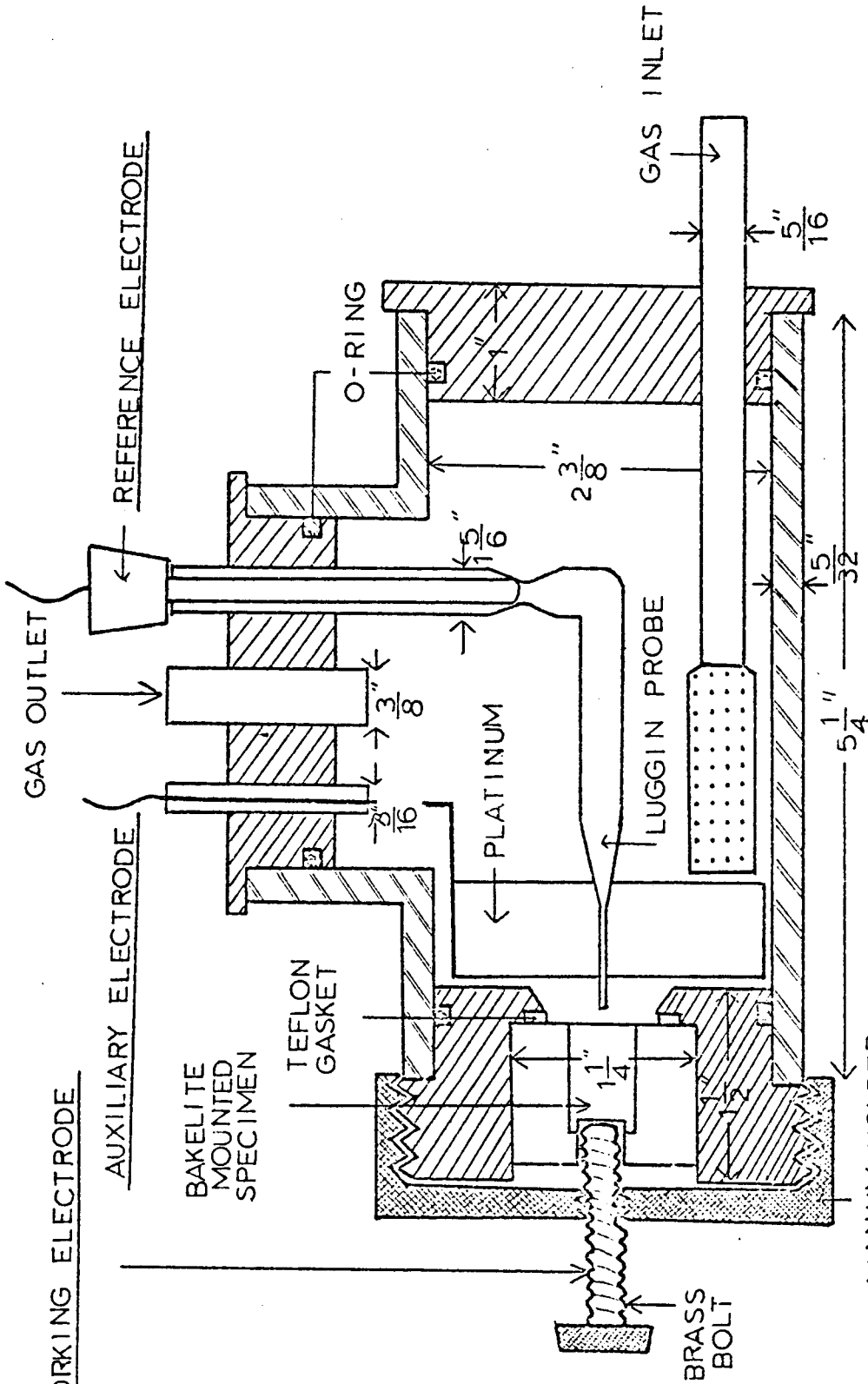


Figure 12. Polarization Cell Used in this Investigation

means of the fritted cylinder. The gas outlet tube, auxiliary electrode are all inserted into the top cap.

The working electrode holder assembly was designed for the metallographic specimens. A circular Teflon gasket co compressed against the specimen by the PVC cap cover provides a leakproof seal. The threaded brass bolt is tightened with sufficient torque to compress the specimen against the Teflon gasket.

A 3/4" x 2" platinum strip spot welded onto a silver wire is used as an auxiliary electrode. A silver-silver chloride electrode is used as a reference electrode in this investigation. The reference electrode was checked with respect to a standard saturated calomel electrode before using in the polarization cell.

After cleaning the polarization cell with acetone and with distilled water, the cell was filled with 1N H_2SO_4 solution. Argon gas was bubbled vigorously through the cell for approximately one hour. The carefully ground and polished specimen was then cleaned and screwed onto the specimen holder assembly. The flow of argon was reduced to less than one cubic foot per hour. The specimen was left in this position for at least one hour to insure that a stable corrosion potential was reached.

The potentiostat was then set at the open-circuit specimen corrosion potential and connected to the electrode leads of the polarization cell. The X-Y recorder was then

synchronized so that the current value coincided with that on the potentiostat, and the potentiostatic polarization curve was recorded by scanning at a preselected rate until a potential of +1.0 volt with respect to the reference electrode was reached.

Controlled Potential Corrosion Test

In order to selectively etch the specimen and detect the minority phase in the etched specimen, a controlled potential etching test was run. The experiments were carried out by presetting the required potential with a suitable probe, and placing the sample in the solution with that potential already applied.

The etching solution used for this test was 5% by volume aqueous sulphuric acid containing 0.1 g/l ammonium thiocyanate.[6, 10] The ammonium thiocyanate addition served to increase the observed current density by a factor of about ten.[6] Samples aged under various conditions were etched at different potentials to determine the nature of the attack corresponding to any particular potential, and in particular cases the range over which intercrystalline attack occurred.

The etching potentials varied from +0.02 volts to +1.40 volts (SHE) depending on the anodic polarization behavior of the specimen. The etching times varied from one minute to ten minutes depending on the current densities at that potential.

After etching, the specimens were washed in soap and water, and dried in methanol. The specimens were then put in a desiccator to prevent oxidation.

The microstructures of the etched specimens were examined by optical microscopy and by scanning electron microscopy (AMR model 900). Energy dispersive X-ray analysis was also applied in order to identify some of the etched particles.

CHAPTER IV

RESULTS AND DISCUSSION

Ferrite Contents and Microstructures of Aged Samples

Throughout this section of results, the following symbols are used; "A" denotes the low ferrite level (0-2 FN) alloys; "D" denotes the high ferrite level (6-8 FN) alloys.

The ferrite number of as-welded, solution treated, and aged samples were measured by using an Aminco-Brenner Magne Gage as previously described.[55] The measured ferrite number before and after heat treatments of high ferrite level metals are shown in Tables 3 and 4. Since the readings of the ferrite number varied from place to place in a weld pad, it is more precise to calculate the fraction of ferrite remaining. This is shown in Tables 3 and 4 and is plotted in Figures 13 and 14.

The influence of temperature on the rate and extent of transformation after various times is clearly evident. The rate of transformation of ferrite into other phases is much higher at 750°C than at 650°C. For example, the fraction of ferrite remaining in type 316 is over 50% after two hours aging at 650°C, while a similar treatment at 750°C reduced the fraction of ferrite remaining to 12%. When the material was solution treated at 1100°C for one hour and water quenched, the ferrite content fell from an initial value of 6-8 to a final of zero.

Table 3. Ferrite Number Readings Before and After Heat Treatments of Types 316L-D and 316-D Welds

Heat Treatment	316L-D			316-D		
	Before	After	Fraction	Before	After	Fraction
As-welded	8.0	8.0	1.00	8.0	8.0	1.00
650°C/2 hrs.	7.5	5.8	0.77	7.6	4.1	0.54
650°C/20 hrs.	7.2	3.1	0.43	7.8	2.5	0.32
650°C/200 hrs.	9.9	0.9	0.09	5.4	0.6	0.11
650°C/2000 hrs.	9.5	0.0	0.00	7.2	0.0	0.00
650°C/5000 hrs.	9.3	0.0	0.00	7.6	0.0	0.00
750°C/2 hrs.	7.3	1.1	0.15	6.6	0.8	0.12
750°C/20 hrs.	7.5	0.3	0.04	5.5	0.1	0.02
750°C/200 hrs.	8.2	0.0	0.00	6.6	0.0	0.00
750°C/2000 hrs.	9.2	0.0	0.00	7.6	0.0	0.00
750°C/5000 hrs.	8.7	0.0	0.00	6.8	0.0	0.00
1100°C/1 hr.	8.6	0.0	0.00	8.3	0.0	0.00

Table 4. Ferrite Number Readings Before and After Heat Treatments of Types 308L-D and 308-D Welds

Heat Treatment	308L-D			308-D		
	Before	After	Fraction	Before	After	Fraction
As-welded	7.6	7.6	1.00	8.9	8.9	1.00
650°C/2 hrs.	7.0	4.0	0.57	7.6	4.2	0.55
650°C/20 hrs.	7.0	3.0	0.43	8.2	4.1	0.50
650°C/200 hrs.	7.0	2.0	0.29	8.1	2.2	0.27
650°C/2000 hrs.	5.2	0.3	0.06	8.8	0.3	0.03
650°C/5000 hrs.	5.7	0.0	0.00	7.6	0.0	0.00
750°C/2 hrs.	7.0	3.2	0.45	7.4	3.0	0.40
750°C/20 hrs.	7.5	1.4	0.19	6.6	1.2	0.18
750°C/200 hrs.	4.6	0.8	0.17	8.1	0.7	0.09
750°C/2000 hrs.	6.4	0.1	0.02	9.1	0.1	0.01
750°C/5000 hrs.	5.6	0.0	0.00	8.6	0.0	0.00
1100°C/1 hr.	7.2	0.0	0.00	8.3	0.0	0.00

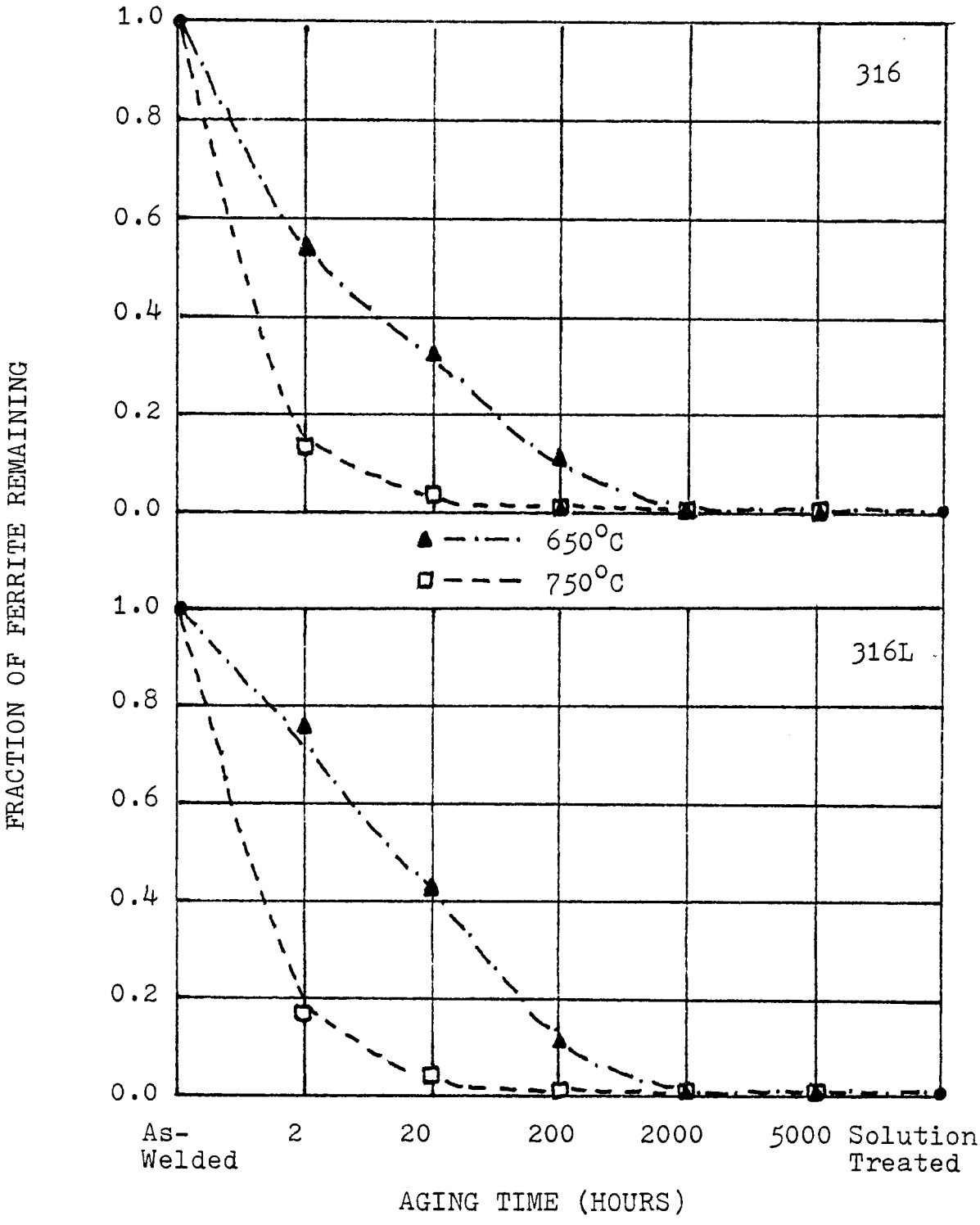


Figure 13. The Fraction of Ferrite Remaining as Function of Heat Treatment of Types 316 and 316L Weld

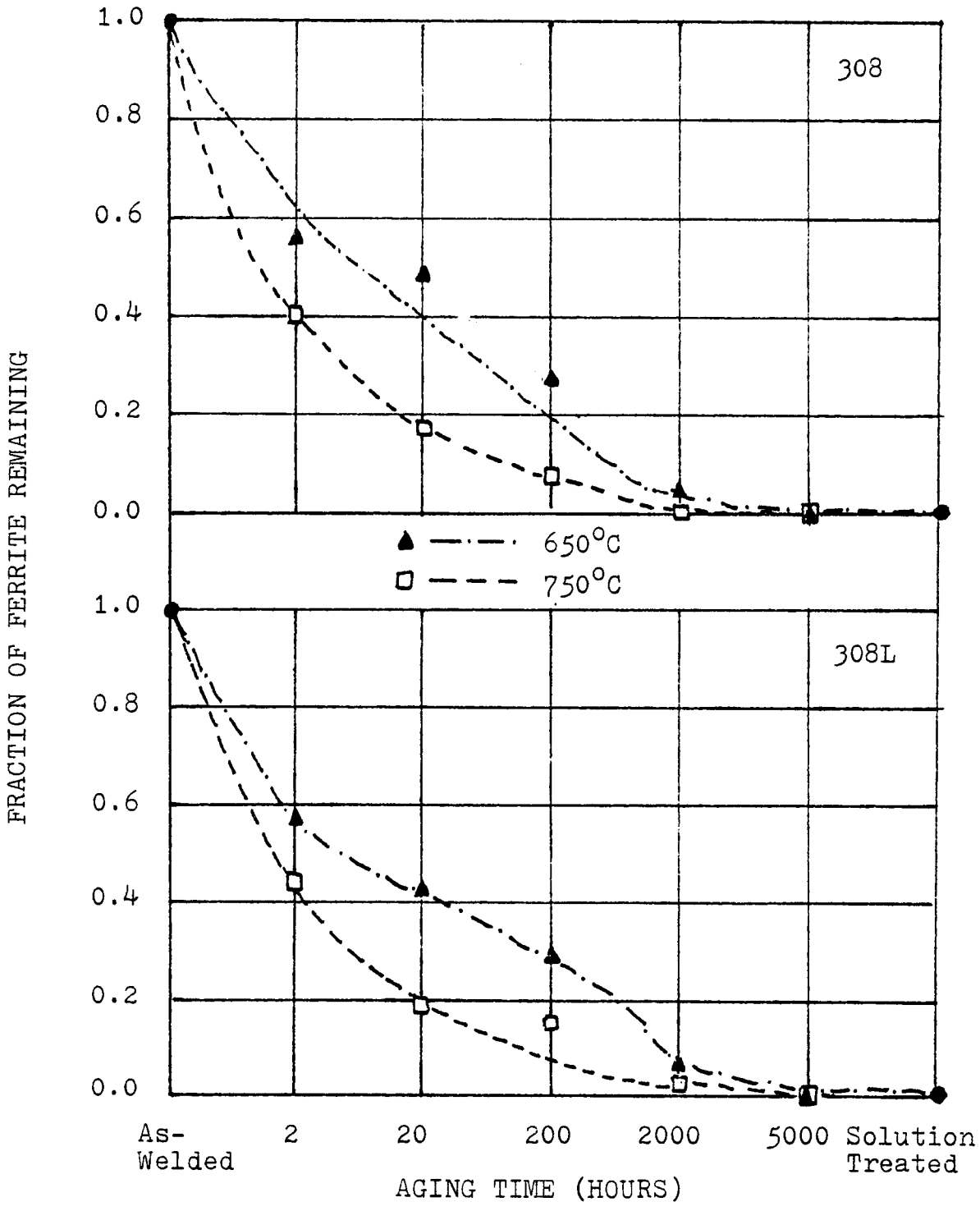


Figure 14. The Fraction of Ferrite Remaining as Function of Heat Treatment of Types 308 and 308L Weld

Table 3 and Table 4 also show that the carbon content, in the range studied, has little effect on ferrite decomposition. Carbon will enhance the ferrite decomposition by forming carbides but may retard the formation of sigma phase. This is true for both 316 and 308 types.

There does appear to be a considerably greater rate of ferrite decomposition in the type 316 materials than in the type 308 materials. The fraction of ferrite remaining in 316 or 316L types is approximately 10% after 200 hours at 650°C while that for 308 and 308L types is approximately 30%. The greater decomposition rate for the 316 and 316L types may be due to the greater chromium equivalent when compared to the 308 and 308L compositions as shown in Table 5. The value of "equivalent chromium" content of each alloy was determined by Hull's calculation[26] with the chemical compositions listed in Table 2. After 2000 hours all ferrite is eliminated in both type 316 alloys as shown in Figure 13. There is no ferrite remaining after 5000 hours aging in all type studied.

Figure 15 shows the effect of aging times on the microstructures of type 316 D at 750°C. It is clear that the longer the aging time the more the intermetallic phases formed. Comparing Figure 15 with Table 3, it is shown that the intermetallic phases can continue to grow after the ferrite is consumed.

The effect of aging temperature is shown in Figure 16 for type 308 samples aged for 2000 hours. There are more

Table 5. The Equivalent Chromium Content of Austenitic Stainless Steel Weld Metals Used in This Investigation.

Type of Welds	Equivalent Chromium Content*
308-A	16.77
308-D	18.16
308L-A	17.06
308L-D	17.92
316-A	20.24
316-D	21.88
316L-A	19.92
316L-D	21.00

* "Equiv. Cr." = Cr + 0.31 Mn + 1.76 Mo + 0.97 W + 2.02 V + 1.58 Si + 2.44 Ti + 1.70 Cb + 1.22 Ta - 0.226 Ni - 0.177 Co

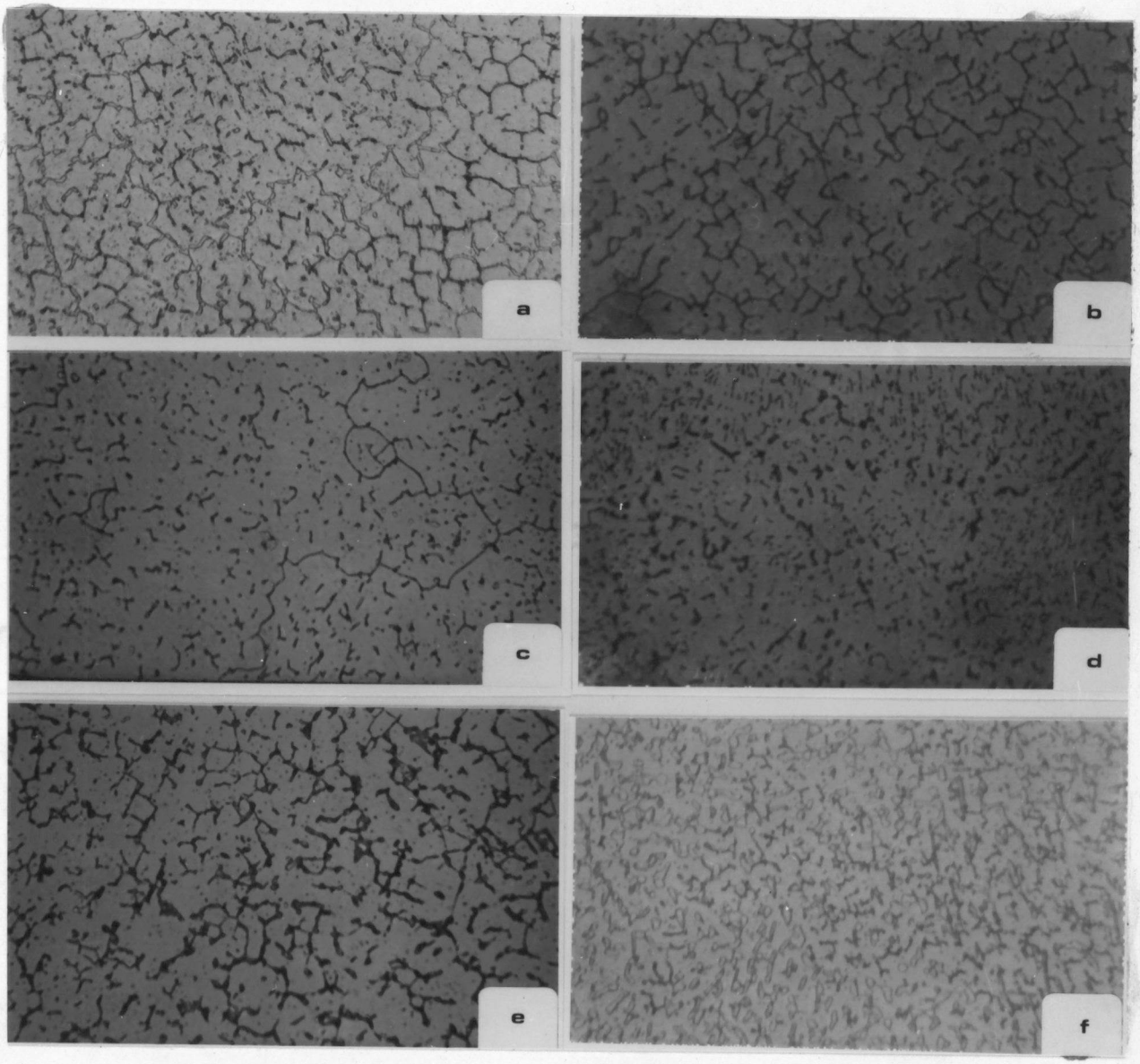


Figure 15. Effect of Aging Times on the Microstructures of 316-D Welds at 750°C. (500X)
(a) 0 Hours; (b) 2 Hours;
(c) 20 Hours; (d) 200 Hours;
(e) 2000 Hours; (f) 5000 Hours.

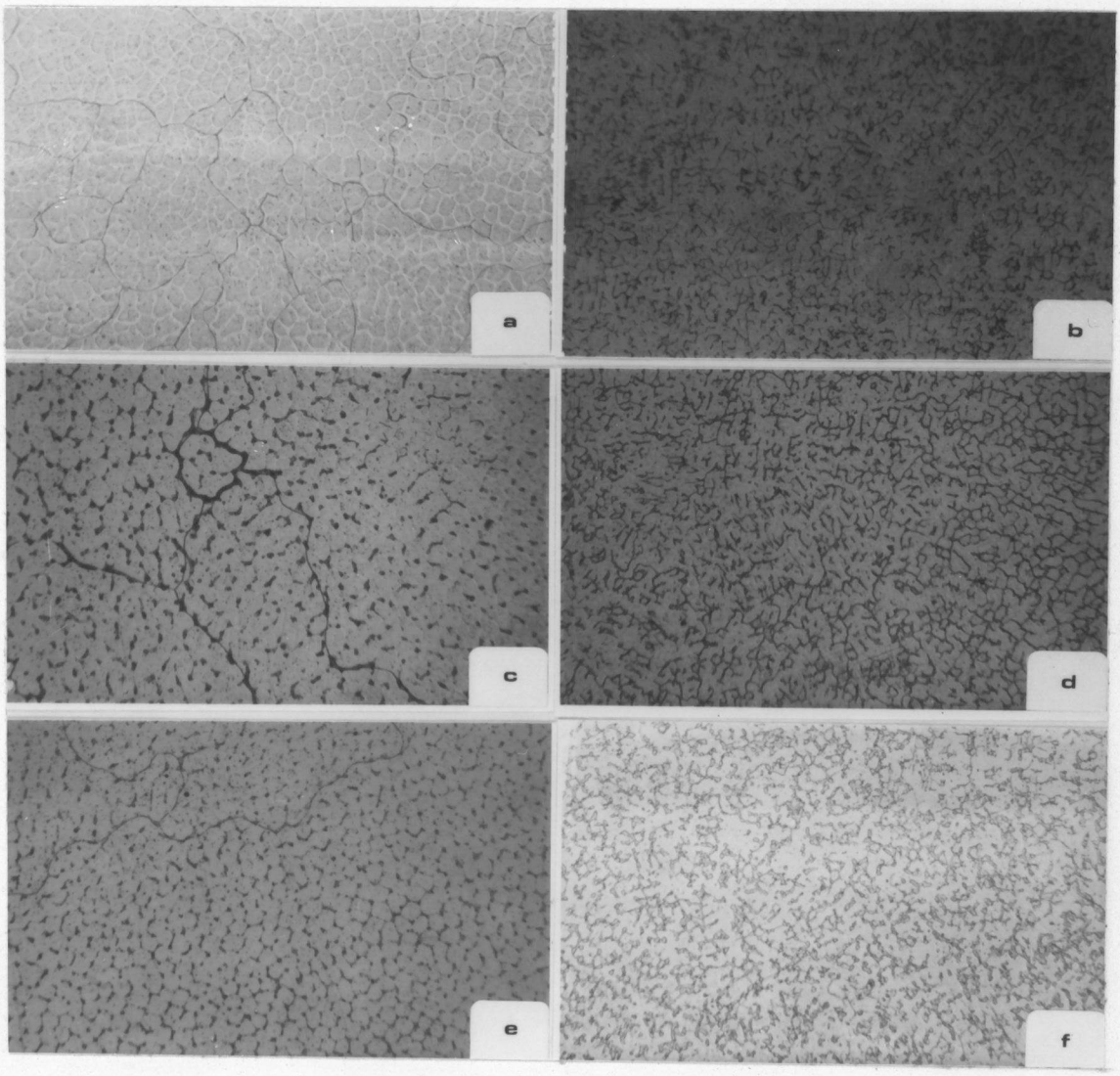


Figure 16. Effect of Temperatures on the Microstructures of Types 308 Welds Aged for 2000 Hours. (200X)
(a) 308-A, 550°C; (b) 308-D, 550°C;
(c) 308-A, 650°C; (d) 308-D, 650°C;
(e) 308-A, 750°C; (f) 308-D, 750°C.

precipitates formed at higher temperature. The effect of initial ferrite level is also shown. The higher initial ferrite the greater the amount of precipitation at any temperature.

Figure 17 shows the effect of solution treatment (one hour at 1100°C, then water quenched) on the microstructures of types 308L D, 316L D, and 308 A. Ferrite phases are reduced and spheriodized after solution treatment.

Ferrite content has a great effect on the microstructures. Figure 18 shows the effect of ferrite content on the microstructures of type 308 welds at different aging treatment. Since the ferrite tends to transform to the carbide, sigma, and chi phases, more precipitates are formed for high ferrite content materials than low ferrite content materials as shown in Figures 16 and 18. But it should be noted that for similar "equivalent chromium contents", the effect of ferrite is more significant at short aging times.

The microstructures of types 316 and 308 are compared in Figure 19. The greater amount of precipitate particles in the type 316 samples than type 308 samples is noticeable. This is probably due to the different "equivalent chromium" contents of the two samples.

Bulk Extraction and X-Ray Diffraction Studies of Precipitates

The phases formed in the aged welds were identified by X-ray diffraction patterns from the extracted residues.

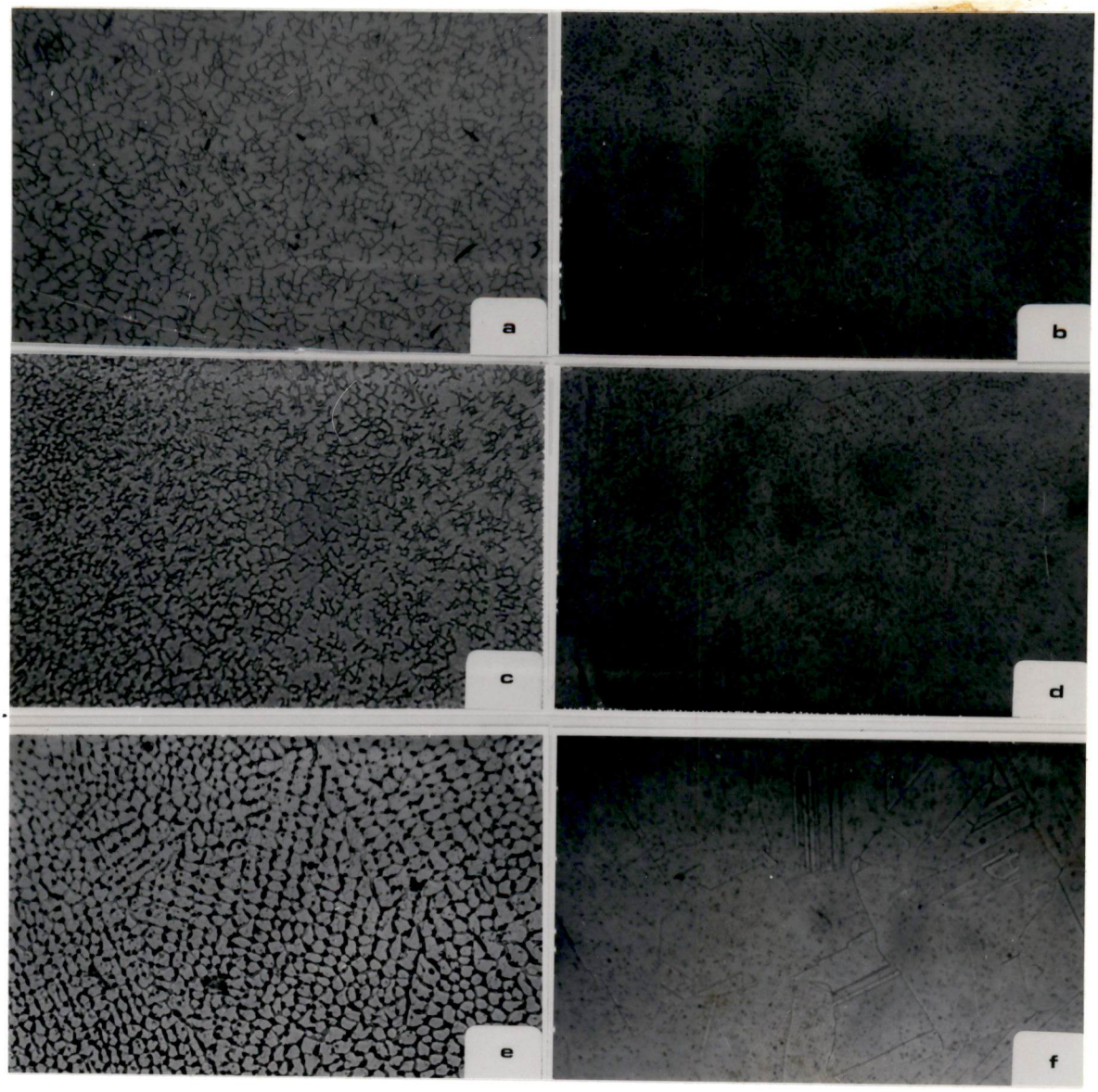


Figure 17. Effect of Solution Treatment on the Microstructures of Austenitic Stainless Steel Welds. (200X)
(a) 308L-D, As-Welded; (b) 308L-D, Solution Treated;
(c) 316L-D, As-Welded; (d) 316L-D, Solution Treated;
(e) 308-A, As-Welded; (f) 308-A, Solution Treated.

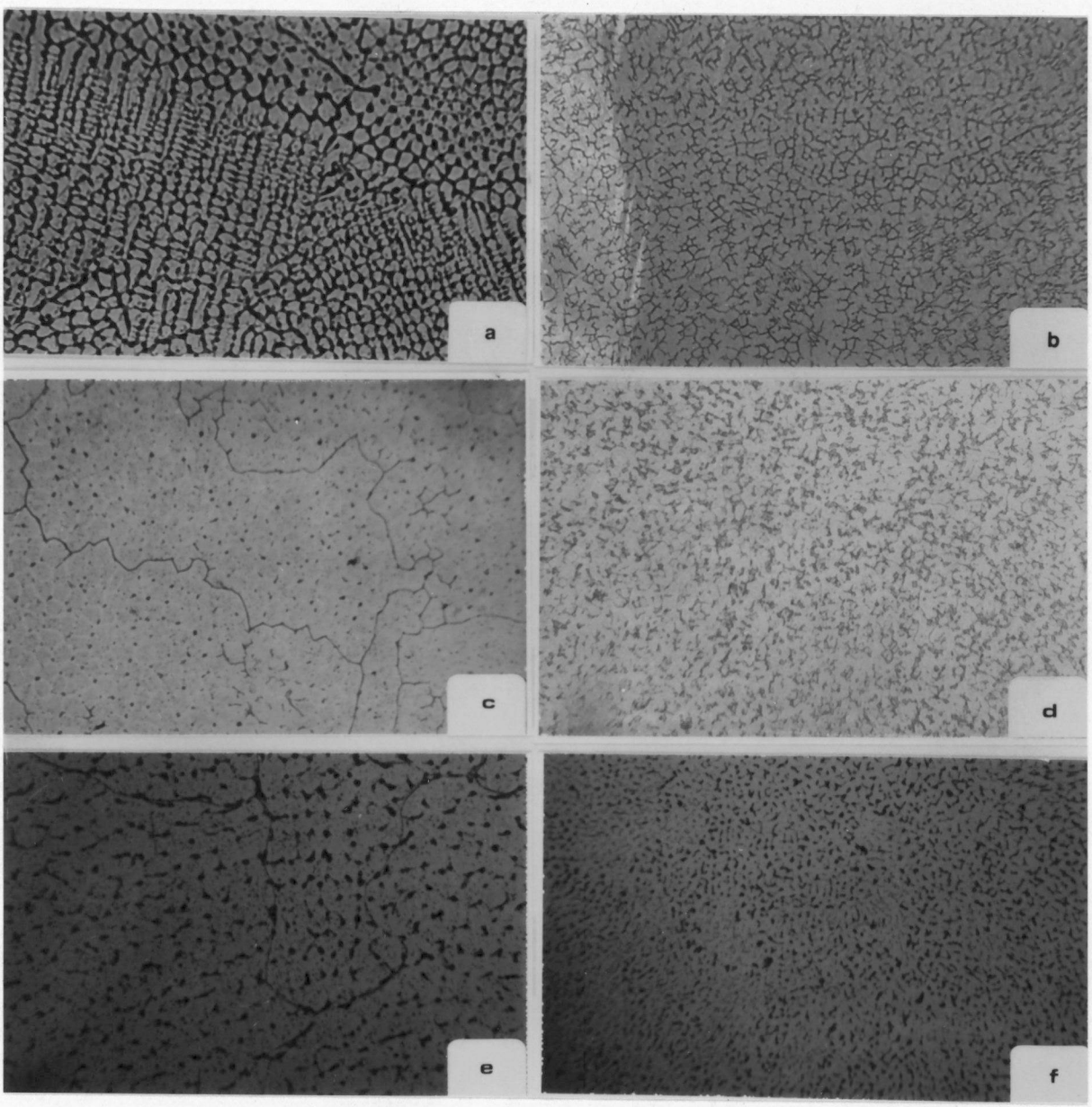


Figure 18. Effect of Ferrite Content on the Microstructures of Types 308 Welds Aged at 750°C. (200X)
(a) 308-A, 0 Hours; (b) 308-D, 0 Hours;
(c) 308-A, 200 Hours; (d) 308-D, 200 Hours;
(e) 308-A, 5000 Hours; (f) 308-D, 5000 Hours.

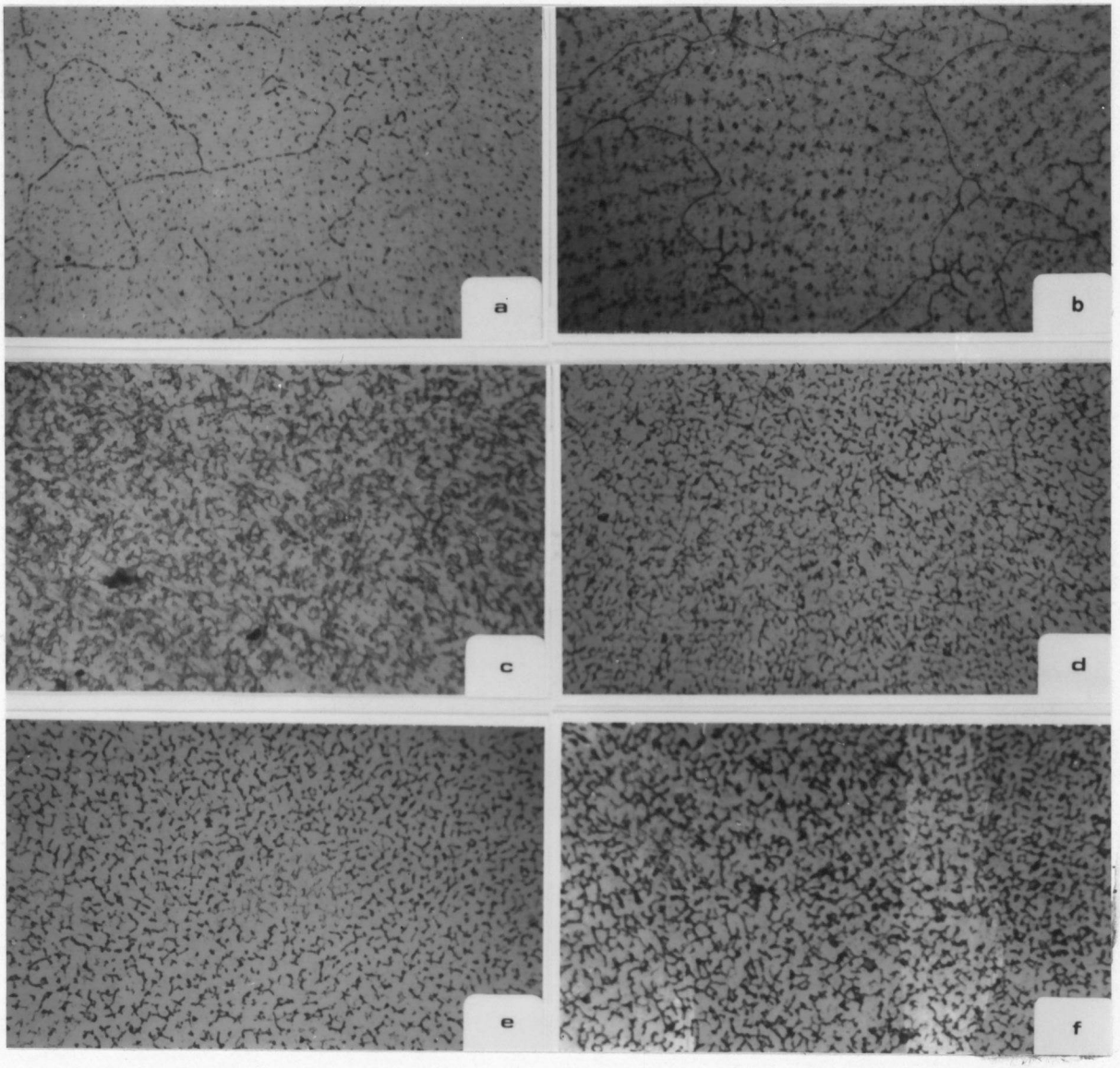


Figure 19. Microstructures of Aged Samples. (200X)
(a) 308L-A and (b) 316L-A, Aged 2000 Hours at 750°C;
(c) 308-D and (d) 316-D, Aged 2000 Hours at 750°C;
(e) 308L-D and (f) 316L-D, Aged 5000 Hours at 750°C.

Samples aged for 200 hours and 2000 hours at 650°C and 750°C were used in this study.

The weight percent of extracted precipitates from aged samples are listed in Table 6. Table 7 shows the identified phases and their relative concentrations in the extracted precipitates. An example of X-ray diffraction pattern analysis from extracted residue is presented in Table 8. The extracted residue was from a type 308 D weld metal aged 2000 hours at 750°C. The X-ray diffraction pattern was then compared with the standard patterns of carbide, sigma, and chi phases which are also listed in Table 8. It was judged by the relative intensities of each line that the extracted residue approximately contained 70% sigma, 30% carbides, and no chi phase. The accuracy of the relative amounts is limited by the subjective estimation of intensities. For this reason another method for calculating the relative amounts of identified phases was also used. It is assumed that all carbon above the solubility limit is present as carbide ($M_{23}C_6$). The amount of carbide was computed and then subtracted from the total amount of extracted residue to obtain the amount of sigma. Table 9 illustrates the calculation of the relative amounts of carbide and sigma phase with the type 308 D weld metal. Figures 20 and 21 show the results from Tables 6 and 7 as a function of heat treatment. While the weight percents of precipitates were plotted on a logrithmic scale, the

Table 6. Weight Percent of Extracted Precipitates from Aged Samples

Heat Treatment	316L-A	316L-D	316-A	316-D	308L-A	308L-D	308-A	308-D
650°C/200 hrs.	1.08	1.75	0.80	0.80	0.49	0.57	0.40	0.83
650°C/2000 hrs.	0.93	1.91	1.13	1.49	0.54	0.85	0.44	1.05
750°C/200 hrs.	0.56	2.29	0.98	2.99	0.44	0.81	0.73	0.99
750°C/2000 hrs.	1.83	4.90	2.67	8.54	0.50	2.01	1.07	2.46

Table 7. Identified Phases and Fraction Content of Extracted Residue

Heat Treatment	316L-A	316L-D	316-A	316-D	308L-A	308L-D	308-A	308-D
650°C/200 hrs.	50% C*	32% C	100% C	100% C	61% C	58% C	100% C	100% C
	50% σ**	68% σ	0% σ	0% σ	39% σ	42% σ	0% σ	0% σ
650°C/2000 hrs.	57% C	30% C	85% C	72% C	55% C	39% C	100% C	92% C
	43% σ	70% σ	15% σ	28% σ	45% σ	61% σ	0% σ	8% σ
750°C/200 hrs.	95% C	25% C	100% C	38% C	61% C	38% C	100% C	98% C
	5% σ	75% σ	0% σ	62% σ	39% σ	62% σ	0% σ	2% σ
750°C/2000 hrs.	29% C	12% C	38% C	13% C	54% C	15% C	78% C	39% C
	71% σ	88% σ	62% σ	87% σ	46% σ	85% σ	22% σ	61% σ

* C : Carbide Phase
** σ : Sigma Phase

Table 8. X-ray Diffraction Pattern Analysis of Weld Metal 308-D Aged 2000 Hours at 750°C

Diffraction Pattern		Standard Patterns						Identified Phases
		Carbide		Sigma		Chi		
d	I	d	I	d	I	d	I	
2.37	vvw	2.39	23.3					C
2.27	vvw			2.30	7.6			σ
2.17	vvw	2.18	44.9					C
2.14	m+			2.15	32.7			σ
						2.10	175	
				2.09	14.5			
2.05	m+	2.06	78.5					C, σ
				2.04	13.0			
1.98	m-			1.99	25.4			σ
1.93	s			1.95	35.5			σ
				1.90	17.0	1.90	50	
1.88	m+	1.89	13.9					σ, C
1.80	vw	1.81	13.6					C
1.60	vvw	1.61	12.3					C
		1.30	10.0					
1.26	m-	1.26	14.7					C
1.24	vw			1.25	6.3			
1.23	vw	1.23	5.7					C, σ
				1.22	4.7			
						1.21	47	
1.09	vw	1.09	15.2					C
0.816	vw	0.82	14.3					C
0.786	vvw			0.79	7.6			
0.78	m-	0.77	12.5	0.77	9.5			C, σ

d : D-spacing
I : Relative Intensity
s : Strong
m+ : Above medium
m- : Below medium
vw : Very weak
vvw : Very very weak
C : Carbide phase
σ : Sigma phase
χ : Chi phase

Table 9. Relative Contents of Extracted Residue from Type 308-D Weld Metal

Heat Treatment	Carbon Content in Weld (wt. %)	Solubility of Carbon in Fe-Cr-Ni-C Alloys (wt. %)	Available Carbon for Carbide Formation (wt. %)	Amount of Carbide Formation (wt. %)	Total Amount of Extract (wt. %)	Fraction of Carbide in Residue
650°C						
200 hrs.	0.060	0.001[58]	0.059	0.926*	0.83	100 %
2000 hrs.	0.060	0.001	0.059	0.926*	1.05	88 %
750°C						
200 hrs.	0.060	0.005	0.055	0.965**	0.99	97 %
2000 hrs.	0.060	0.005	0.055	0.965**	2.46	39 %

* At 650°C, 1 gm C = 15.70 gm carbide[59]
** At 750°C, 1 gm C = 17.55 gm carbide

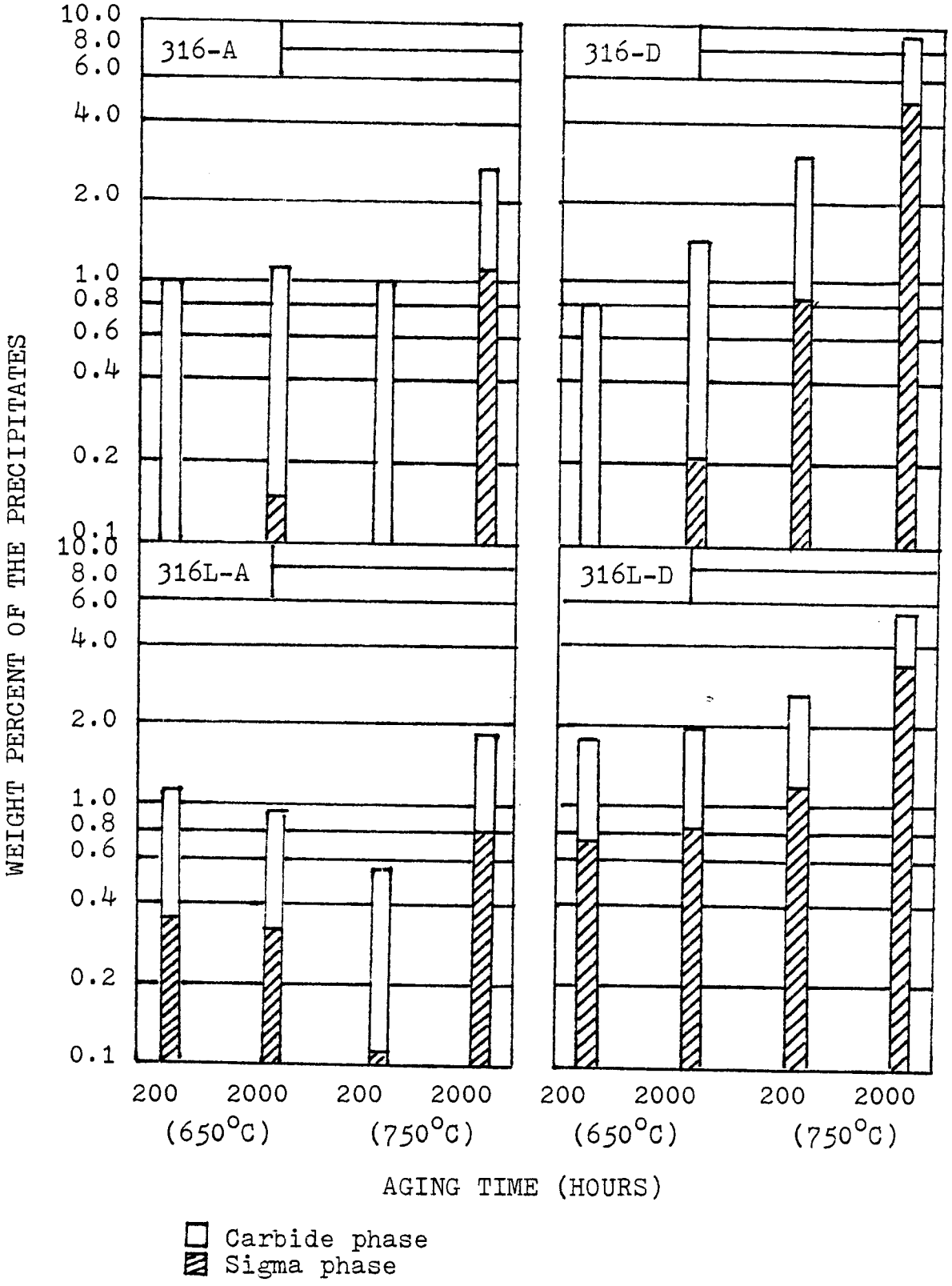


Figure 20. Weight Percent of Precipitates as Function of Heat Treatment for Types 316 and 316L Weld

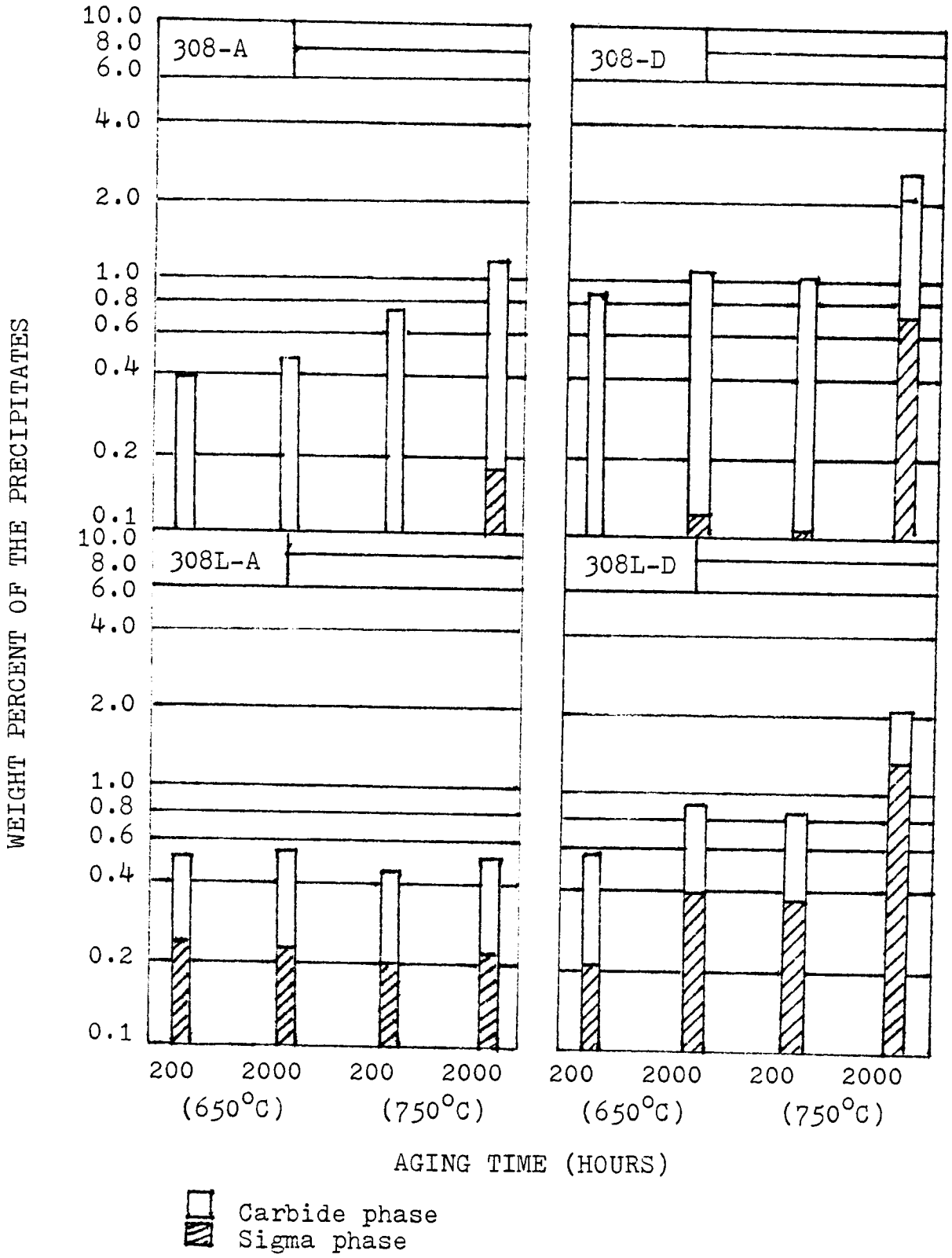


Figure 21. Weight Percent of Precipitates as Function of Heat Treatment for Types 308 and 308L Weld

fraction contents of each phase were indicated as a linear decimal fraction of the bar height.

It is clearly observed that there were more precipitates in the high ferrite level welds than in the low ferrite level welds. This can be explained by the fact that the ferrite present in the as-deposited welds is replaced by the carbides, sigma, and chi phases during aging at elevated temperatures. Also the ferrite-austenite boundaries serve as easy nucleating sites for both carbides and the intermetallic phases, thus enhancing the rate of formation of such phases in welds containing ferrite as compared to materials of similar composition in which no ferrite exists. High ferrite welds formed more sigma phase than low ferrite weld formed. This is probably due to greater concentration of ferrite forming elements in the ferrite than in the austenite matrix. These localized concentrations enhance the formation of sigma phase because the ferrite formers, chromium, molybedum, and niobium, are also the sigma formers.

The aging time and temperature also have significant effects on the phase transformation. After longer aging time or at higher aging temperature, more precipitates are formed. The fraction of sigma phase formed is large for aging at higher temperature or aging for longer time. This shows again that the sigma phase can continue to grow after the ferrite is consumed.

The 316 and 316L types specimens have more precipitates and more sigma phase formed than 308 and 308L types have. This is true for both low and high ferrite content welds and consistent with the microstructures shown in Figure 19, page 61. The reason for that was probably because of the greater chromium equivalent of types 316 and 316L welds as previously stated.

Anodic Polarization Measurements

Throughout this section of results, the following conventions are used: all potentials are referred to the standard hydrogen electrode (SHE); current density is calculated by dividing measure currents by the geometric surface area.

Crevices between the specimen and the resin mount are known to introduce error and a lack of reproducibility in the passive current densities recorded during anodic polarzation measurements; crevice effects markedly increase the apparent passive current. To check the absence of this and other experimental sources of error, the polarization curves of two samples of stainless steel type 430 were run under the standard procedures (ASTM G-1/XI). The samples were solution treated at 1050^{o}C for one hour and then mounted in bakelite. The polarization curves of these two samples generally lie in the standard band of the ASTM results as shown in Figure 22.

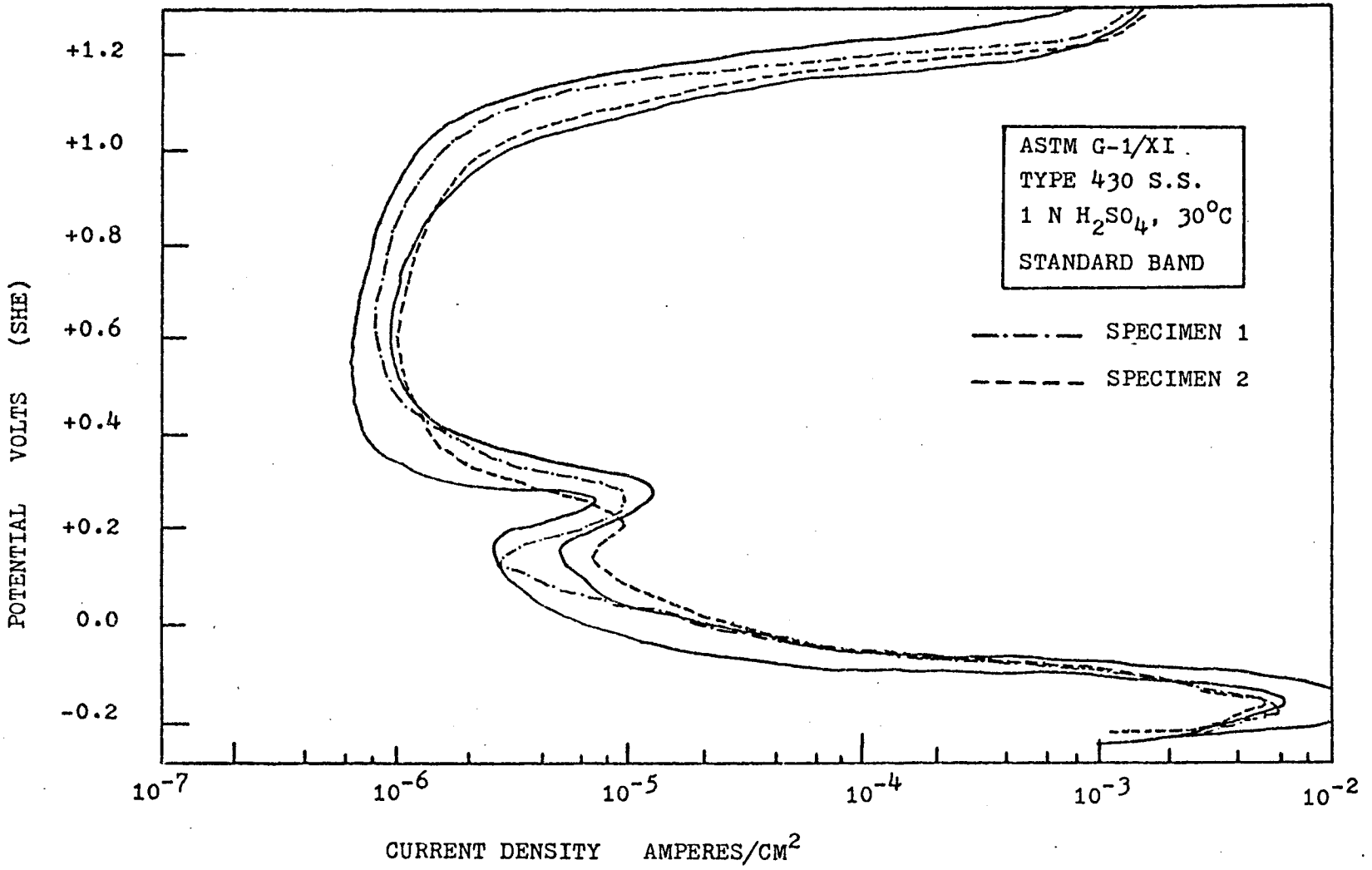


Figure 22. Standard Band of the Polarization Curves of Stainless Steel 430 Under the Standard Procedures of ASTM G-1/XI

The scan rate also has a significant effect on the polarization curves. This is illustrated in Figure 23. As traverse rate is increased, the anodic polarization curves are shifted to higher current densities over the entire range of potentials investigated. The primary passive potentials also move to a positive (noble) direction.

The effect of the surface finish on the polarization curves is shown in Figure 24. There is only a slight difference on the passive region of the polarization curves after polishing through a 600 grit polishing. For this reason 600 grit polishing was used in this investigation. This is also suggested by the ASTM standard procedures.

Figure 25 represents the effect of polarization pretreatment of the specimen on the polarization curves. The specimen used was a type 308 A stainless steel weld and sensitized by aging two hours at 750°C. It is shown that the second maximum peak increases slightly for longer immersion time. The passive current density is independent on the polarization pretreatment.

The reproducibility of the polarization curves is shown in Figure 26. Three sets of polarization curves were run under the same procedures except a little difference in temperature ($25^{\circ}C \pm 2^{\circ}C$). There is no change at the passive region of the polarization curve but a slight change at the active region of the polarization curve. The reason of these phenomena is that the critical current density is very sensitive to the temperature, pretreatment, and the

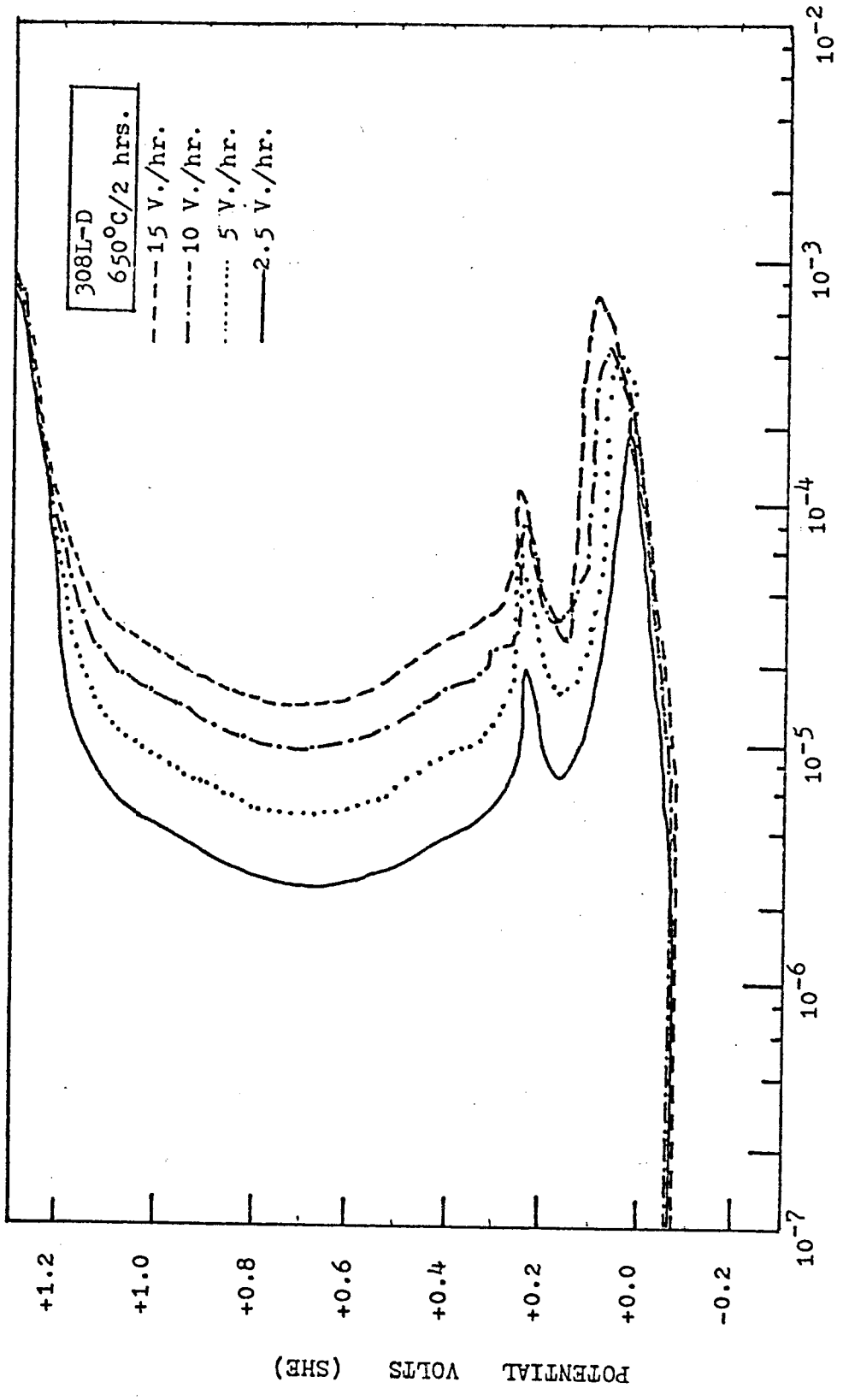


Figure 23. Effect of the Scan Rate on the Polarization Curves

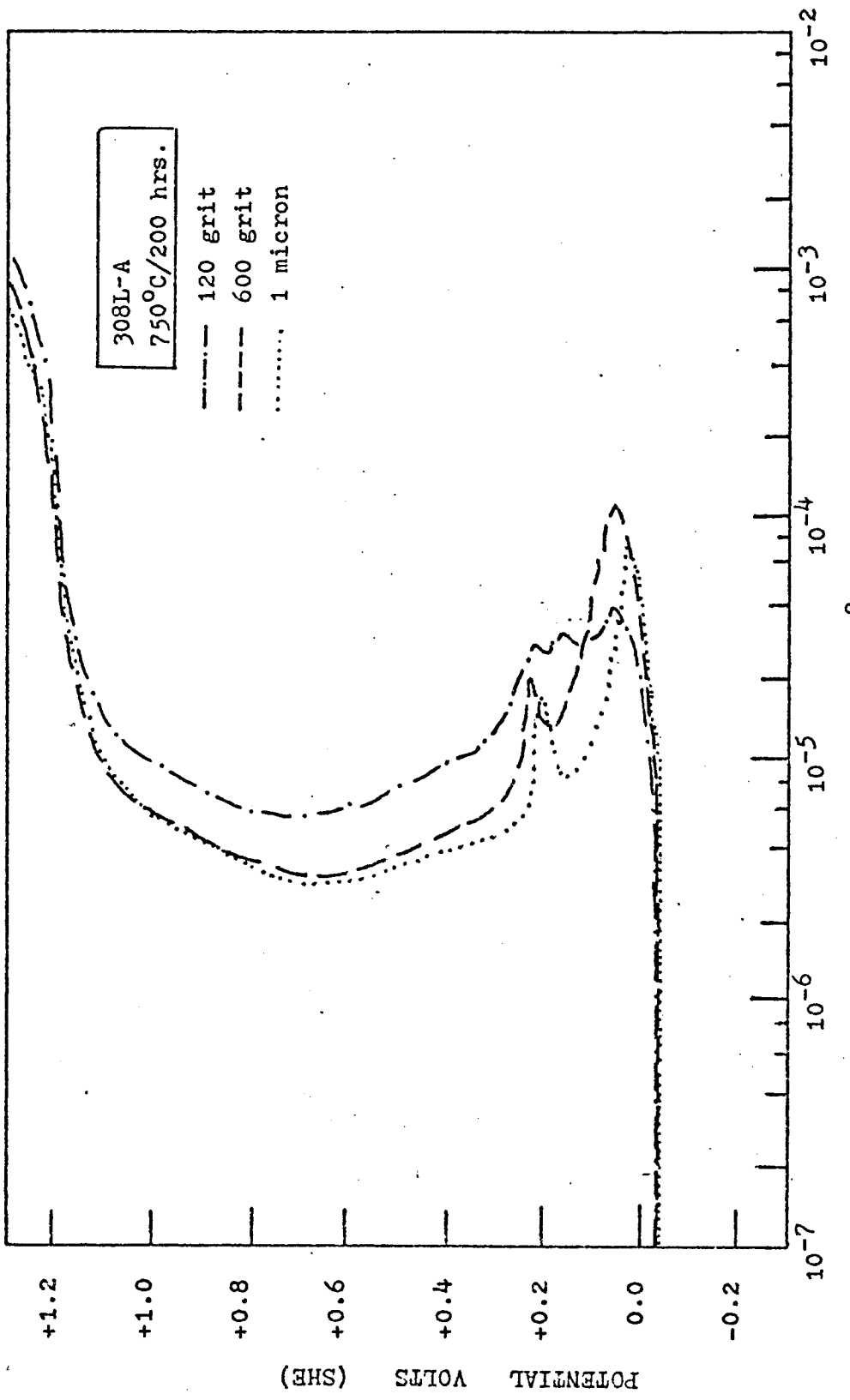


Figure 24. Effect of Surface Finish on the Polarization Curves

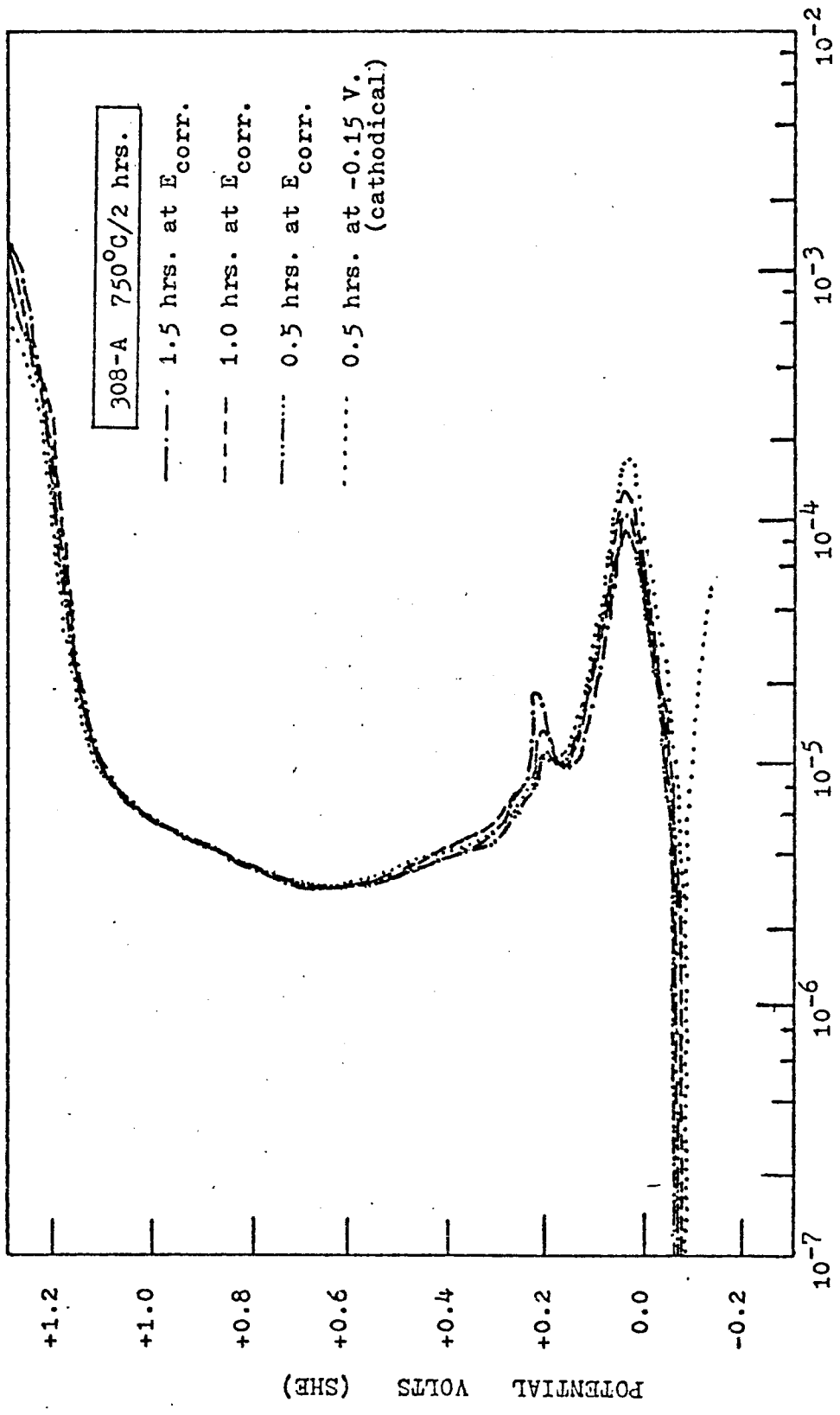


Figure 25. Effect of Immersion Time of Specimen on the Polarization Curves

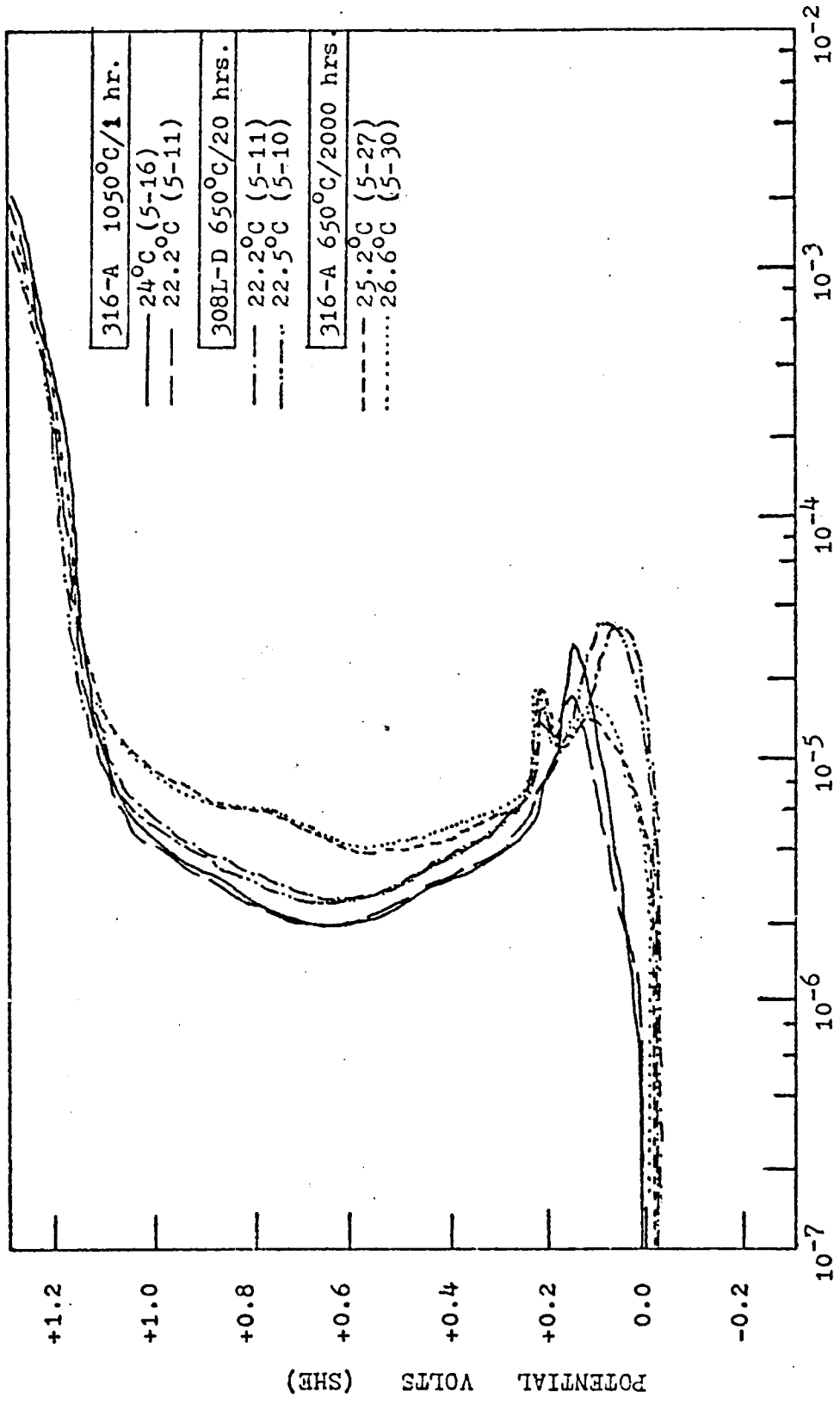


Figure 26. The Reproducibility of the Anodic Polarization Curves

composition of the specimen.

Anodic polarization curves for as-welded, heat treated at 650°C and 750°C, and solution treated materials of all eight types austenitic stainless steel welds were run under the ASTM standard procedures except the temperature (25°C ± 2°C). Figures 27 to 34 show some of the results. The electrochemical parameters of the polarization curves for all the specimens are listed in Tables 10 through 17. Figure 35 presents a typical polarization curve obtained in this investigation and gives the definition of each parameter.

It is obvious that the sensitization has a great effect on the anodic polarization curves, especially on the passive region, as shown in Figures 27 through 30. This phenomena comes from the fact that carbides were formed along the austenite grain boundaries. The metal immediately around the carbides is depleted in chromium to below the level necessary to maintain passivity, and becomes susceptible to preferential corrosive attack. The passive current density decreases after longer aging times. This is caused by further diffusion of chromium into the chromium-depleted grain boundary region after complete precipitation of chromium carbides. For the low carbon grade stainless steel welds the sensitization effect is not significant as is shown in Figures 31 through 34.

Stainless steels are normally used in environments corresponding to the passive region. For this reason, the

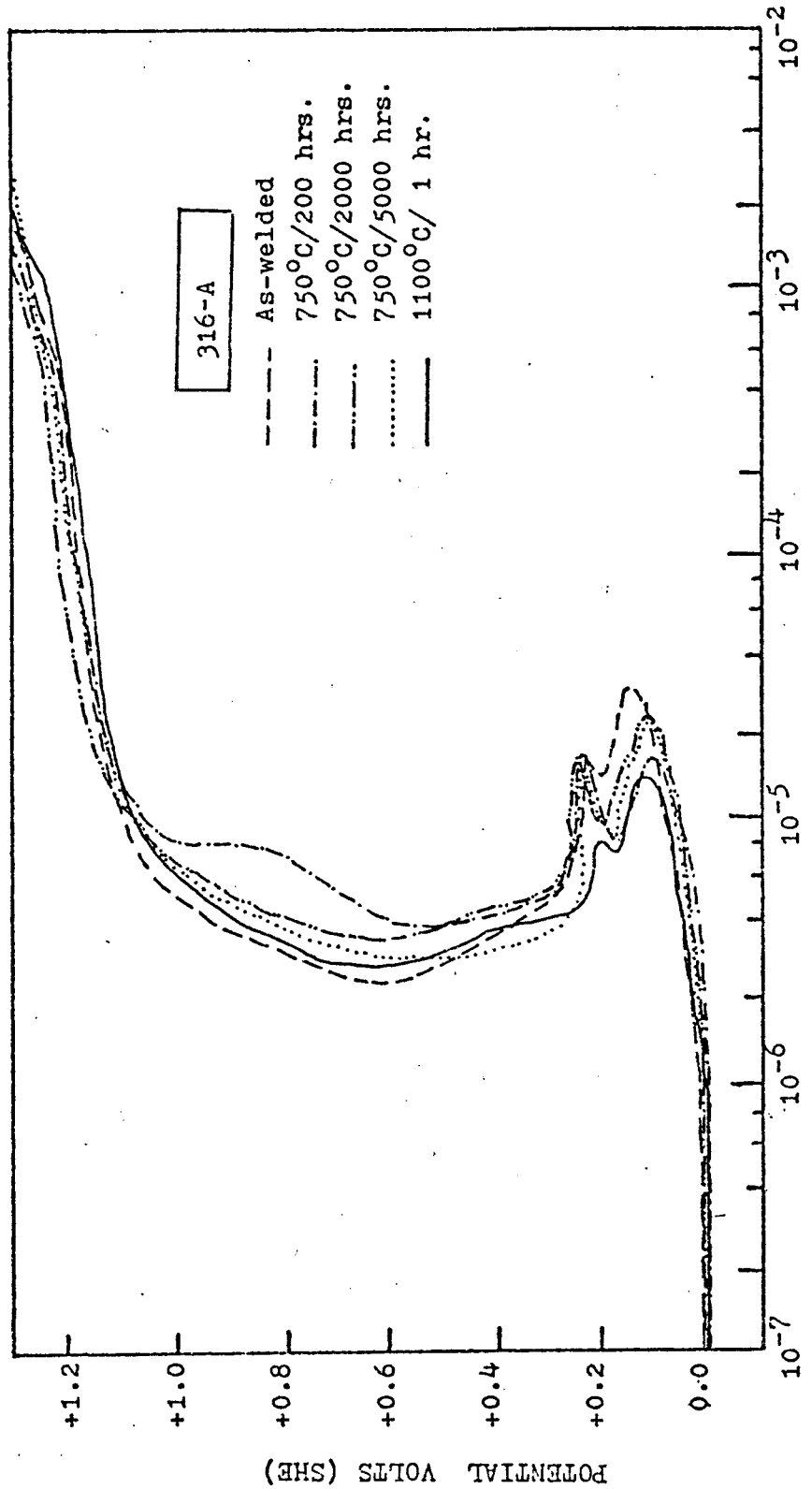


Figure 27. Anodic Polarization Curves of Type 316-A Weld

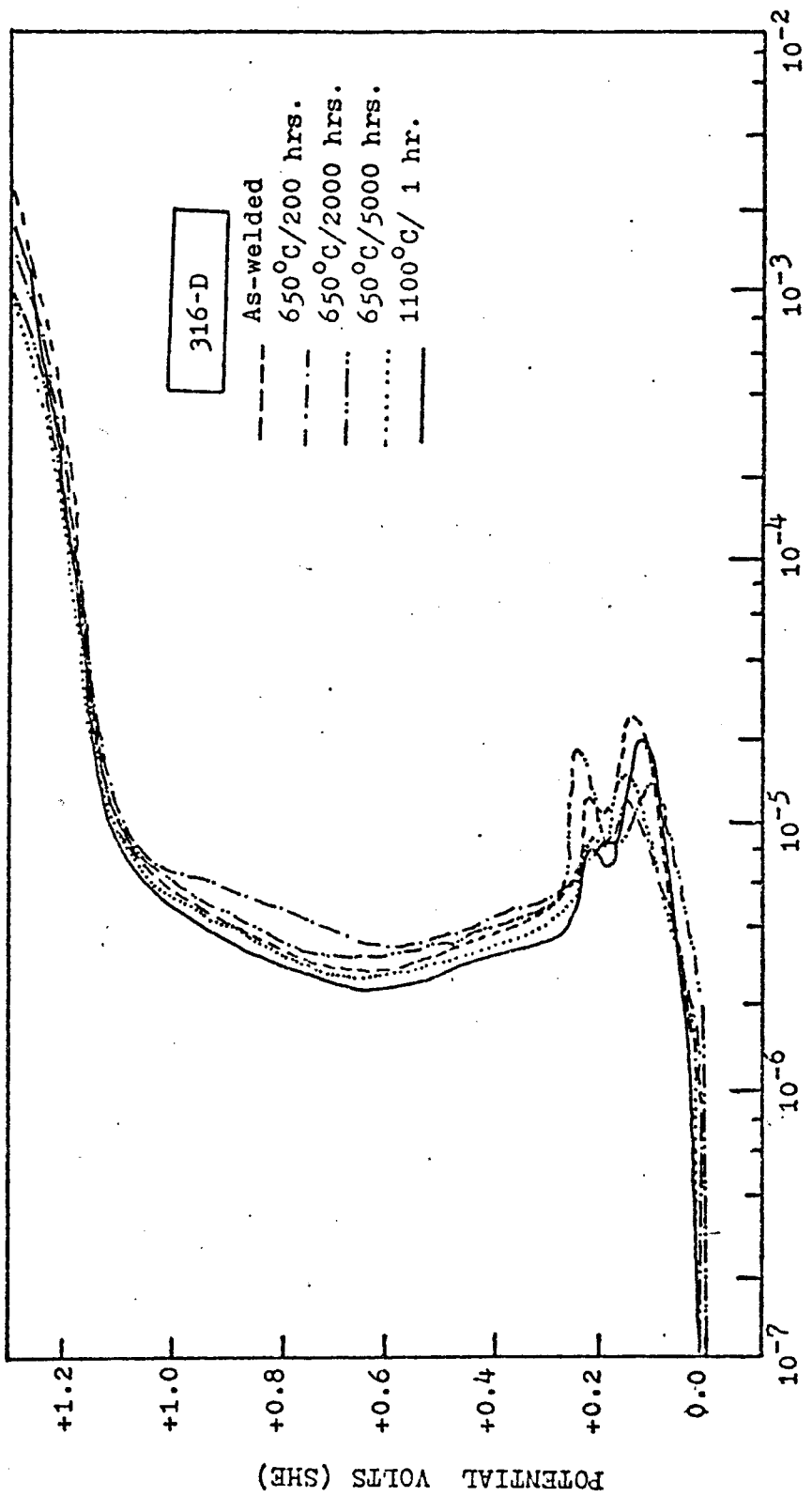


Figure 28. Anodic Polarization Curves of Type 316-D Weld

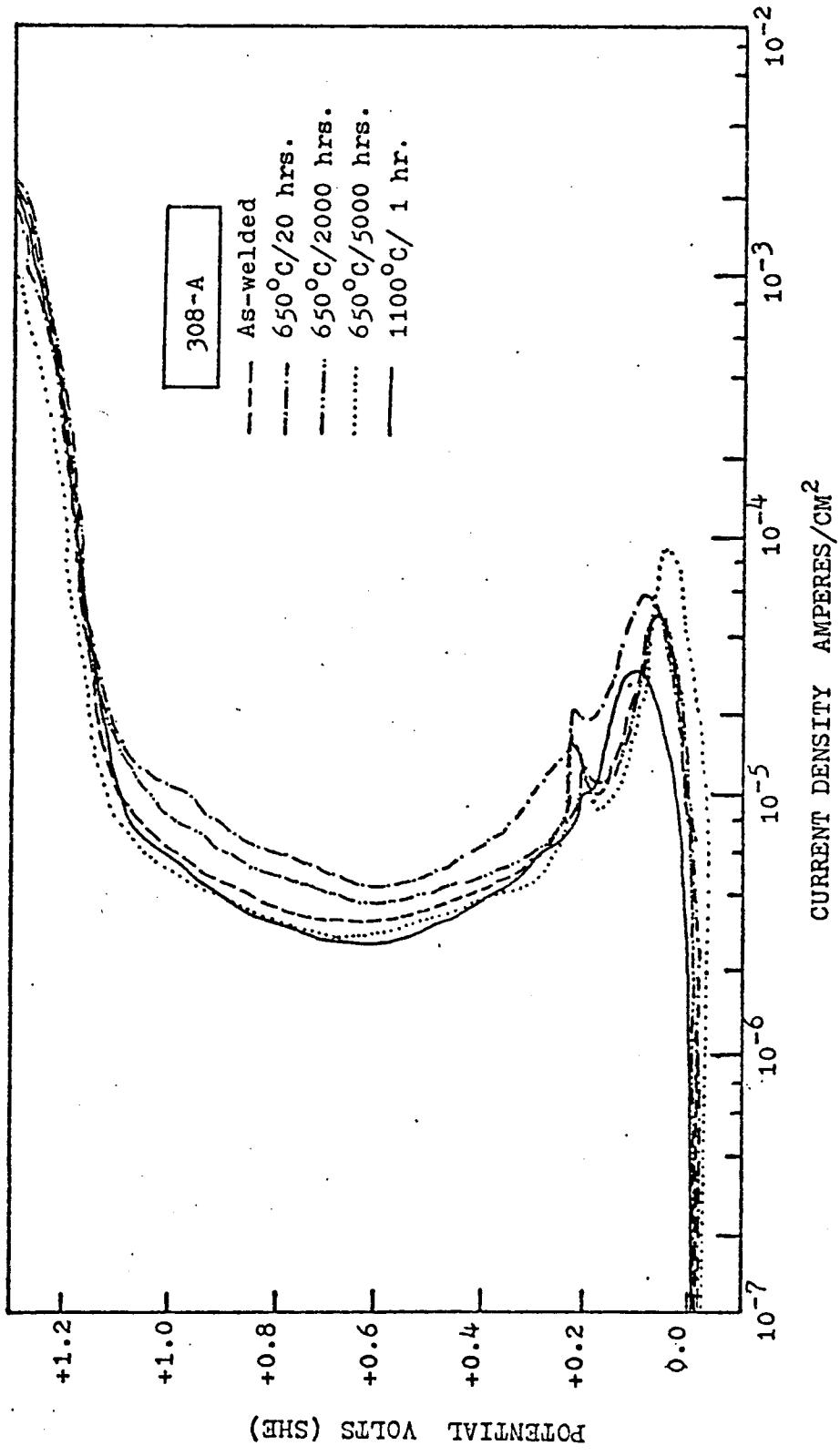


Figure 29. Anodic Polarization Curves of Type 308-A Weld

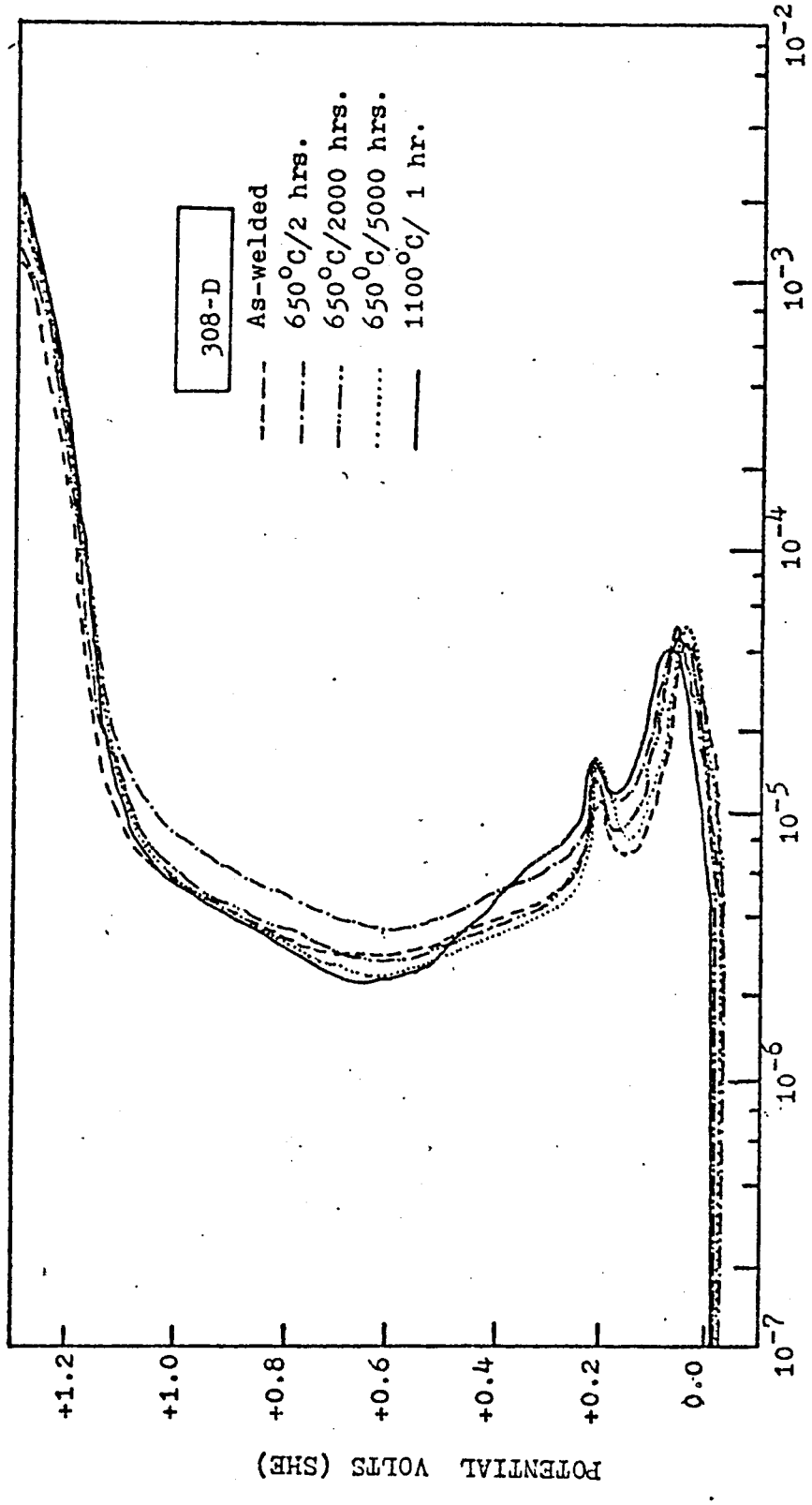


Figure 30. Anodic Polarization Curves of Type 308-D Weld

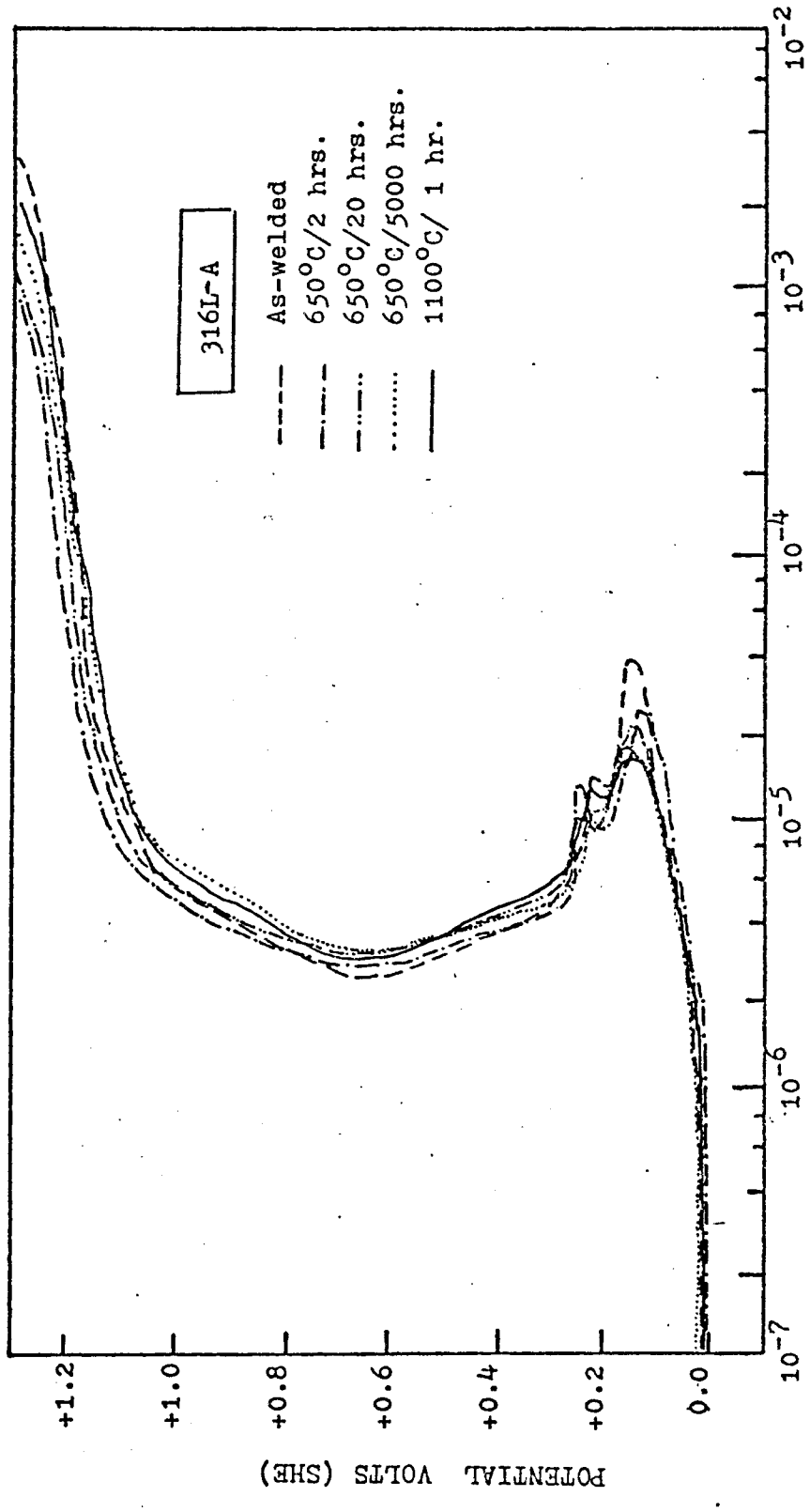


Figure 31. Anodic Polarization Curves of Type 316L-A Weld

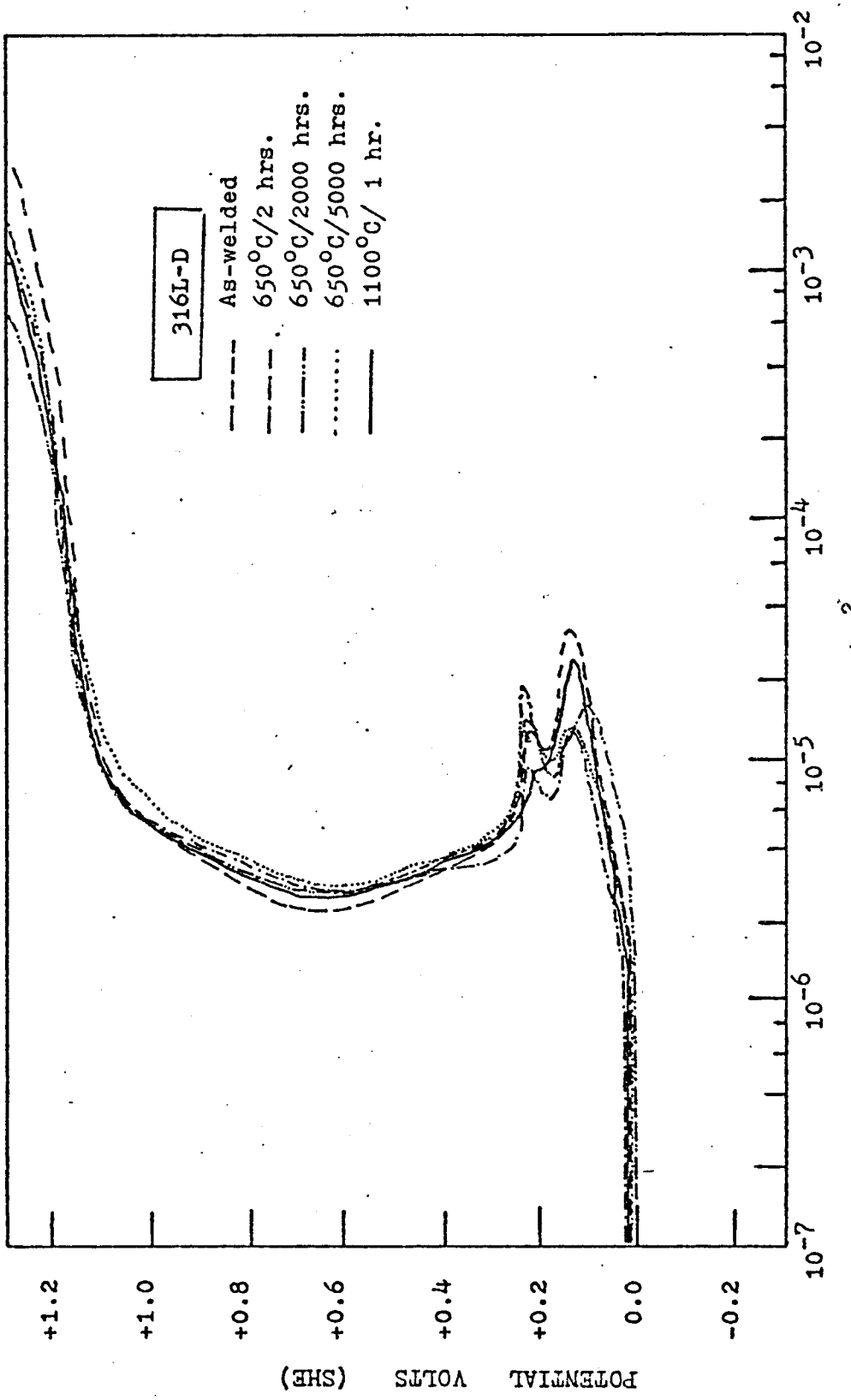


Figure 32. Anodic Polarization Curves of Type 316L-D Weld

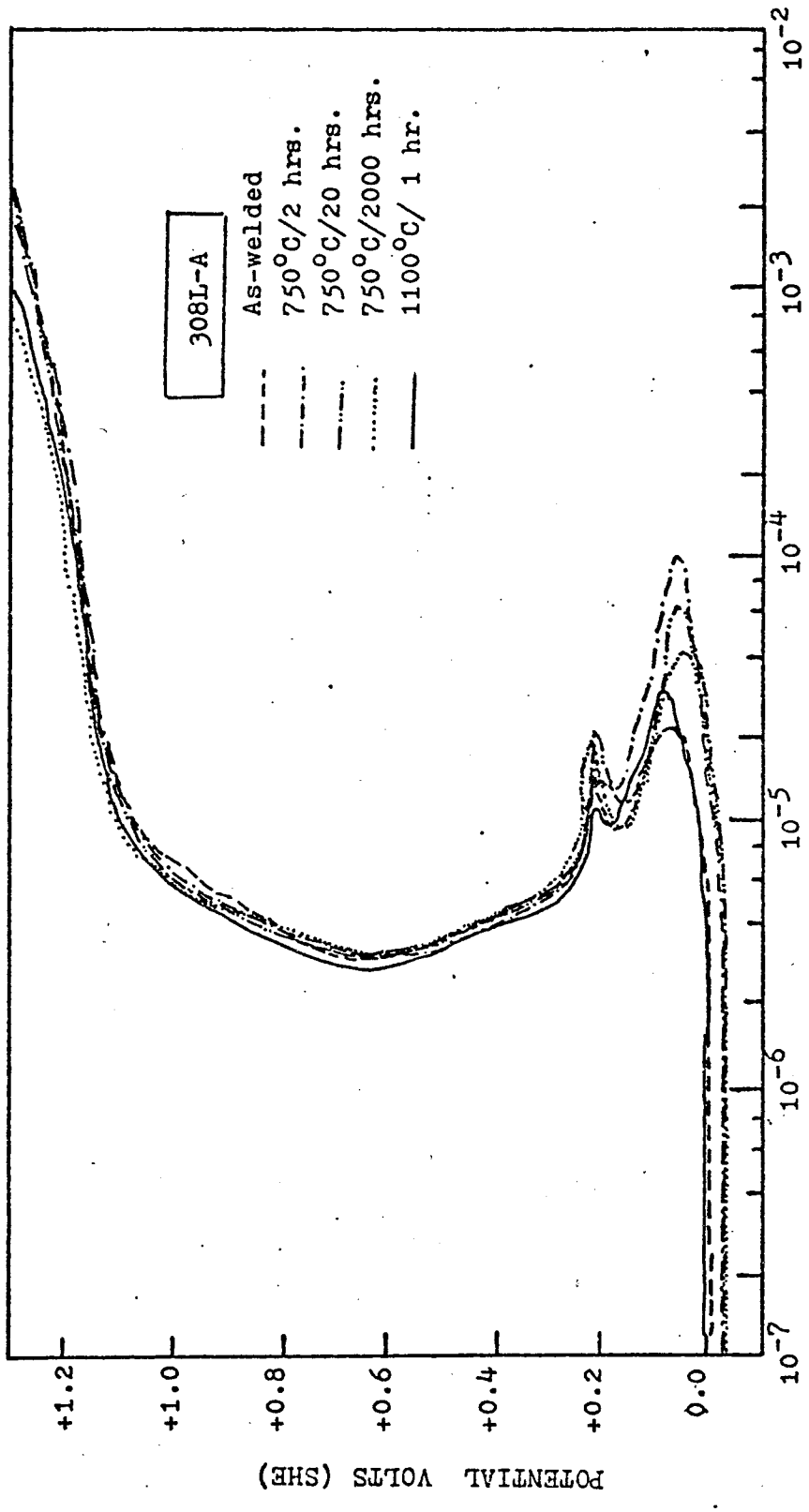


Figure 33. Anodic Polarization Curves of Type 308L-A Weld

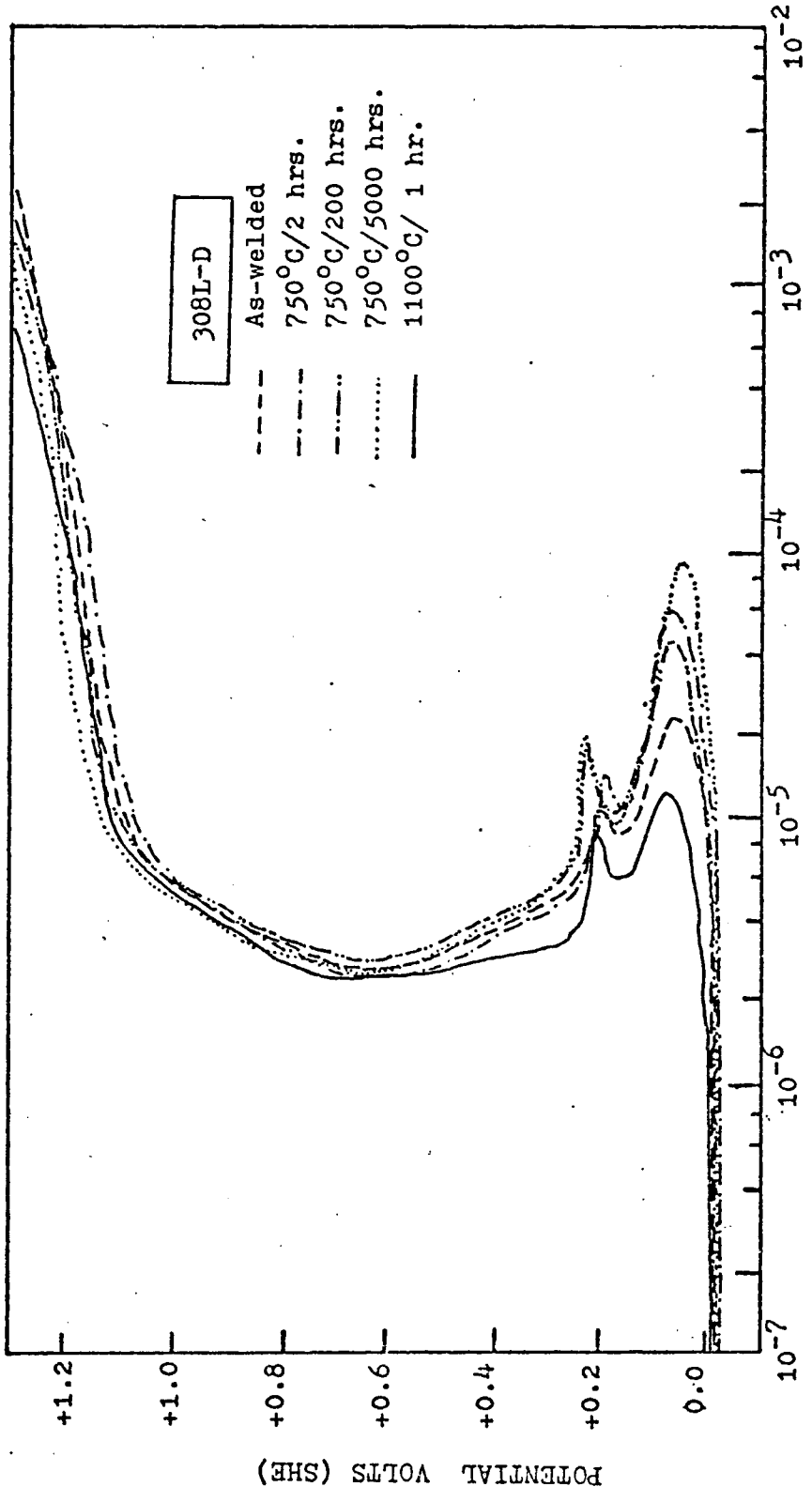


Figure 34. Anodic Polarization Curves of Type 308L-D Weld

Table 10. Electrochemical Parameters of Polarization Curves of Type 316-A Weld Metal

Heat Treatment	Current Density (10^{-6} Amperes/cm^2)			Potential (Volts, SHE)			
	I_1	I_2	I_p	E_c	E_1	E_2	E_p
As-welded	32.0	17.0	2.4	0.00	0.13	0.21	0.64
650°C/2 hrs.	36.0	26.0	5.0	-0.04	0.10	0.20	0.63
650°C/2000 hrs.	14.0	18.0	4.0	-0.02	0.13	0.22	0.60
650°C/5000 hrs.	27.0	12.0	3.2	-0.02	0.10	0.20	0.62
750°C/2 hrs.	40.2	17.0	3.2	-0.04	0.12	0.20	0.62
750°C/20 hrs.	32.5	16.5	2.8	-0.01	0.13	0.22	0.60
750°C/200 hrs.	17.0	17.5	3.8	0.00	0.10	0.22	0.60
750°C/2000 hrs.	25.0	16.0	3.3	0.00	o.10	0.23	0.65
750°C/5000 hrs.	23.0	15.0	2.7	0.00	0.10	0.21	0.60
1100°C/1 hr.	14.0	8.0	2.6	-0.01	0.11	0.20	0.65
Average Value	26.1	16.3	3.3	-0.02	0.11	0.21	0.62

Table 11. Electrochemical Parameters of Polarization Curves of Type 316-D Weld Metal

Heat Treatment	Current Density (10^{-6} Amperes/cm^2)			Potential (Volts, SHE)			
	I_1	I_2	I_p	E_c	E_1	E_2	E_p
As-welded	25.0	12.1	2.6	0.00	0.12	0.21	0.65
650°C/2 hrs.	47.0	28.0	2.8	-0.02	0.10	0.23	0.65
650°C/20 hrs.	19.0	8.9	2.8	0.00	0.13	0.20	0.60
650°C/200 hrs.	11.4	8.0	3.2	0.00	0.13	0.20	0.60
650°C/2000 hrs.	15.0	20.0	2.9	0.00	0.10	0.23	0.65
650°C/5000 hrs.	15.0	8.8	2.5	0.00	0.13	0.20	0.65
750°C/2 hrs.	17.0	7.0	2.7	-0.01	0.07	0.22	0.65
750°C/20 hrs.	10.0	7.0	2.7	+0.01	0.13	0.20	0.65
750°C/2000 hrs.	22.0	10.7	2.6	0.00	0.10	0.20	0.60
750°C/5000 hrs.	9.0	10.0	2.8	-0.01	0.10	0.21	0.65
1100°C/1 hr.	20.0	9.0	2.3	0.00	0.10	0.21	0.60
Average Value	19.1	11.8	2.7	-0.01	0.11	0.21	0.63

Table 12. Electrochemical Parameters of Polarization Curves of Type 308-A Weld Metal

Heat Treatment	Current Density (10^{-6} Amperes/cm^2)			Potential (Volts, SHE)			
	I_1	I_2	I_p	E_c	E_1	E_2	E_p
As-welded	53.0	17.0	3.2	-0.04	0.03	0.20	0.65
650°C/20 hrs.	61.0	20.7	4.2	-0.04	0.06	0.20	0.60
650°C/200 hrs.	160.0	27.6	3.1	-0.06	0.07	0.20	0.65
650°C/2000 hrs.	50.0	13.0	3.6	-0.03	0.04	0.20	0.60
650°C/5000 hrs.	100.0	16.8	2.8	-0.05	0.04	0.21	0.65
750°C/2 hrs.	96.0	16.0	3.8	-0.06	0.03	0.17	0.60
750°C/20 hrs.	62.0	15.0	3.2	-0.03	0.05	0.22	0.70
750°C/200 hrs.	51.0	12.0	3.1	-0.05	0.04	0.18	0.60
750°C/2000 hrs.	100.0	26.0	3.0	-0.05	0.04	0.23	0.60
750°C/5000 hrs.	82.0	15.0	2.6	-0.04	0.05	0.20	0.65
1100°C/1 hr.	60.0	16.0	3.0	-0.02	0.07	0.20	0.65
Average Value	79.5	17.7	3.2	-0.05	0.04	0.20	0.63

Table 13. Electrochemical Parameters of Polarization Curves of Type 308-D Weld Metal

Heat Treatment	Current Density (10^{-6} Amperes/cm^2)			Potential (Volts, SHE)			
	I_1	I_2	I_p	E_c	E_1	E_2	E_p
As-welded	51.0	13.5	2.7	-0.05	0.05	0.22	0.65
650°C/2 hrs.	50.0	15.0	3.2	-0.04	0.03	0.20	0.60
650°C/20 hrs.	21.0	17.0	2.2	-0.04	0.03	0.22	0.65
650°C/200 hrs.	24.0	12.0	2.4	-0.04	0.04	0.20	0.65
650°C/2000 hrs.	47.0	13.0	2.7	-0.04	0.04	0.20	0.60
650°C/5000 hrs.	50.0	18.0	2.4	-0.05	0.02	0.20	0.60
750°C/2 hrs.	38.0	13.0	3.1	-0.04	0.03	0.18	0.60
750°C/200 hrs.	36.0	12.5	2.6	-0.04	0.03	0.20	0.65
750°C/2000 hrs.	35.0	21.0	2.7	-0.03	0.03	0.22	0.65
750°C/5000 hrs.	25.0	12.0	2.0	-0.04	0.03	0.22	0.70
1100°C/1 hr.	43.5	17.0	2.3	-0.03	0.06	0.20	0.62
Average Value	38.2	14.9	2.6	-0.04	0.03	0.20	0.63

Table 14. Electrochemical Parameters of Polarization Curves of Type 316L-A Weld Metal

Heat Treatment	Current Density (10^{-6} Amperes/cm^2)			Potential (Volts, SHE)			
	I_1	I_2	I_p	E_c	E_1	E_2	E_p
As-welded	40.0	15.0	2.5	0.02	0.14	0.21	0.65
650°C/2 hrs.	25.	22.0	2.6	0.00	0.10	0.23	0.65
650°C/20 hrs.	22.0	10.0	3.0	0.00	0.10	0.21	0.65
650°C/200 hrs.	25.0	10.2	3.0	-0.02	0.10	0.20	0.65
650°C/2000 hrs.	41.0	20.0	2.7	0.00	0.10	0.21	0.60
650°C/5000 hrs.	17.0	11.5	3.0	-0.02	0.11	0.20	0.60
750°C/2 hrs.	45.0	12.0	2.7	-0.01	0.07	0.22	0.60
750°C/20 hrs.	54.0	15.0	3.0	-0.01	0.05	0.22	0.65
750°C/200 hrs.	30.0	20.0	3.3	0.00	0.10	0.22	0.65
750°C/2000 hrs.	19.5	11.2	3.3	0.00	0.12	0.20	0.65
750°C/5000 hrs.	21.5	11.5	4.0	0.00	0.12	0.20	0.60
1100°C/1 hr.	17.0	13.0	2.9	0.00	0.13	0.23	0.65
Average Value	29.8	13.6	3.0	-0.01	0.10	0.21	0.63

Table 15. Electrochemical Parameters of Polarization Curves of Type 316L-D Weld Metal

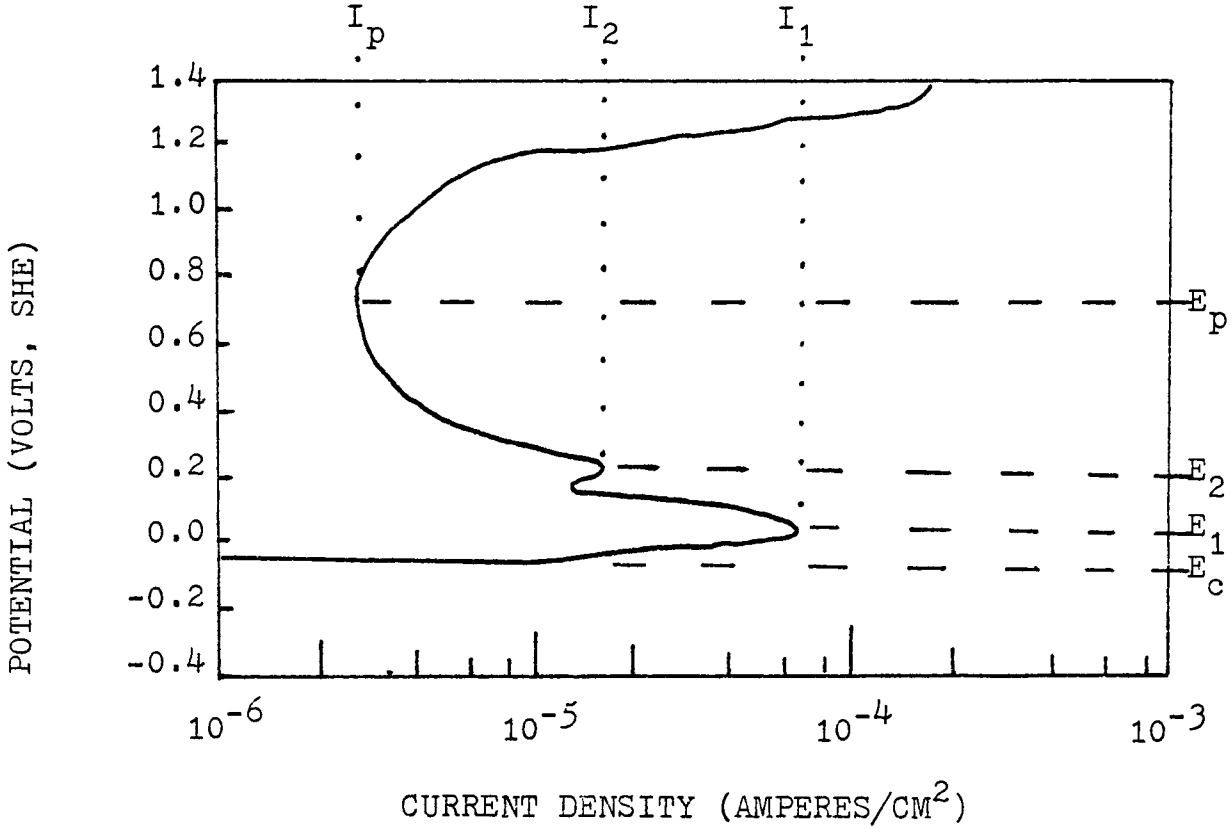
Heat Treatment	Current Density (10^{-6} Amperes/cm^2)			Potential (Volts, SHE)			
	I_1	I_2	I_p	E_c	E_1	E_2	E_p
As-welded	34.5	13.0	2.2	0.00	0.13	0.22	0.65
650°C/2 hrs.	14.0	9.5	2.8	0.02	0.13	0.22	0.62
650°C/20 hrs.	21.0	13.0	2.6	0.00	0.12	0.22	0.65
650°C/200 hrs.	17.0	21.0	2.9	0.00	0.10	0.22	0.60
650°C/5000 hrs.	13.0	16.0	2.9	0.00	0.12	0.22	0.62
750°C/2 hrs.	11.5	8.5	3.1	0.00	0.13	0.21	0.60
750°C/20 hrs.	25.0	16.0	2.9	0.00	0.13	0.22	0.65
750°C/200 hrs.	26.0	12.0	3.0	0.00	0.13	0.22	0.65
750°C/2000 hrs.	22.5	21.0	2.9	-0.01	0.13	0.20	0.60
750°C/5000 hrs.	25.0	12.3	2.9	0.00	0.12	0.22	0.65
1100°C/1 hr.	10.0	8.6	2.7	0.00	0.10	0.22	0.65
Average Value	20.0	13.7	2.8	0.00	0.12	0.22	0.63

Table 16. Electrochemical Parameters of Polarization Curves of Type 308L-A Weld Metal

Heat Treatment	Current Density (10^{-6} Amperes/cm^2)			Potential (Volts, SHE)			
	I_1	I_2	I_p	E_c	E_1	E_2	E_p
As-welded	22.5	15.5	3.0	-0.02	0.06	0.20	0.65
650°C/2 hrs.	69.0	22.0	3.2	-0.01	0.06	0.22	0.62
650°C/20 hrs.	100.0	17.0	2.6	-0.05	0.05	0.20	0.65
650°C/200 hrs.	210.0	17.0	2.7	-0.05	0.05	0.20	0.65
650°C/2000 hrs.	136.0	15.0	2.5	-0.05	0.05	0.20	0.55
650°C/5000 hrs.	40.0	10.0	2.5	-0.03	0.06	0.20	0.60
750°C/2 hrs.	110.0	15.0	3.0	-0.05	0.05	0.20	0.60
750°C/20 hrs.	69.0	21.0	3.2	-0.04	0.05	0.22	0.65
750°C/200 hrs.	110.0	20.0	3.2	-0.04	0.05	0.23	0.65
750°C/2000 hrs.	47.0	22.0	3.1	-0.04	0.04	0.22	0.65
750°C/5000 hrs.	150.0	26.0	3.1	-0.44	0.04	0.22	0.60
1100°C/1 hr.	31.0	11.8	2.8	-0.02	0.06	0.20	0.60
Average Value	91.2	17.7	2.9	-0.04	0.05	0.21	0.62

Table 17. Electrochemical Parameters of Polarization Curves of Type 308L-D Weld Metal

Heat Treatment	Current Density (10^{-6} Amperes/cm^2)			Potential (Volts, SHE)			
	I_1	I_2	I_p	E_c	E_1	E_2	E_p
As-welded	24.0	10.0	2.6	-0.03	0.04	0.20	0.60
650°C/2 hrs.	70.0	14.0	2.4	-0.04	0.02	0.20	0.65
650°C/20 hrs.	34.0	15.0	2.5	-0.03	0.04	0.20	0.65
650°C/200 hrs.	40.0	12.0	2.8	-0.05	0.05	0.18	0.60
650°C/2000 hrs.	40.5	20.5	2.4	-0.04	0.02	0.20	0.65
650°C/5000 hrs.	25.0	11.0	2.7	-0.05	0.05	0.21	0.65
750°C/2 hrs.	60.0	11.0	2.4	-0.05	0.03	0.18	0.60
750°C/20 hrs.	40.0	15.0	2.4	-0.03	0.03	0.20	0.65
750°C/200 hrs.	46.0	17.0	2.8	-0.04	0.03	0.22	0.62
750°C/2000 hrs.	28.0	19.5	2.8	-0.04	0.03	0.22	0.65
750°C/5000 hrs.	105.0 25.0	23.0	2.5	-0.05	0.02	0.20	0.65
1100°C/1 hr.	25.0	10.0	2.2	-0.03	0.10	0.20	0.65
Average Value	44.8	14.8	2.5	-0.04	0.04	0.20	0.63



Definition of terms:

E_c - Corrosion potential
E_1 - Primary passive potential (Critical potential)
E_2 - Secondary passive potential
E_p - Minimum passive potential
I_1^p - Primary passive current density (Critical current density)
I_2 - Secondary passive current density
I_p^2 - Minimum passive current density

Figure 35. Typical Anodic Polarization Curve Obtained in This Investigation

passive current density as a function of heat treatment is plotted in Figures 36 through 39. It is evident that ferrite content has a significant effect on the passive current density of the polarization curves, particularly for the specimens aged for shorter aging times. High ferrite content welds have lower passive current densities than the low ferrite content welds. The reason for this beneficial role of ferrite in austenitic stainless steel welds aged during the sensitization period are as follows: (1) The total area of grain boundaries and phase interface is increased in the presence of ferrite, thereby reducing the quantity of carbide predipitates per unit area; (2) The ferrite is significantly higher in chromium than is the austenite. Therefore, it can lose chromium to a grain boundary precipitate and not become sufficiently depleted to be preferentially attacked; (3) Chromium diffuses more readily in ferrite than austenite so there is less chromium depletion; (4) The islands of ferrite present minimize the formation of continuous grain bouncary precipitates in the austenite grain boundaries. After longer aging times, the chromium will diffuse back into the chromium depleted region. The susceptibility to intergranular attack will be reduced and the difference of passive current densities between low ferrite and high ferrite level welds becomes smaller and smaller. This is also observed in Figures 36 through 39.

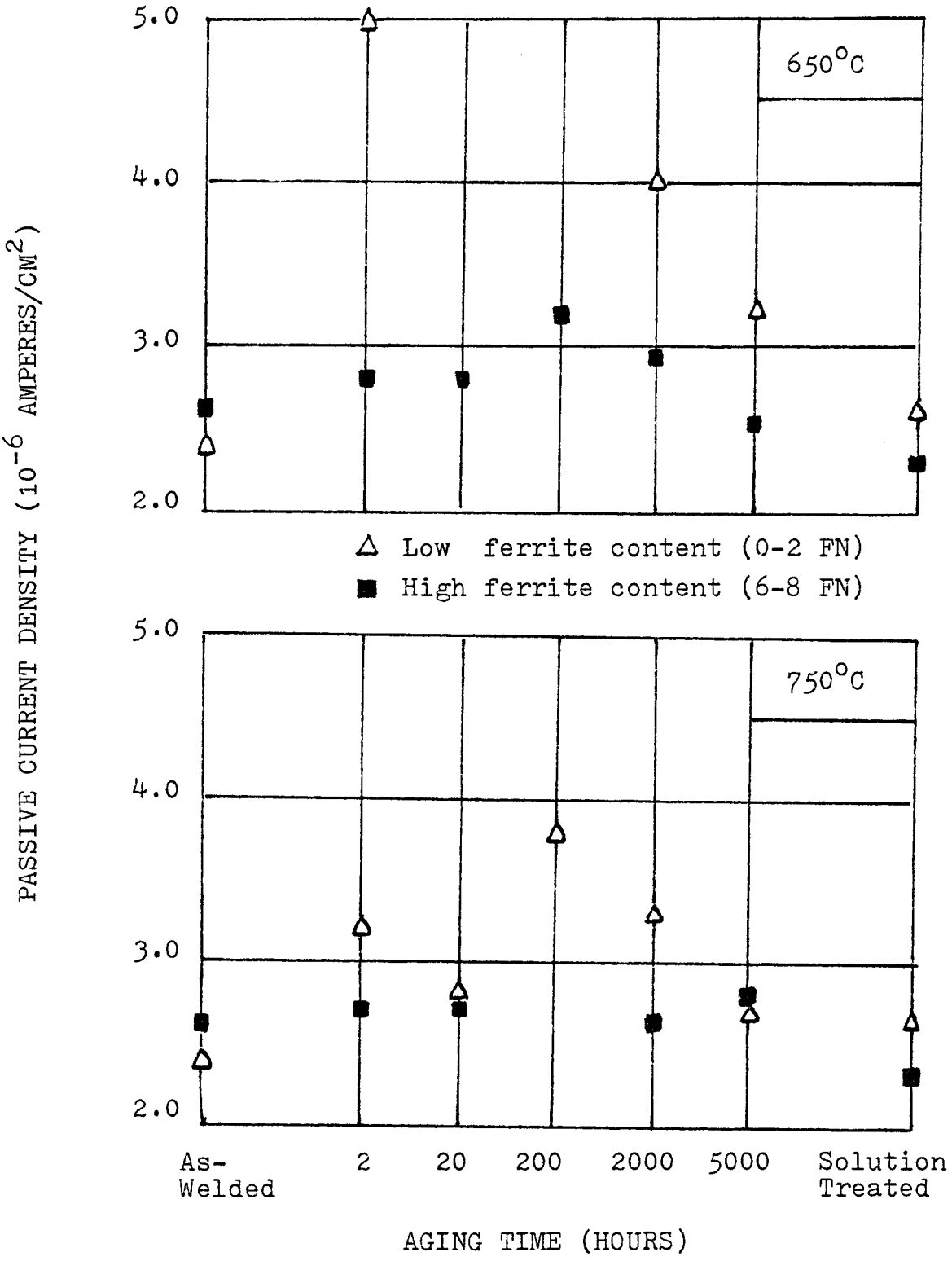


Figure 36. Passive Current Density as A Function of Heat Treatment for Type 316 Welds

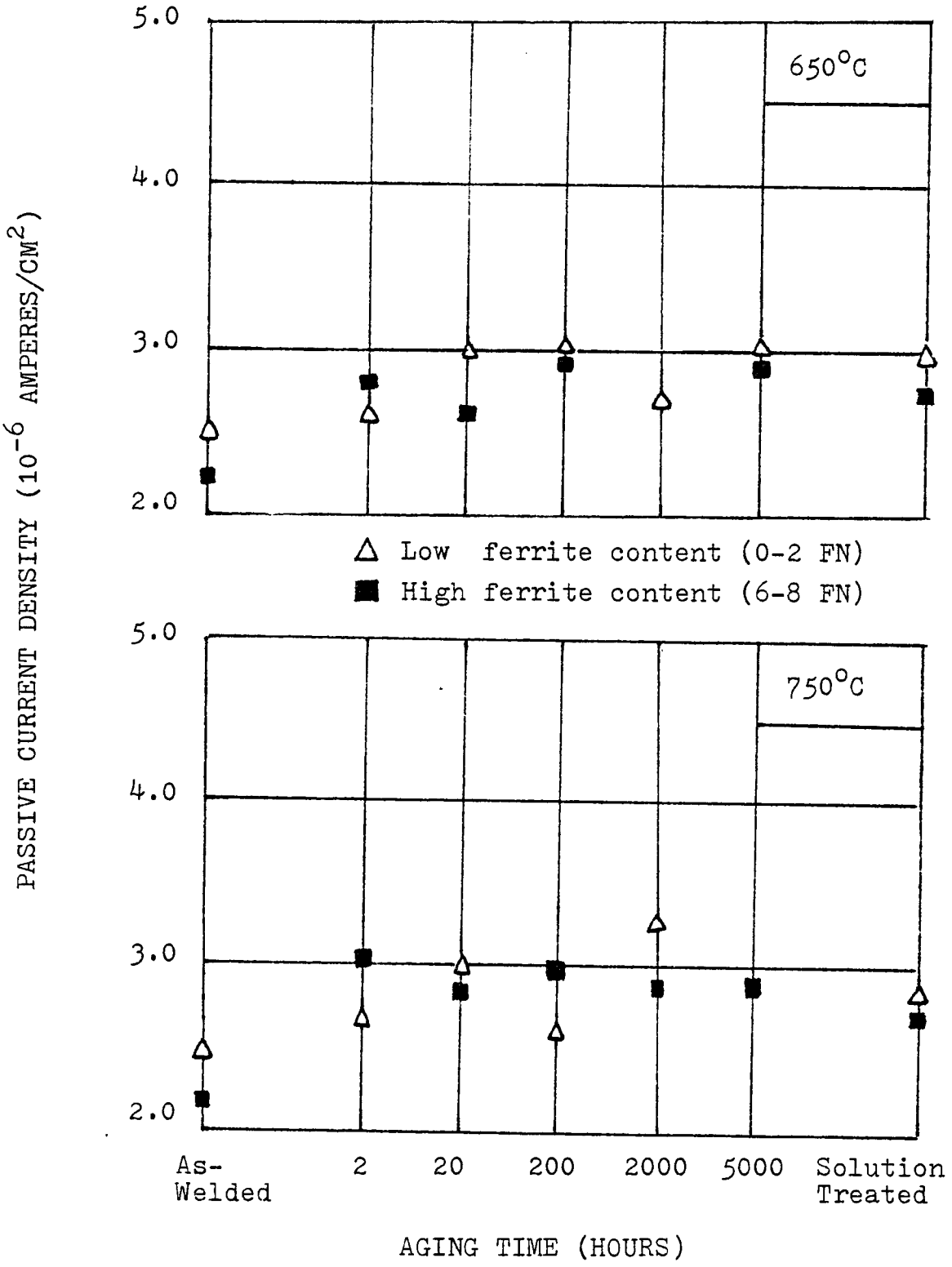


Figure 37. Passive Current Density as A Function of Heat Treatment for Type 316L Welds

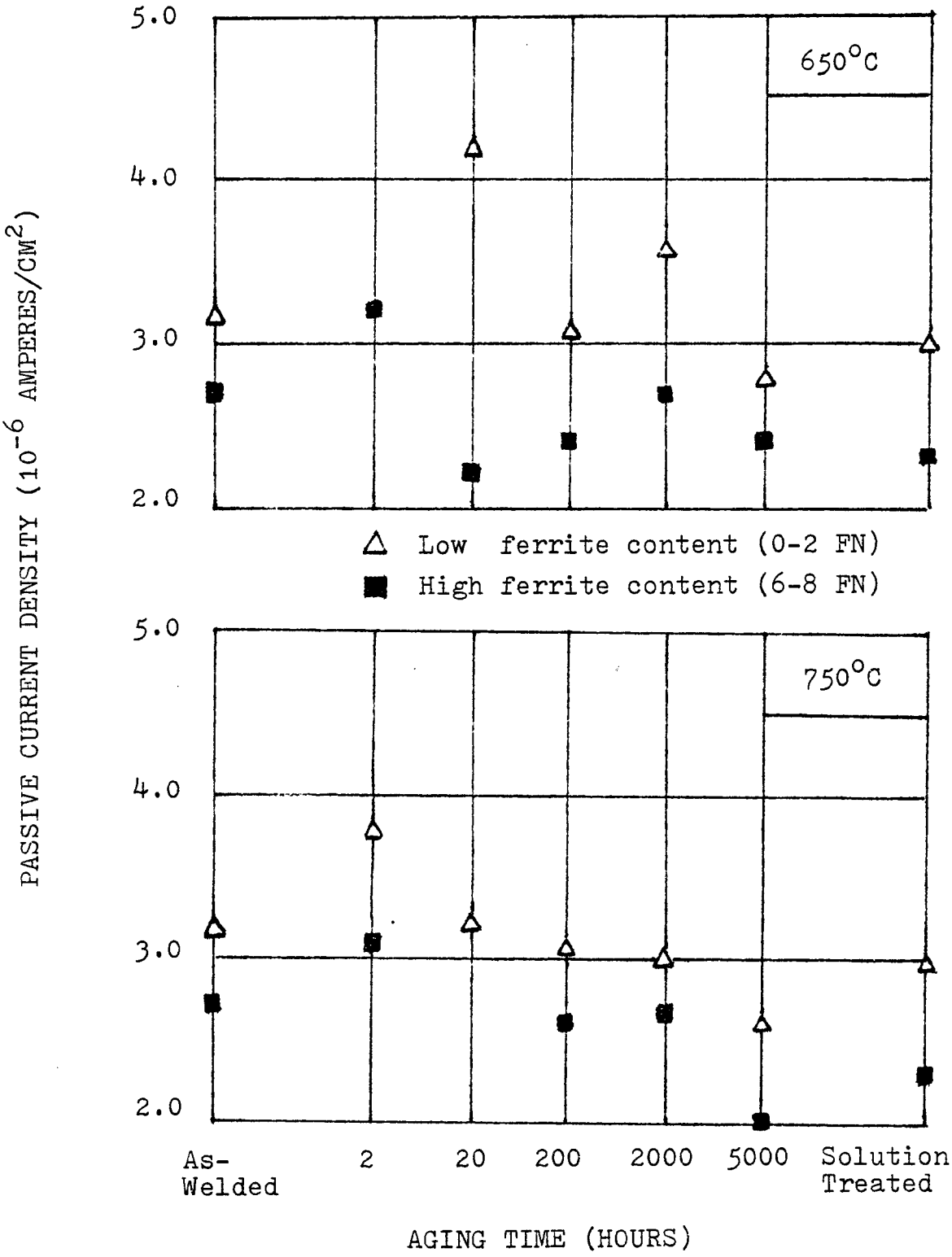


Figure 38. Passive Current Density as A Function of Heat Treatment for Type 308 Welds

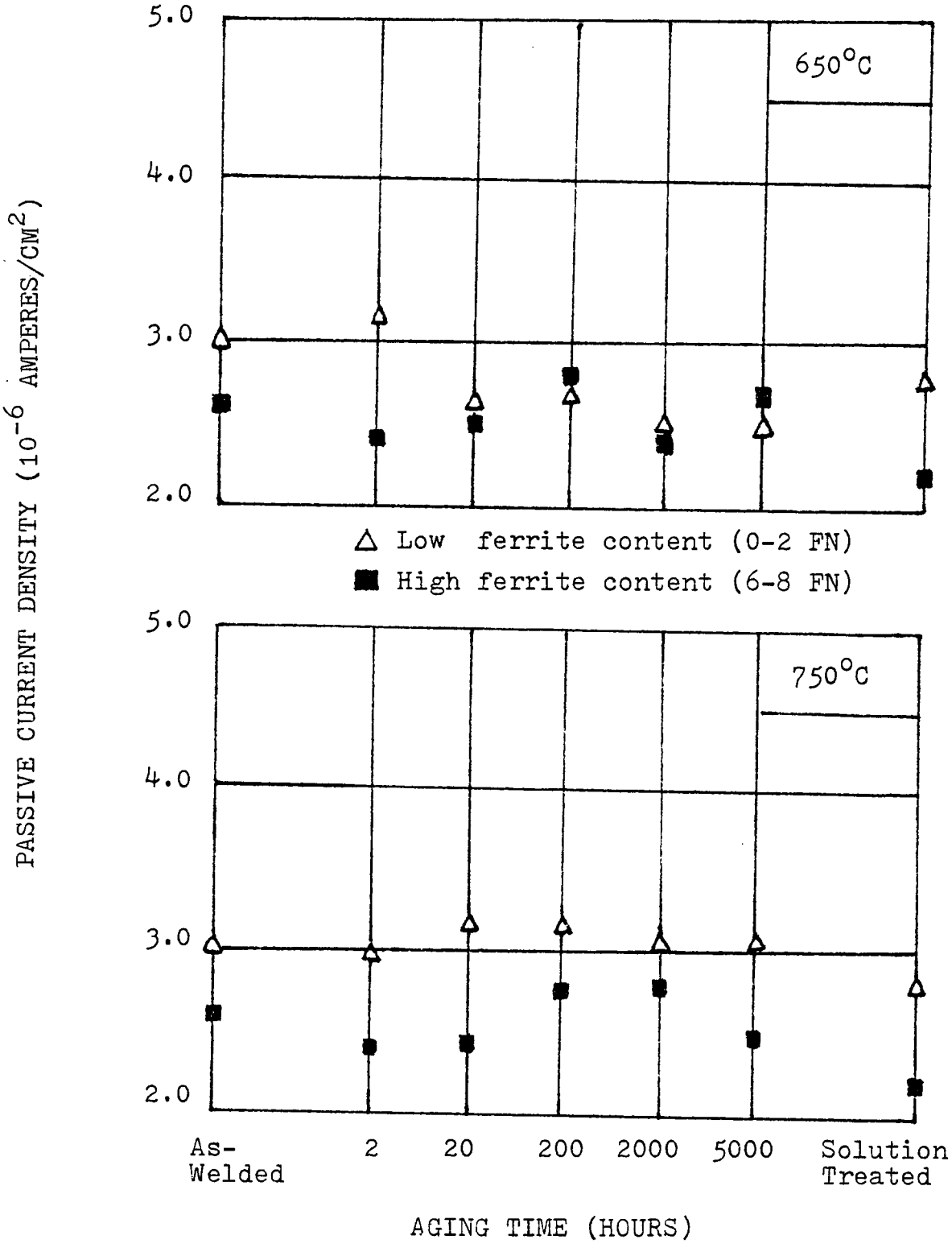


Figure 39. Passive Current Density as A Function of Heat Treatment for Type 308L Welds

The critical current density as a function of heat treatment for all alloys studied are plotted in Figures 40 through 43. It is clear that high ferrite content welds have low critical current densities. This is probably due to the compositional effect. Reference to Table 2, page 40, shows that high ferrite metals have greater chromium and carbon contents than the low ferrite metals have. This is consistent with Greene and Wilde's results[56] in which they found that chromium, carbon, and molybdenum contents can decrease the critical current densities of stainless steel 304 in 1N H_2SO_4 at 30°C.

In order to compare the general characteristics of the anodic polarization curves for all types of stainless steel weld metals, the average values of the electrochemical parameters of each type weld were calculated and listed in Table 18. Several features are observed as follows:

(1) Both the passive current density and critical current density are lower in the high ferrite content welds than in the low ferrite content welds.

(2) The difference of passive current densities between low carbon grade and high carbon grade steels is larger in the low ferrite content welds than in the high ferrite content welds.

(3) The critical current densities of low carbon grade steels are higher than the high carbon grade steels. The difference of critical current densities between

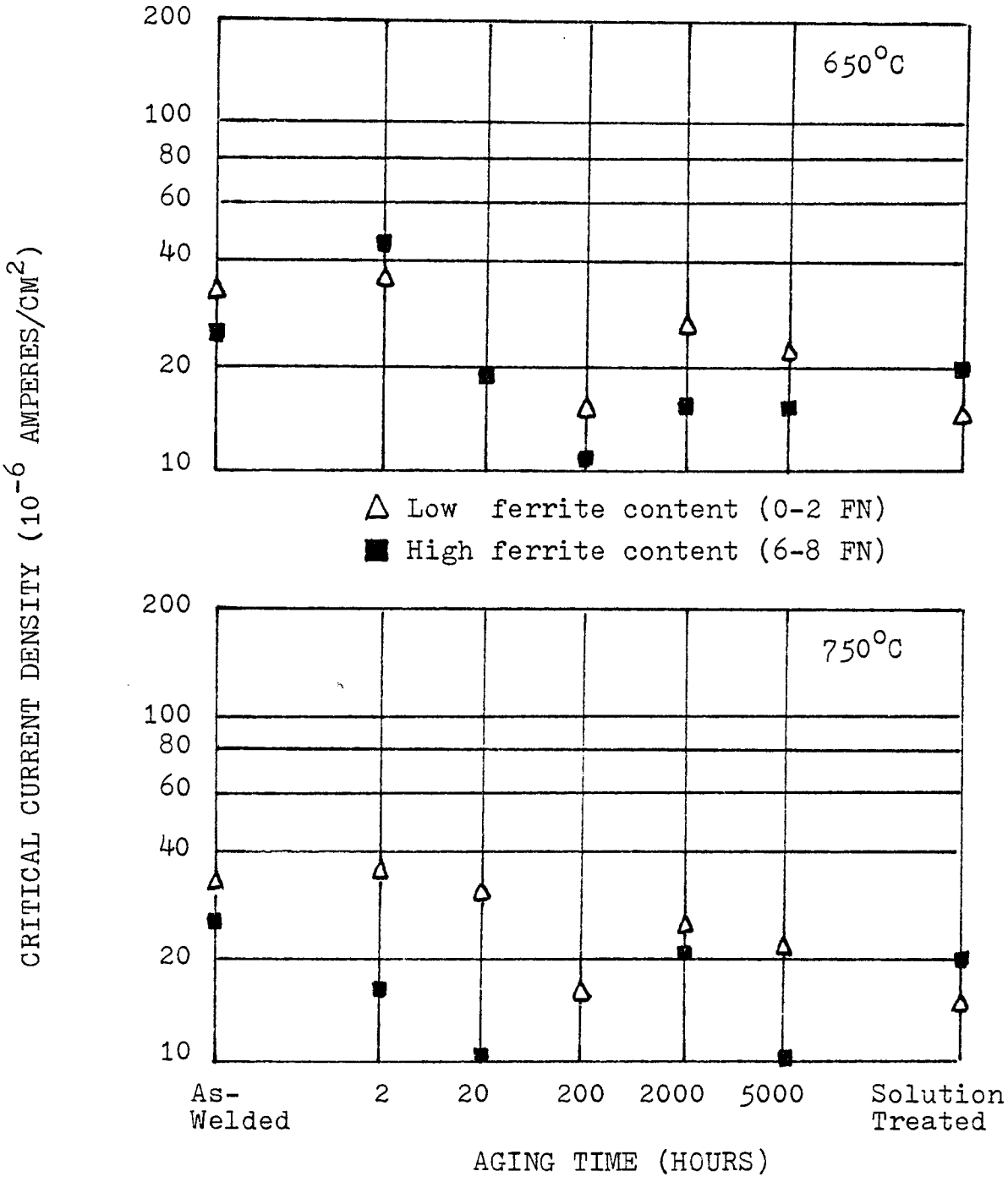


Figure 40. Critical Current Density as A Function of Heat Treatment for Type 316 Welds

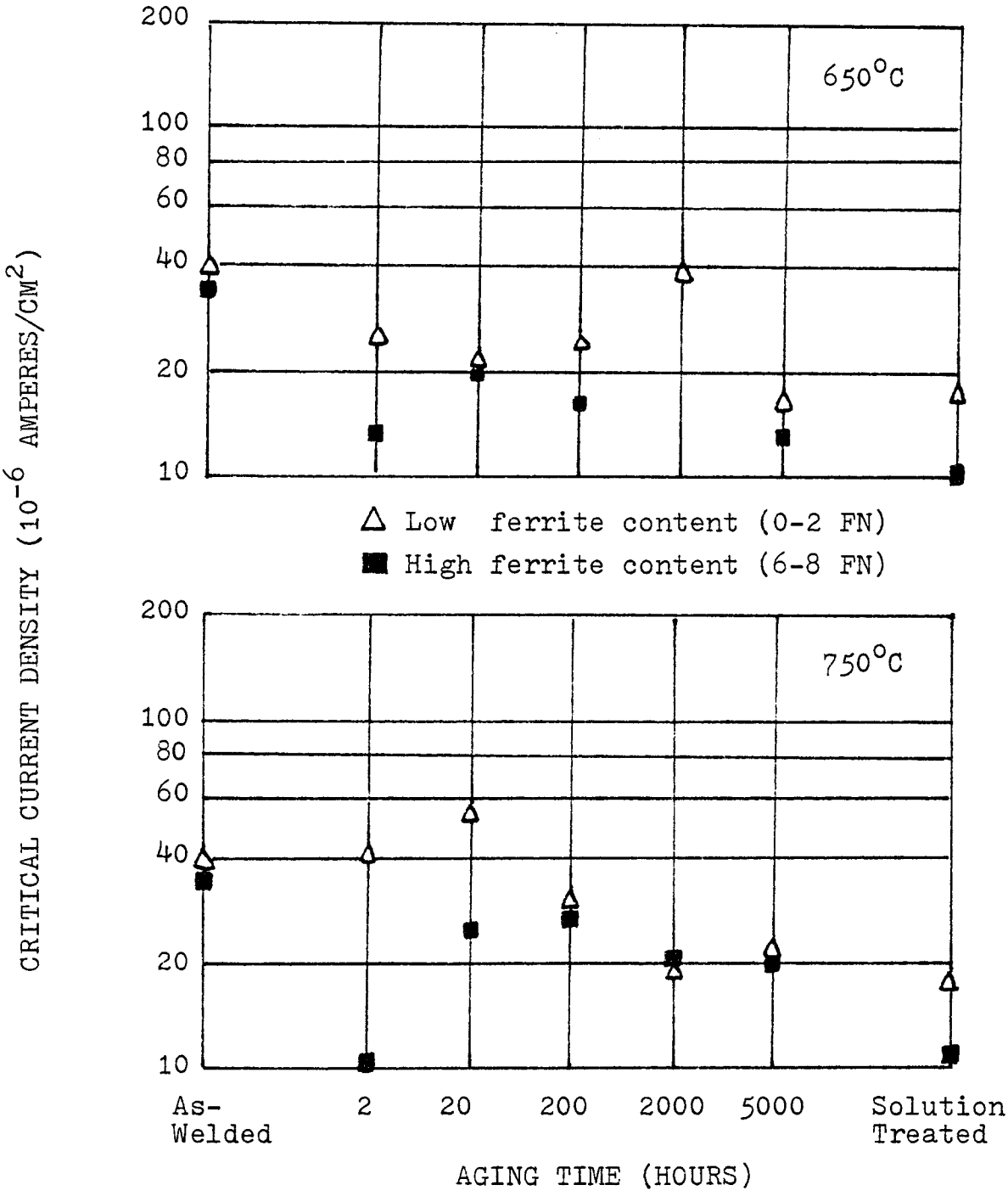


Figure 41. Critical Current Density as A Function of Heat Treatment for Type 316L Welds

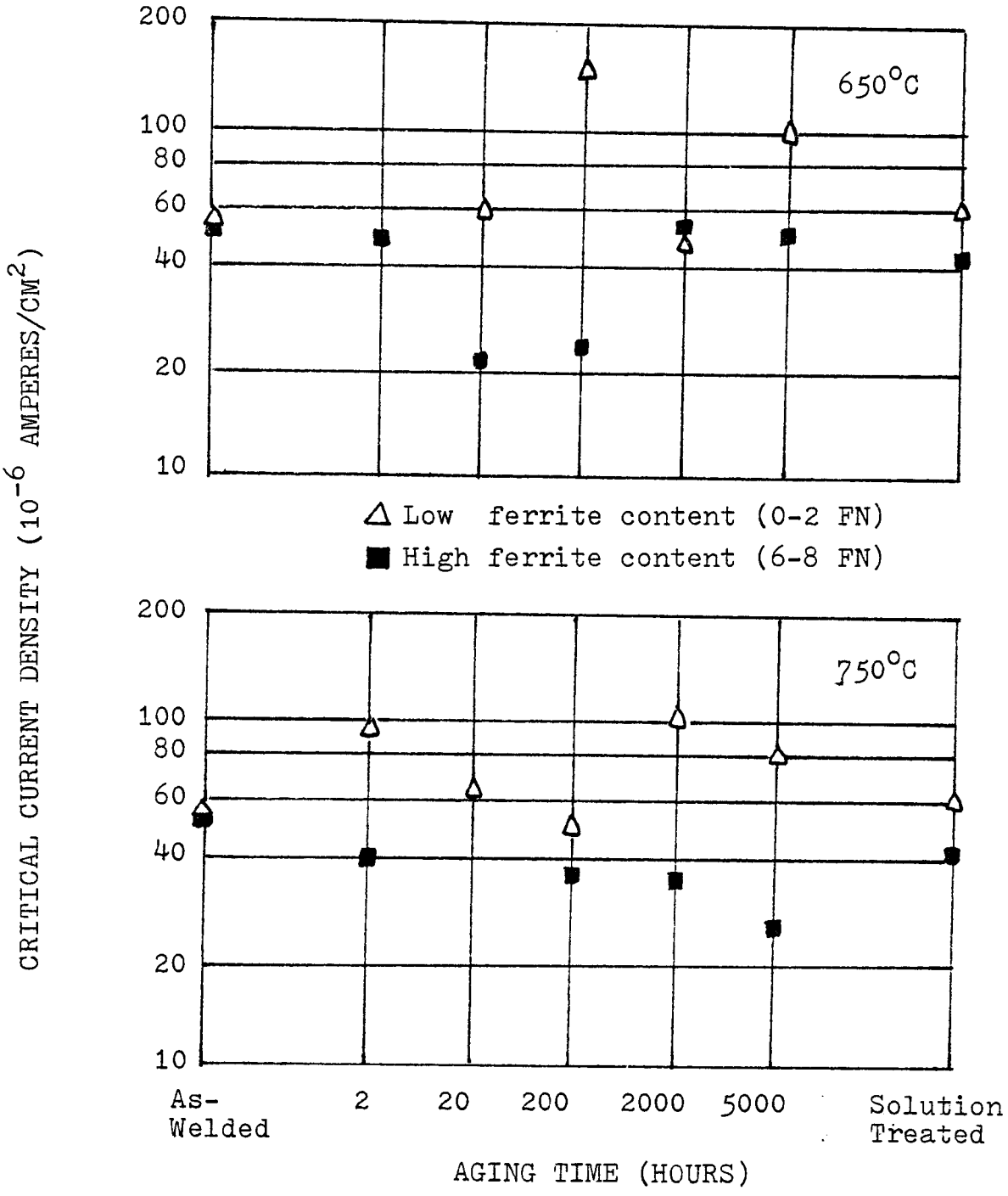


Figure 42. Critical Current Density as A Function of Heat Treatment for Type 308 Welds

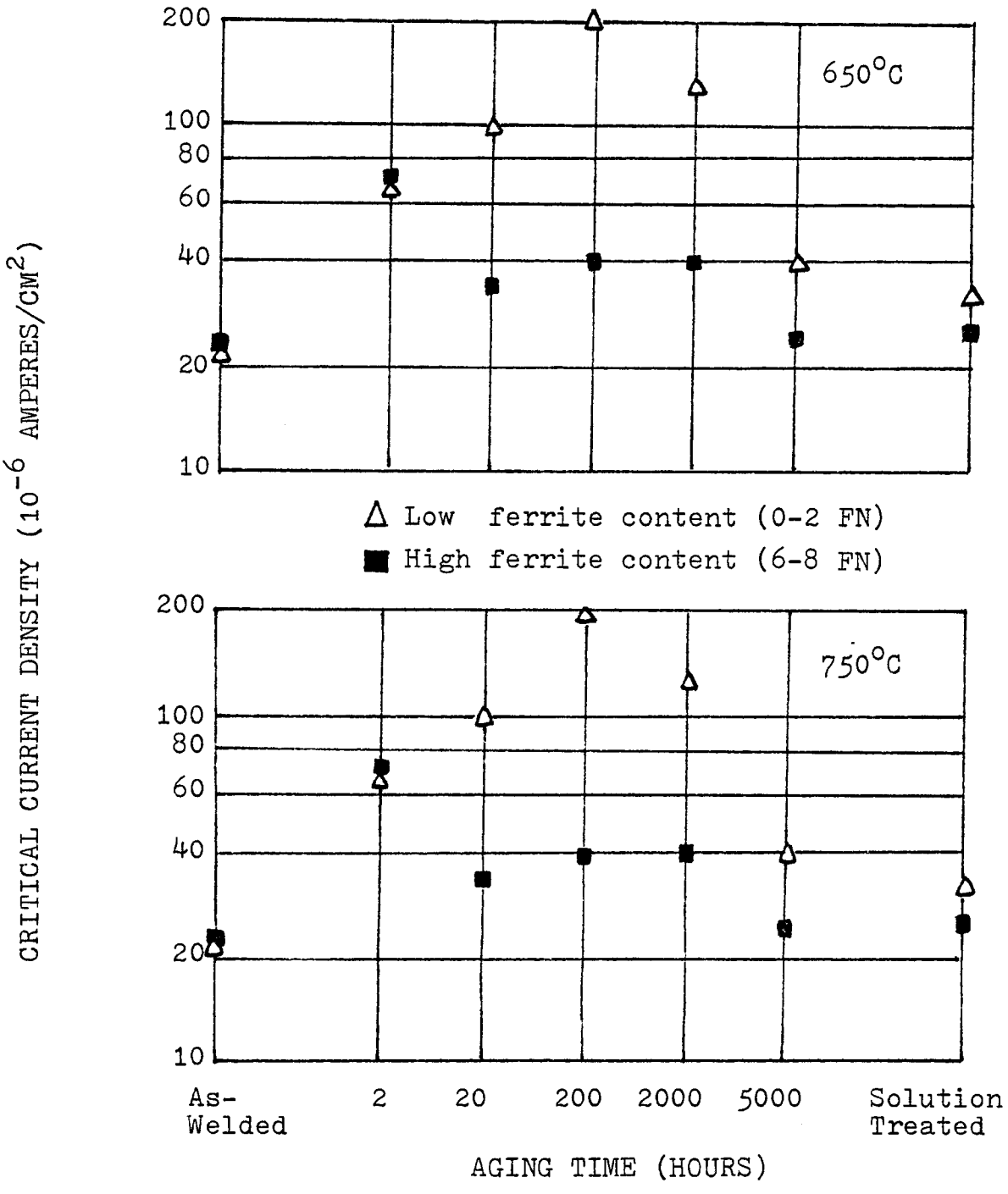


Figure 43. Critical Current Density as A Function of Heat Treatment for Type 308L Welds

Table 18. Average Values of Electrochemical Parameters for Each Type of Stainless Steel Weld Metal

Weld Metal	Current Density (10^{-6} Amperes/cm^2)			Potential (Volts, SHE)			
	I_1	I_2	I_p	E_c	E_1	E_2	E_p
316L-A	29.8	13.6	3.0	-0.01	0.10	0.21	0.63
316L-D	20.0	13.7	2.8	0.00	0.12	0.22	0.63
316-A	26.1	16.3	3.3	-0.02	0.11	0.21	0.62
316-D	19.1	11.8	2.7	-0.01	0.11	0.21	0.63
308L-A	91.2	17.7	2.9	-0.04	0.05	0.21	0.62
308L-D	44.8	14.8	2.5	-0.04	0.04	0.20	0.63
308-A	79.5	17.7	3.2	-0.05	0.04	0.20	0.63
308-D	38.2	14.9	2.6	-0.04	0.03	0.20	0.63

low carbon grade and high carbon grade welds is again larger in the low ferrite metals than in the high ferrite metals.

(4) Type 316 welds have lower critical current densities than type 308 welds have. There is no difference between the passive current densities of type 316 and 308 welds.

(5) The corrosion potentials and the critical potentials do not change during heat treatments at least in the experimental error range.

(6) The corrosion potentials of type 316 welds are about 35 mV higher than the corrosion potentials of type 308 welds. Also the critical potentials of type 316 welds are 65 mV higher than that of type 308 welds.

From the results of section I and II, it is found that more sigma phase forms in high ferrite content welds than in low ferrite content welds during aging. The lower passive current density of high ferrite weld metals shows that chromium depletion in the boundary itself was the cause of attack rather than the precipitates themselves. It is felt that the distribution of chromium was a major cause of the intergranular corrosion in aged austenitic stainless steel weld metals.

It is also found that the chemical composition played an important role in controlling the corrosion resistance of austenitic stainless steel weld metals in 1N H_2SO_4 at

room temperature. Increased chromium, molybdenum, and carbon favors reduced critical current densities in 1N H_2SO_4.

Controlled Potential Corrosion Test and
Scanning Electron Microscope Studies

Controlled potential corrosion tests were conducted in a solution of 5% H_2SO_4 and 0.1 g/l NH_4SCN at room temperature (25°C ± 2°C). All tests were run in the polarization cell which facilitated measurement and control of specimen potential (measured relative to a SHE with a Luggin probe).

Three etching potentials were used in this test. They are: (a) + 0.02 Volts (SHE) in the active region; (b) + 0.10 Volts (SHE) at the beginning of passivity; (c) + 1.40 Volts (SHE) at the beginning of transpassivity. The etching times varied from one minute to ten minutes depending on the current densities at that potential.

Figure 44 shows the effect of etching potential on the microstructures of austenitic stainless steel weld type 308 A aged 20 hours at 750°C. It is shown that in the active region corrosive attack depends on the orientation of the grains. There is much difference between etching at the beginning of passivity and etching at the beginning of transpassivity as is shown in Figure 44. This is also shown in Figures 45 through 47. The microstructures of type 308L welds aged two hours at 650°C and 2000 hours at 750°C are shown in Figure 45 and Figure 46, respectively. Figure 47 shows the microstructures of type 308 welds aged

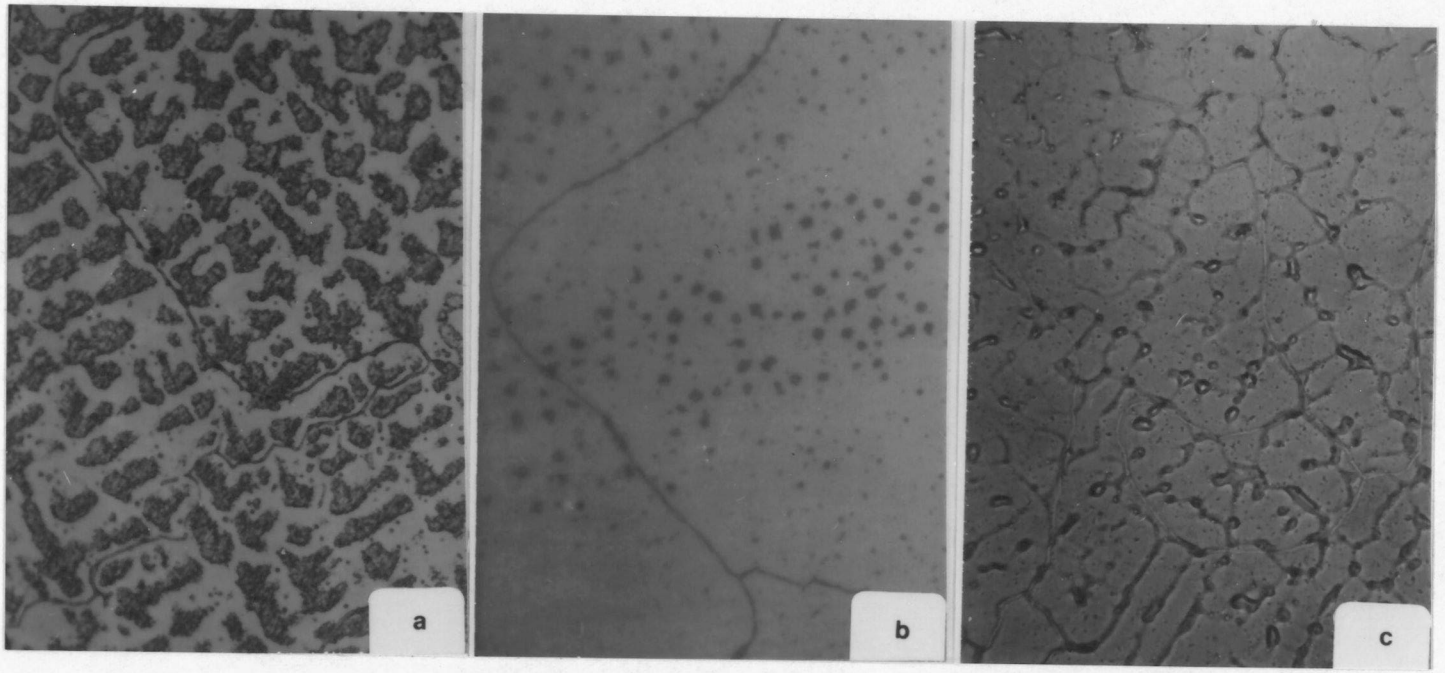


Figure 44. Microstructures of Type 308-A Weld Aged 20 Hours at 650°C. (500X)
(a) Etched 2 Minutes at + 0.02 V. (SHE);
(b) Etched 10 Minutes at + 0.10 V. (SHE);
(c) Etched 1¼ Minutes at + 1.40 V. (SHE).

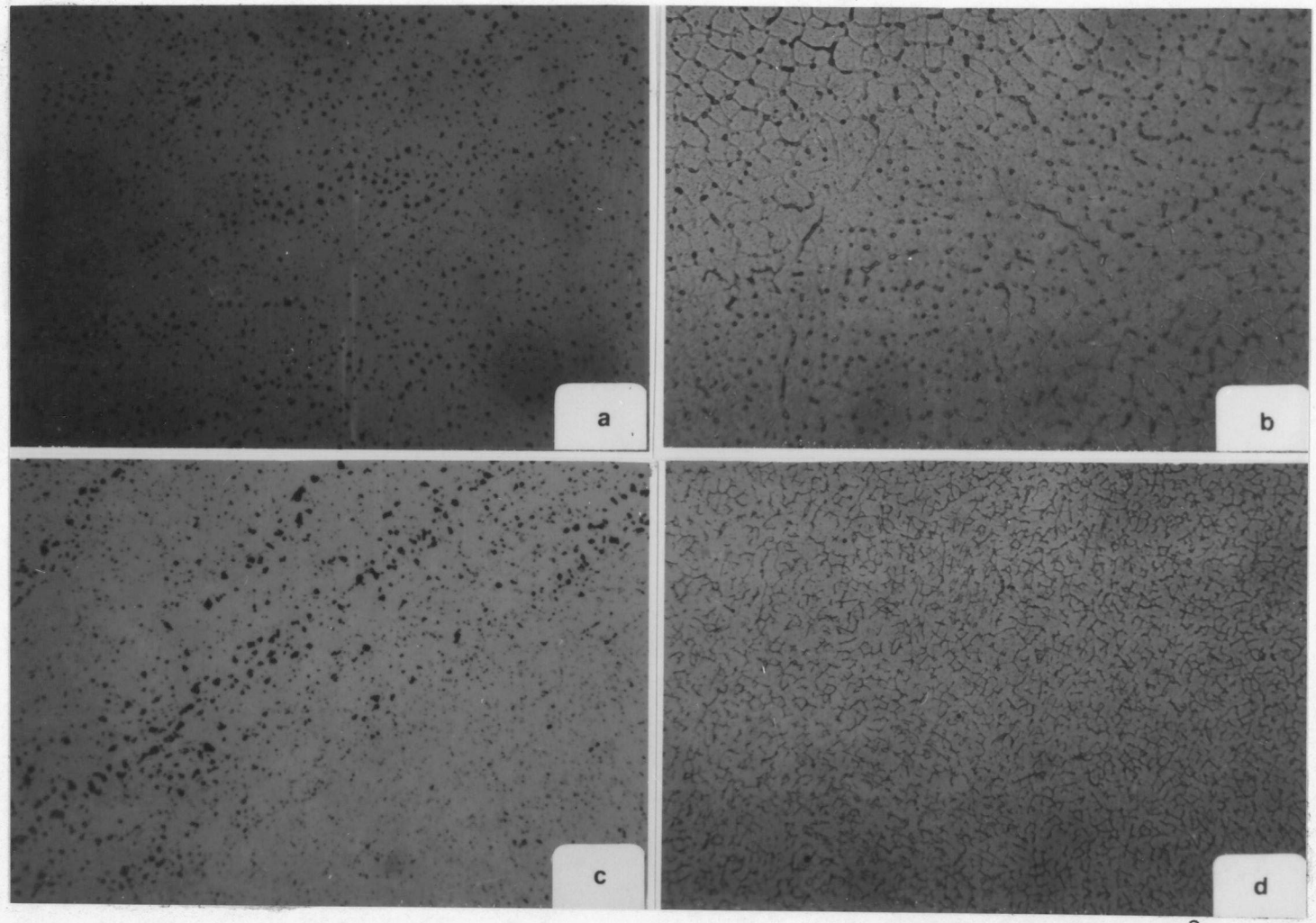


Figure 45. Microstructures of Type 308 Welds Aged Two Hours at 650°C. (200X)
(a) 308L-A, 10 Minutes at + 0.10 V. (SHE);
(b) 308L-A, 1½ Minutes at + 1.40 V. (SHE);
(c) 308L-D, 10 Minutes at + 0.10 V. (SHE);
(d) 308L-D, 1½ Minutes at + 1.40 V. (SHE).

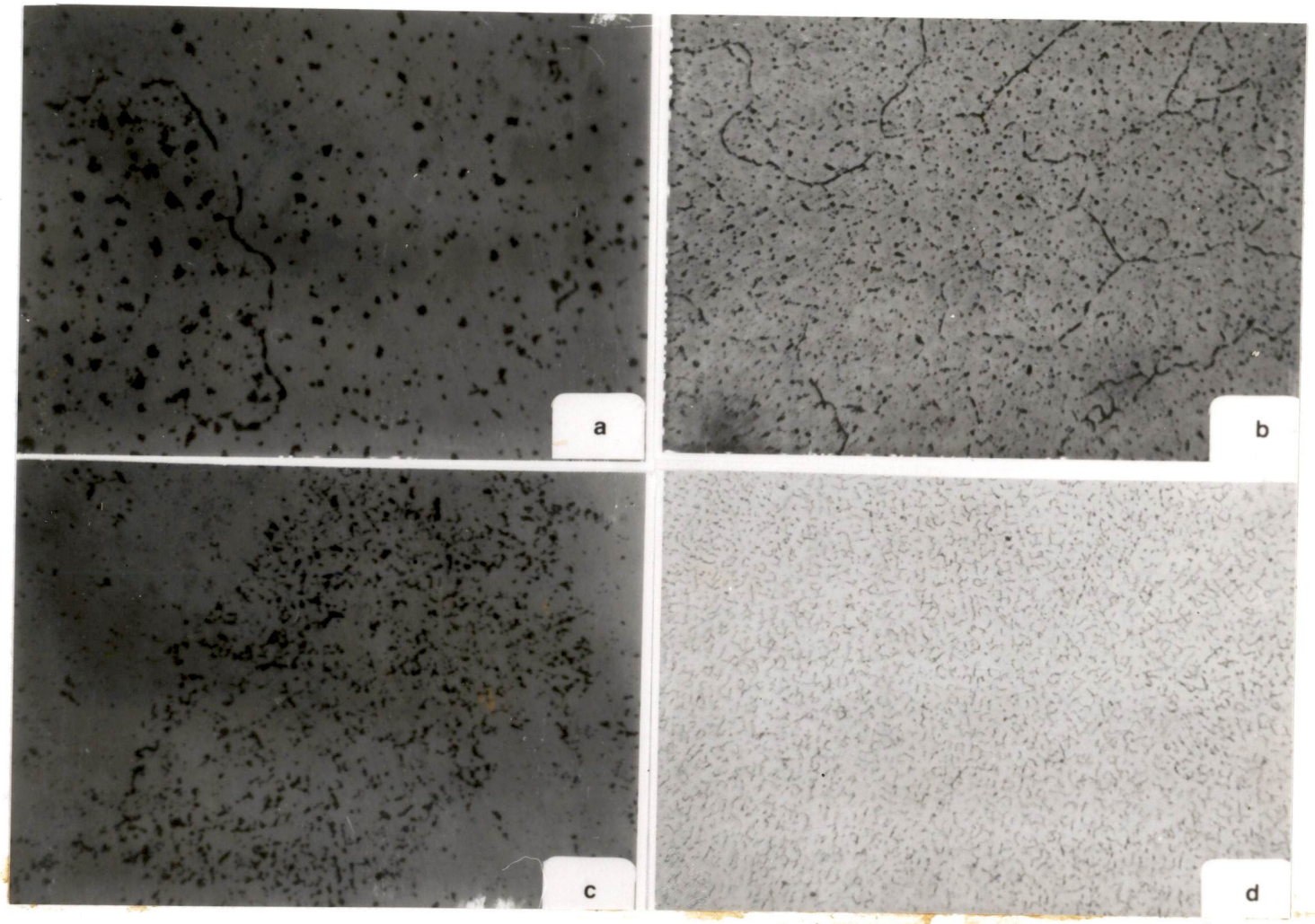


Figure 46. Microstructures of Type 308L Welds Aged 2000 Hours at 750°C. (200X)
(a) 308L-A, 8 Minutes at + 0.10 V. (SHE);
(b) 308L-A, 2 Minutes at + 1.40 V. (SHE);
(c) 308L-D, 8 Minutes at + 0.10 V. (SHE);
(d) 308L-D, 2 Minutes at + 1.40 V. (SHE).

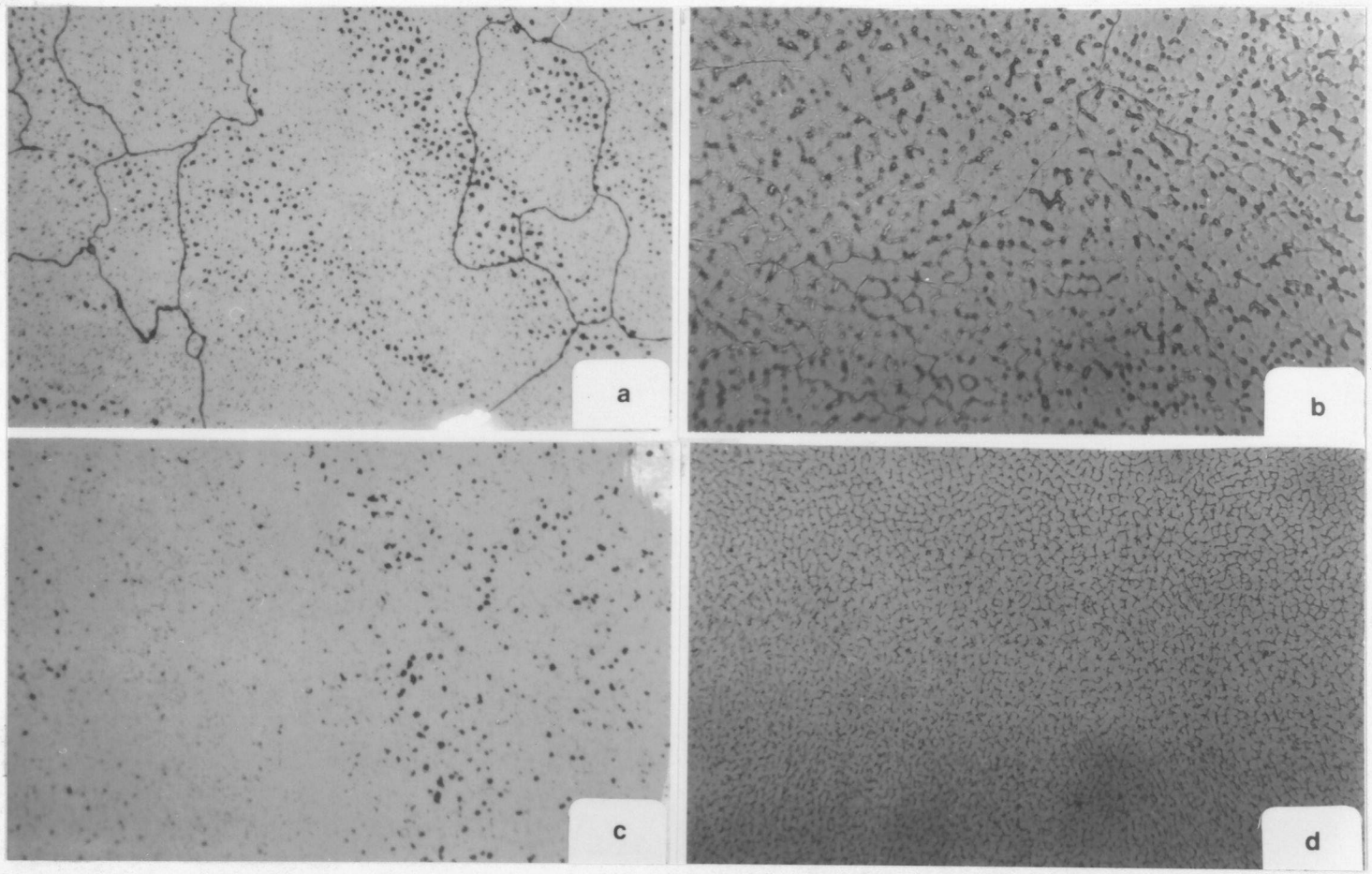


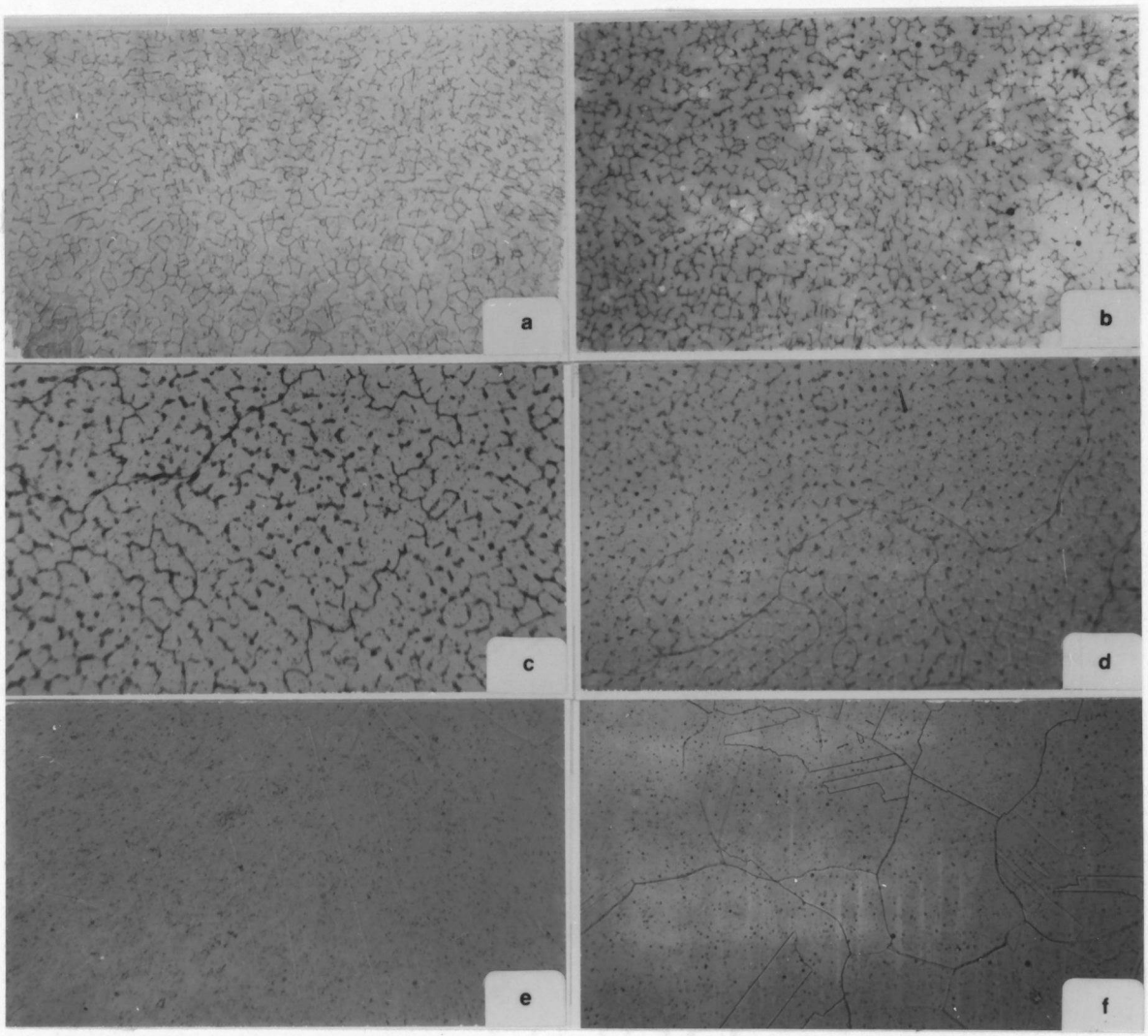
Figure 47. Microstructures of Type 308 Welds Aged 20 Hours at 650°C. (200X)
(a) 308-A, 10 Minutes at + 0.10 V. (SHE);
(b) 308-A, 1¼ Minutes at + 1.40 V. (SHE);
(c) 308-D, 10 Minutes at + 0.10 V. (SHE);
(d) 308-D, 1¼ Minutes at + 1.40 V. (SHE).

20 hours at 650°C.

It is found that specimens etched beyond + 1.40 volts (SHE) have the same microstructures as etched electrically in the conventional etching solution for austenitic stainless steel (25 gm CrO_3, 133 ml acetic acid, 7 ml H_2O). This is shown in Figure 48. The reason is that beyond + 1.40 volts both etching solutions attack the chromium-rich region in the specimen.

In Figures 45 through 47 it is observed that in high ferrite content welds the corrosive attack is uniformly distributed around the second phases. While in the low ferrite welds attack was also concentrated along the austenite grain boundaries. This is also shown at higher magnification in Figures 49 and 50 for high carbon grade and low carbon grade welds respectively. In practical application this is harmful since the attacked grain boundaries will become the starting sits of stress cracking.

In this investigation it is also found that sigma and remaining ferrite can corrode rapidly beyond the transpassive region (highly oxidizing condition). This is shown in Figures 49a and 50b also. The characteristic X-ray spectra of the precipitate (A) and matrix (B) shows that the attacked phases are either sigma phase or remaining ferrite. Since ferrite will enhance the formation of sigma phase, it is suggest that under highly oxidizing condition ferrite control may be necessary to avoid heavy attack on the sigma phase.



(a), (c), (e): Etched 1-2 mins. at 9 V. in 25 gm CrO_3, 133 ml acetic acid, and 7 ml distilled water.
(b), (d), (f): Etched 1-2 mins. at +1.40 V. (SHE) in 5% H_2SO_4 and 0.1 g/l NH_4SCN.
(a) and (b): 308-D, 750°C/2 hrs.
(c) and (d): 316L-A, 650°C/5000 hrs.
(e) and (f); 316-D, 1100°C/1 hr.

Figure 48. Effect of Etching Solution on the Microstructures of Austenitic Stainless Steel Weld Metal. (200X)

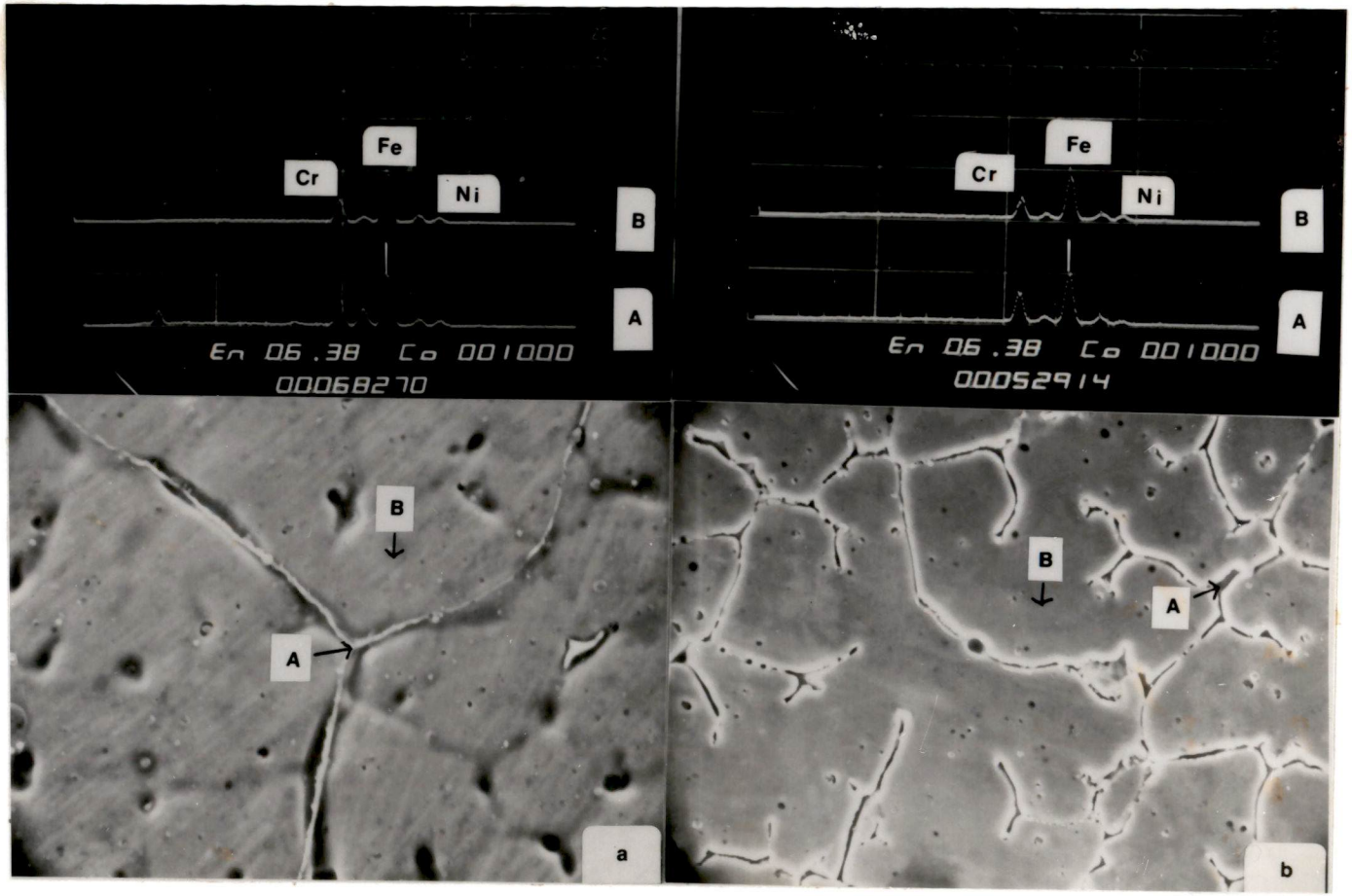


Figure 49. Microstructures of Type 308 Welds Aged Two Hours at 750°C. (2000X)
(a) Low Ferrite Weld Etched Two Minutes at + 1.40 Volts (SHE);
(b) High Ferrite Weld Etched Two Minutes at + 1.40 Volts (SHE).

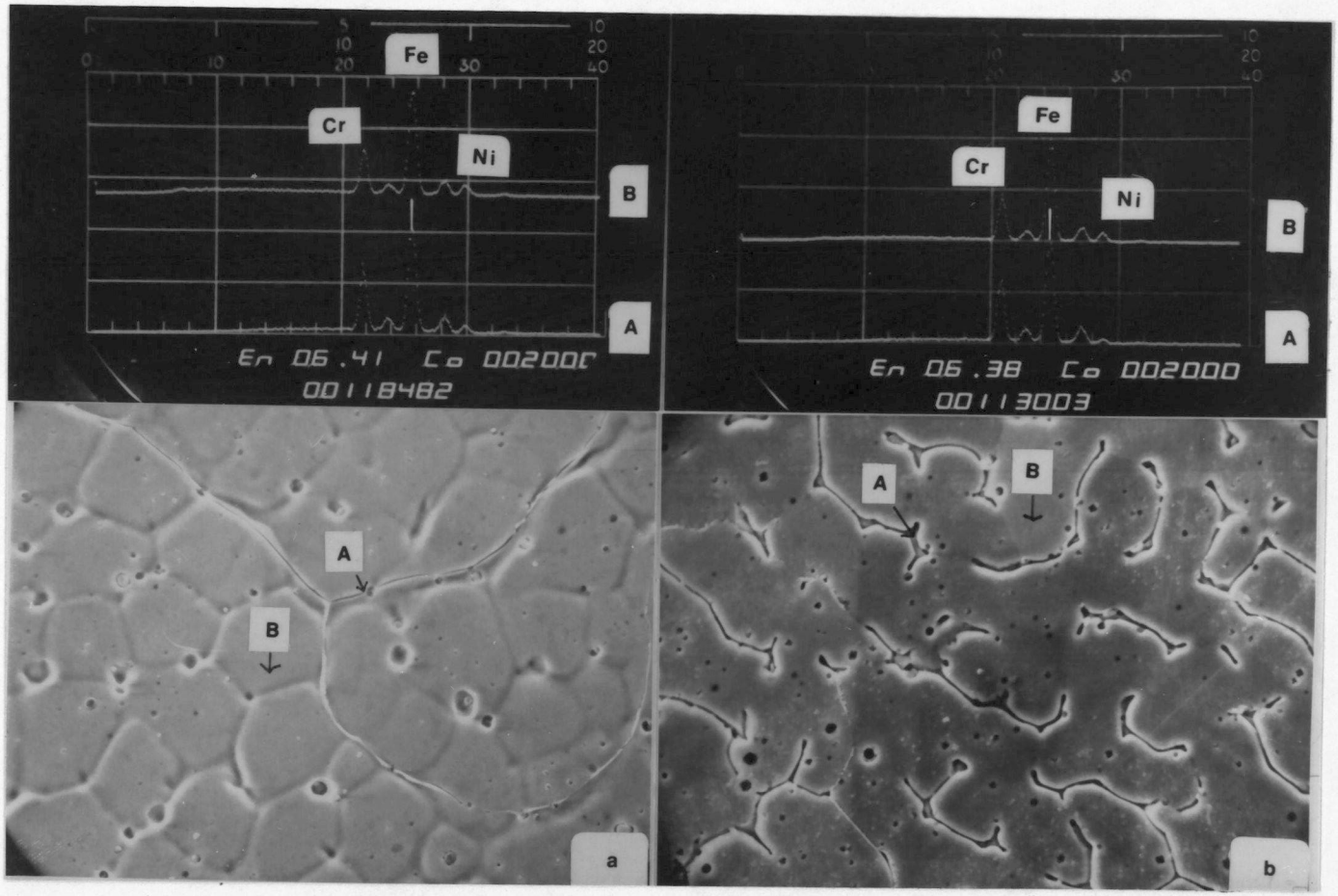


Figure 50. Microstructures of Type 308L Welds Aged Two Hours at 750°C. (2000X)
(a) Low Ferrite Weld Etched Two Minutes at + 1.35 Volts (SHE);
(b) High Ferrite Weld Etched Two Minutes at + 1.35 Volts (SHE).

CHAPTER V

CONCLUSIONS

The results of this investigation allow the following conclusions to be made. It is emphasized that unless otherwise stated reference to polarization curve data applies to deaerated 1N H_2SO_4 at room temperature.

(1) The ferrite present in the as-deposited welds is replaced by the intermetallic sigma and chi phases during aging at elevated temperatures. Also the ferrite-austenite boundaries serve as easy nucleating sites for both carbides and the intermetallic phases, thus enhancing the rate of formation of such phases in welds containing ferrite as compared to materials of similar composition in which no ferrite exists.

(2) Because of the greater chromium equivalent, types 316 and 316L welds have more precipitates and more sigma phase formed than 308 and 308L types have.

(3) The sensitization has a great effect on the anodic polarization curves, especially on the passive region. The passive current density decreases after longer aging times. For the low carbon grade stainless steel welds the sensitization effect is not significant.

(4) Both the passive current density and critical current density are lower in the high ferrite content welds than in the low ferrite content welds.

(5) Type 316 welds have lower critical current densities than type 308 welds have. There is no difference between the passive current densities of types 316 and 308 welds.

(6) Chromium depletion in the boundary itself was the cause of intergranular attack rather than the precipitates themselves. It is felt that the distribution of chromium was a major cause of the intergranular corrosion in aged austenitic stainless steel weld metals.

(7) The chemical composition plays an important role in controlling the corrosion resistance of austenitic stainless steel weld metals in 1N H_2SO_4 at room temperature. Increased chromium, molybdenum, and carbon favors recuced critical current densities in 1N H_2SO_4.

(8) From the controlled potential corrosion test it was found that the corrosive attack is uniformly distributed around the second phases in the high ferrite welds. In the low ferrite welds attack is concentrated along the grain boundaries.

(9) Sigma phase can corrode rapidly beyond the transpassive region (highly oxidizing condition). Since ferrite will enhance the formation of sigma phase, it is suggest that under highly oxidizing condition ferrite control may be necessary to avoid heavy attack on the sigma phase.

LIST OF REFERENCES

LIST OF REFERENCES

1. J. E. Spruiell, "Studies on Microstructure-property Relationships in Austenitic Stainless Steels." A proposal to ERDA, Univ. of Tennessee (1975).

2. D. F. Spond, "A Study of the Ferrite-Fissuring Relationship in Austenitic Stainless Steel Weld Metals," M.S. Thesis, Univ. of Tennessee (1975).

3. F. C. Hull, "Effect of Delta Ferrite on the Hot Cracking of Stainless Steel," Welding J., 46, 399s-409s (1967).

4. T. G. Gooch, "Welding and Corrosion Resistance of Austenitic Stainless Steels," International Institute of Welding Annual Assembly (1975).

5. N. D. Greene, "Experimental Electrode Kinetics," Reselaer Polytechnic Institute, Troy, New York (1965).

6. T. G. Gooch, "Corrosion of AISI Type 304 Austenitic Stainless Steels," British Welding J., 15 (7), 345-357 (1968).

7. N. D. Greene, "Predicting the Behavior of Corrosion Resistant Alloys by Potentiostatic Polarization Methods," Corrosion, 18, 136t-142t (1962).

8. C. D. Lundin, W. T. Delong, and D. F. Spond, "Ferrite-Fissuring Relationship in Austenitic Stainless Steel Weld Metals," Welding J., 54 (8), 241s-246s (1975).

9. W. D. France, Jr., "Controlled Potential Corrosion Tests, Their Applications and Limitations," Material Research & Standards, 9 (8), 21-26 (1969).

10. V. Cihal and M. Prazak, "Corrosion and Metallographic Study of Stainless Steels Using Potentiostatic Techniques," JISI, 193, 360-367 (1959).

11. F. C. Bell and D. E. Sonon, "Improved Metallograhic Etching Techniques for Stainless Steel and for Stainless Steel to Carbon Steel Weldments," Metallography, 9, 91-107 (1976).

12. C. Edeleanu, "The Potentiostat as a Metallographic Tool," JISI, 191, 482-488 (1957).

13. W. T. Delong, "Ferrite in Austenitic Stainless Steel Weld Metal," Welding J., 53, 273s-286s (1974).

14. J. A. Scott, "Microstructural and Mechnical Behavior of Post-treated Austenitic Stainless Steel Weldments," M.S. Thesis, Univ. of Tennessee (1975).

15. J. R. Hawthorne and H. E. Watson, "Notch Toughness of Austenitic Stainless Steel Weldments with Nuclear Irradiation," Welding J., 52, 255s-260s (1973).

16. R. W. Emerson and Morrow, "Welding High-temperature Austenitic Steel Piping," Welding J., 30, 15s-39s (1951).

17. B. Weiss and R. Stickler, "Phase Instabilities During High Temperature Exposure of 316 Austenitic Stainless Steels," Metal Trans., 3, 851-866 (1972).

18. H. Thielsh, "Physical Metallurgy of Austenitic Stainless Steels," Welding J., 29, 577s-621s (1950).

19. E. C. Bain, R. H. Aborn, and J. B. Rutherford, Transactions, ASST, TASTA, 21, 481-509 (1933).

20. H. Goldschmidt, "Interstitial Alloys," Plenum Press, New York (1967).

21. D. M. Haddrill and C. Humphries, "Stainless Steel," British Welding Research Association Bulletin, (Sept. & Nov., 1964, Jan., 1965).

22. J. E. Spruiell, J. A. Scott, C. S. Ary, and R. L. Hardin, "Microstructural Stability of Thermal-Mechanically Pretreated Type 316 Austenitic Stainless Steel," Metal Trans., 4, 1533-1544 (1973).

23. P. Duhaj, J. Ivan, and E. Makovicky, "Sigma Phase Precipitation in Austenitic Steels," JISI, 206, 1245-1251 (1968).

24. H. Wiegand and M. Doruk, Arch. Eisenhuttenw., 8, 559 (1962).

25. T. M. Williams, D. R. Harries, and J. Furnival, "Creep-Rupture Behavior of Type 316 Austenitic Steel in Relation to Boron Content," JISI, 210, 351 (1972).

26. F. C. Hull, "Effect of Composition on Embrittlement of Austenitic Stainless Steels," Welding J., 52, 104s-113s (1973).

27. D. Warren, "The Effect of Sigma Phase Vs Chromium Carbides on the Intergranular Corrosion of Type 316 and 316L Stainless Steel," Corrosion, 15, 221t-232t (1959).

28. R. F. Hills and D. R. Harries, "Sigma Phase in Austenitic Stainless Steels," Chem. & Proc. Engr., Sept., 391-396 (1960).

29. A. S. Grot and J. E. Spruiell, "Microstructural Stability of Titanium-Modified Type 316 and Type 321 Stainless Steel," Metal Trans., 6A, 2023-2030 (1975).

30. A. S. Grot, "Time-Temperature-Precipitation Studies of Titanium Modified Type 316 and 321 Stainless Steels," M.S. Thesis, Univ. of Tennessee (1974).

31. N. C. Cole, C. M. Goodwin, and C. M. Slaughter, "Effect of Heat Treatments on the Microstructures of Stainless Steel Weld Metal," Microstructural Science, 3, 789-822 (1975).

32. W. L. Wilcox, "Welding Stainless Steel-The 200 and 300 Series," Metal Progress, July, 121-130 (1964).

33. O. W. Albritton and P. E. Kadleck, "Microstructural Variations in Welded Austenitic Stainless Steel Caused by Heating at 1350°F," Welding J., 47 (2), 73s-81s (1968).

34. M. G. Fontana and N. D. Greene, "Corrosion Engineering," McGraw-Hill Book Co. (1967).

35. H. H. Uhling, "Corrosion and Corrosion Control," John Wiley & Sons Inc. (1971).

36. M. C. T. Bystram, "Some Aspects of Stainless Alloy Metallurgy and their Application to Welding Problems," British Welding J., 3 (2), 41-46 (1956).

37. G. V. T. Ranzetta, "The Corrosion of Stainless Steel Welds," Australasian Corrosion Engineering, 19 (7), 5-11 (1975).

38. T. G. Gooch and D. C. Willingham, "Weld Decay in AISI 304 Stainless Steel," Metal Constr. & Brit. Weld Journal, 3 (10), 366-369 (1971).

39. T. G. Gooch, "A question of Ferrite," The Welding Institute Research Bulletin, 15 (7), 183-188 (1974).

40. T. G. Gooch and D. C. Willingham, "Weld Decay in Austenitic Stainless Steel," The Welding Institute, Abington, Cambridge (1975).

41. E. E. Stansbury, "A Set of Supplement Notes to Met. Eng. 3150, Corrosion," Dept. of Chem. and Met. Engr., Univ. of Tennessee (1974).

42. L. L. Shreir, "Corrosion, Volume 1," Newnes-Butterworths, (1976).

43. R. F. Steigerwald, "Electrochemistry of Corrosion," 24, 1-10 (1968).

44. M. Henthorne, "Corrosion and the Process Plant," Refresher Series on Corrosion, Chem. Engr., (1971-1972).

45. The Reproducibility of Potentiostatic and Potendynamic Anodic Polarization Measurements - An ASTM G-1/XI Interlaboratory Testing Program, June 29, (1967).

46. B. E. Wilde, " A Relationship between Steady-State Corrosion Potential and the Anodic Dissolution Kinetics of the 300 Series Austenitic Stainless Steels," Corrosion Science, 7, 315-324 (1967).

47. W. D. France, Jr., and N. D. Greene, "Interpretation of Passive Current Maximum during Polarization of Stainless Steels," Corrosion, 24, 403-406 (1968).

48. C. D. Kim and B. F. Wilde, "Influence of Cathodic Pretreatment of the Anodic Dissolution Kinetics of Stainless Steels in Dilute Acid Media," Corrosion, 10, 735-744 (1970).

49. J. R. Myers, F. H. Beck, and M. G. Fontana, "Anodic Polarization Behavior of Nickel-Chromium Alloys in Sulfuric Acid Solution," Corrosion, 21, 277-287 (1965).

50. K. Osozawa and H. J. Engell, "The Anodic Polarization Curves of Iron-Nickel-Chromium Alloys," Corrosion Science, 6, 389-393 (1966).

51. K. Osozawa, K. Bohenkamp, and H. J. Engell, "Potentiostatic Study on the Intergranular Corrosion of an Austenitic Chromium-Nickel Stainless Steel," Corrosion Science, 6, 421-433 (1966).

52. M. B. Rockel, "Interpretation of the Second Anodic Current Maximum on Polarization Curves of Sensitized Chromium Steels in 1N H_2SO_4," Corrosion, 27 (3), 95- 103 (1971).

53. M. Henthorne, "Intergranular Corrosion in Iron and Nickel Base Alloys," Process Corrosion Engineering, NACE, 66-85 (1976).

54. R. L. Cowan II. and C. S. Tedmon Jr., "Intergranular Corrosion of Iron-Nickel-Chromium Alloys," Advances in Corrosion Science and Technology, Vol. 3, 293-389 (1971).

55. W. T. Delong, "Calibration Procedure for Instruments to Measure the Delaa Ferrite Content of Austenitic

56. N. D. Greene and B. E. Wilde, "Variable Corrosion Resistance of 18-8 Stainless Steels: Influence of Environmental and Metallurgical Factors," Corrosion, 26 (12), 533-538 (1970).

57. B. D. Cullity, "Elements of X-ray Diffraction," Addison-Wesley Co. (1956).

58. L. Patel, "Effect of Carbon Content on the Sigma Formation in Austenitic Stainless Steel," M.S. Thesis, Univ. of Tennessee (to be published).

59. H. Tuma, M. Vyklicky, and K. Lobl, Archiv. fur das Eisenkuttenwesen, 41, p.983 (1970). English translation: BNWL-TR-73 (Report).

VITA

The author was born in Sen-Tung Province of Mainland China on June 5, 1947. He moved with his family to Taiwan in 1948 before the Communist regime took over the mainland. He completed his elementary and high school education in Taipei, and earned his Bachelor of Science degree in the field of physics at the Fu Jen University in 1969. He served in the Chinese Army as a second lieutenant in 1970.

The author came to the United States in the Fall of 1971 and earned his Master of Science degree in the field of physics at the Montana State University in 1973. He entered the Metallurgical Engineering Department of The University of Tennessee, Knoxville, in the Fall of 1975. He is a member of the American Society for Metals, the American Welding Society, and Sigma Xi.

The author wishes to continue his graduate work toward a Ph.D. degree at The University of Tennessee in the field of Metallurgical Engineering.

He is married to the former Pin-Ying Wang of Taiwan, Republic of China.